https://ntrs.nasa.gov/search.jsp?R=19690013610 2020-03-12T03:51:44+00:00Z

N 69 22975

RESEARCH AND DEVELOPMENT STUDY ON WIDE BAND-GAP SEMICONDUCTOR FILMS

By A. J. Noreika, M. H. Francombe and S. A. Zeitman

December 1968

Distribution of this report is provided in the interest of information exchange and should not be construed as endorsement by NASA of the material presented. Responsibility for the contents resides with the organization that prepared it.

Prepared under Contract No. NAS 12-568 by
WESTINGHOUSE ELECTRIC CORPORATION
Pittsburgh, Pa.

Electronics Research Center
NATIONAL AERONAUTICS AND SPACE ADMINISTRATION

Dr. Robert F. Adamsky
Technical Monitor
NAS 12-568
Electronics Research Center
575 Technology Square
Cambridge, Massachusetts 02139

Requests for copies of this report should be referred to:

NASA Scientific and Technical Information Facility
P.O. Box 33
College Park, Maryland 20740

RESEARCH AND DEVELOPMENT STUDY
ON WIDE BAND-GAP SEMICONDUCTOR FILMS

By A. J. Noreika, M. H. Francombe and S. A. Zeitman

December 1968

Interim Report

June 1967 - November 1968

Prepared under Contract No. NAS 12-568 by
WESTINGHOUSE ELECTRIC CORPORATION
Pittsburgh, Pa.

Electronics Research Center
NATIONAL AERONAUTICS AND SPACE ADMINISTRATION

TABLE OF CONTENTS

	Page
LIST OF ILLUSTRATIONS	
LIST OF TABLES	
SUMMARY	1
1. INTRODUCTION	5
2. EVAPORATED FILMS	9
2.1 Aluminum Antimonide (AlSb)	9
2.1.1 Preparation	9
2.1.2 Structural Properties	14
2.1.3 Optical Studies	15
2.1.4 Chemical Stability	18
2.1.5 Electrical Studies	19
2.2 Aluminum Antimonide - Reactively Sputtered	27
2.2.1 Preparation	27
2.2.2 Structural and Optical Properties	29
2.3 Aluminum Arsenide (AlAs)	29
2.3.1 Preparation	29
2.3.2 Structural Properties	36
2.3.3 Optical Studies and Chemical Stability	38
2.3.4 Electrical Studies	40
2.4 Aluminum Phosphide (AlP)	42
2.4.1 Preparation	42
2.4.2 Structural, Optical and Electrical Studies	43
2.5 Discussion	48
3. SPUTTERED FILMS	50
3.1 Reactively Sputtered AlN (Diode System)	50
3.1.1 Preparation	50
3.1.2 Structural Studies	53
3.1.3 Chemical Stability	58
3.1.4 Optical Properties	60
3.1.5 Capacitance Measurements	66
3.1.6 Capacitive Properties of Annealed Films	70
3.1.7 I-V Measurements	73
3.1.8 I-V Data for Annealed Films	79
3.1.9 C-V Measurements	85

TABLE OF CONTENTS (Cont'd.)

	Page
3.2 Reactively Sputtered AlN (Triode System)	88
3.2.1 Preparation	89
3.2.2 Composition and Growth Rate Evaluation	90
3.2.3 Optical Properties	91
3.2.4 Electrical Measurements	93
3.3 Mixed Al-Si Nitrides	94
3.3.1 Preparation	94
3.3.2 Structural and Optical Properties	94
3.3.3 Electrical Measurements	95
3.4 Reactively Sputtered BN	100
3.4.1 Preparation	100
3.4.2 Structure	101
3.4.3 Optical and Electrical Data	104
3.5 Discussion	106
4. CONCLUSIONS AND FUTURE PLANS	111
4.1 Conclusions	111
4.2 Future Plans	112
5. REFERENCES	116
6. APPENDIX (NEW TECHNOLOGY)	119

LIST OF ILLUSTRATIONS

Fig. 1A — Schematic of system for co-evaporation of AlSb films, (a) front elevation of reaction chamber.

Fig. 1B — (b) plan view of mounting system used for sequential exposure of four substrates.

Fig. 2 — System for growth of AlSb films by three temperature evaporation methods.

Fig. 3 — System for three-temperature evaporation of AlSb films showing close-up of substrate assembly.

Fig. 4 — Absorption spectra of AlSb films (significant features found by reflectance spectra are indicated by the arrows, including the band-gap value of 1.6 eV). Samples Z-197-3 and Z-199-1 are on CaF_2; Z-197-4 is on sapphire.

Fig. 5 — Spectral variation of photovoltaic effect in AlSb film evaporated on Ta contacts.

Fig. 6 — Spectral variation of photoresponse from AlSb films.

Fig. 7 — Temperature dependence of resistance measured in situ on AlSb films deposited at 600°C; (Z-212) thickness 1μ, (Z-215) thickness 2μ.

Fig. 8 — Schematic of arrangement for diode reactive sputtering of AlSb films; recesses in cathode contain the Group V element (Sb).

Fig. 9 — Schematic of alternate sputtering system with external Sb source.

Fig. 10 — Transmission electron diffraction patterns from sputtered AlSb films deposited on cleaved CaF_2 at (a) 400°C, approximate thickness 1500 A and (b) 650°C, approximate thickness 1000 A.

Fig. 11 — Modified system for co-evaporation of AlAs films.

Fig. 12 — Electron diffraction pattern from evaporated aluminum-rich AlAs film showing Wurtzite structure.

Fig. 13 — Absorption spectra from evaporated AlAs films, (Z-222-2) 650°C, thickness 6000 A, (Z-223) 750°C, thickness 3000 A, (KB59-1) 480°C, thickness 1500 A.

Fig. 14 Temperature dependence of resistance measured on AlAs film (Z-234) deposited at 720°C, thickness 2 microns.

Fig. 15 Electron diffraction pattern of AlP film deposited on silica at 720°C.

Fig. 16 Temperature dependence of resistance measured on AlP film (Z-237) deposited at 720°C, thickness 9100 A.

Fig. 17 Absorption spectrum of AlP film, obtained with sample immersed in ethyl alcohol. (Absorption of cell and alcohol shown as "blank").

Fig. 18 Schematic of arrangement for diode reactive sputtering of AlN films. Resistive heating of substrates in Ta envelopes via the solid and split disks of the substrate holder.

Fig. 19A Electron diffraction patterns of AlN films reactively sputtered on (111)Si; (a) unheated substrate; (b) substrate temperature, 900°C.

Fig. 19B Electron diffraction patterns of AlN films reactively sputtered on (111)Si; (c) substrate temperature, 950°C; (d) substrate temperature, 1000°C.

Fig. 20 Electron diffraction patterns of AlN films reactively sputtered on (0001) faces of 6H-type SiC crystals: electron beam along (a) [11.0] and (b) [10.0].

Fig. 21 Transmission electron micrograph of reactively sputtered AlN film (1000 A thick) deposited on (111) Si at 900°C.

Fig. 22 Absorption spectrum of AlN film on CaF_2.

Fig. 23 Optical absorption data comparing properties of reactively sputtered AlN to bulk single crystals. Film Z-203-2 is an as-grown film; film Z-203-3 has been similarly deposited but has been annealed at 900°C in N_2. T_1 is an as-grown crystal (Cox, et al.). T_2 is a crystal annealed in Argon.

Fig. 24 Absorption difference spectrum obtained from nitrogen anneal of sputtered AlN film.

Fig. 25 Optical absorption in four AlN films, thickness 8000 A, deposited on vitreous silica and sapphire under same sputtering conditions. One film on each substrate was given standard annealing treatment in nitrogen.

Fig. 26 Variation of dielectric constant, $\varepsilon/\varepsilon_0$, with temperature at several frequencies.

Fig. 27 Variation of dissipation factor, D, with temperature at several frequencies.

Fig. 28 Variation of ac resistivity with temperature at several frequencies.

Fig. 29 Effects of thermal anneal on dissipation factor (loss) of reactively sputtered AlN films.

Fig. 30 Current-voltage data for Al/AlN/Ta film sandwich structure, AlN film thickness 8000 A. Also shown are data of Kawabe, et al. for single crystal AlN.

Fig. 31 Current-voltage data for Al/AlN/Ta film sandwich structure, AlN film thickness 8000 A. Curves A, B and C obtained from adjacent test samples on same film.

Fig. 32 Photoconductivity effect for Al/AlN/Ta film sandwich (sample illuminated with mercury-argon lamp).

Fig. 33 Current-voltage data for Ta/AlN/Ta film sandwich structure, AlN film thickness 4000 A.

Fig. 34 I-V relationships of an AlN film at various temperatures. The dielectric is part of a Ta/AlN/Ta structure. AlN thickness is 4500 A.

Fig. 35 I-V relationships of an AlN film for various annealing schedules. Annealing temperature is 220°C; AlN thickness is 6000 A.

Fig. 36 Capacitance-voltage traces for Al-AlN-Si with varying sweep voltages. The transient at the ends of the sweep is an instrumental artifact.

Fig. 37 Optical absorption in three AlN films deposited on vitreous silica, two having been prepared by diode reactive sputtering, the third by triode reactive sputtering. The shift toward higher wavelength for the unannealed diode-prepared film is likely due to a N_2 deficiency in the film. The triode prepared film does not suffer in a like manner.

Fig. 38 Electron diffraction patterns of mixed AlN-Si_3N_4 film. Substrate temperature, 900°C; thickness 6000 Å.

Fig. 39 Dielectric polarization effect observed in mixed AlN-Si_3N_4 films. Film thickness is approximately 4500 A.

Fig. 40 I-V data for mixed $AlN-Si_3N_4$ film. Cathode Al:Si ratio is approximately 1:1.

Fig. 41 Electron micrograph and selected area diffraction pattern from reactively sputtered BN film deposited on heated (800°C) Si substrate.

Fig. 42 Electron micrograph and selected area diffraction pattern from reactively sputtered BN film deposited on unheated Si substrate.

Fig. 43 Optical absorption data for two BN films deposited under similar sputtering conditions. BN-002-1 was annealed in pure N_2. Note the slight shift to shorter wavelength (higher energy).

LIST OF TABLES

Table I Aluminum-V Compounds Collected Properties

Table II X-Ray Diffraction Data for Evaporated AlSb Films

Table III Summary of Selected Results for Co-Evaporated AlAs Films Deposited on Vitreous Silica

Table IV Electron Diffraction Data for Reactively Sputtered AlN Films

Table V Frequency Variation of Capacitance and Loss Values of Some Annealed AlN Films

Table VI Data for Triode Reactively Sputtered AlN Films

Table VII Diffraction Data for BN

Table VIII Dielectric Data for Reactively Sputtered BN Films

SUMMARY

Thin films of AlSb, AlAs and AlP have been prepared by a three-temperature reactive evaporation technique, while films of AlN were deposited using a reactive sputtering method. Reactive sputtering was also used to produce films of AlSb. The structural, optical and electrical properties of these films were examined and related to conditions of deposition. The properties were compared with published data for these materials in (where available) thin film, or alternatively bulk, single-crystal form.

The freshly deposited films of AlSb were found to be structurally and optically similar to bulk crystals. It was observed, however, that in times varying from a few hours to several weeks, both structural and optical properties altered. The changes were caused by hydrolysis of the compound when exposed to the laboratory environment and were observed also in films of AlAs and AlP. The structural alteration took the form of a change from a well-crystallized deposit to an amorphous-like one, the change taking place initially at the exposed surface. Granular deposits prepared at elevated temperatures were observed to degrade most rapidly. Optical change was evident in the form of marked increase of absorption in the visible and ultraviolet. Electrical measurements on some films contacted with tantalum showed the presence of a strong photovoltaic effect. Measurements of the spectral variation of this effect indicated that it arose from a barrier-like phenomenon. Analyses of the data led to reasonable values both for the band gap of AlSb and the work function of Ta.

Sputtered films of AlSb acquired a highly oriented structure at temperatures near 650°C, while evaporated films were only partly oriented. An investigation of relative growth rates at these temperatures showed the following: AlSb (evaporated) $\sim$ 300 A/min; AlSb (sputtered) $\sim$ 50 A/min. The effect of exposure to the atmosphere was identical to that reported for the evaporated films.

AlAs films were prepared by the reactive evaporation method and are believed to be the first produced by this method. X-ray examination showed the films to consist mainly of the bulk cubic phase although electron diffraction studies on some Al-rich films revealed that surface layers comprised a highly oriented wurtzite modification. Optical data were consistent with indirect band gap of 2.1 eV (in agreement with the bulk form). Electrical measurements suggested that the measured conductivity of the films was dominated by a spread of shallow impurity levels which could not be characterized by a single activation energy. The change in properties when exposed to air was less drastic than that experienced by the AlSb films, the optical absorption decreasing after a prolonged exposure.

AlP was also prepared in thin film form by the reactive evaporation method. Experience with the chemical instability of both the AlSb and AlAs films led to use of alcohol-filled containers to protect the film during optical and electrical studies. The optical absorption data are consistent with a compound with an absorption edge near 2.5 eV, again in good agreement with the bulk compound. Structurally the film was found to adopt the cubic bulk form possessing a weak (110) fiber

texture. The electrical resistivity studies suggested that conductivity was influenced (as in the AlAs films) by a spread of shallow impurity levels.

Study of the properties of reactively sputtered AlN films comprised a considerable part of the overall program. The emphasis on this compound was motivated by excellent chemical stability characteristics and by the observations of good dielectric behavior. Structurally, films of AlN assumed the bulk, wurtzite (hexagonal) arrangement. Epitaxial deposits were prepared on oriented Si and SiC substrates together with strongly textured films on vitreous silica. Optically, the films as-deposited in a high-pressure glow-discharge system showed absorption characteristics with an anomalously low edge, which suggested the presence of nitrogen vacancies or argon occlusion (a similar effect had been observed by Cox, et. al. (Ref. 1) in argon annealed single crystals). Annealing in nitrogen at temperatures near the depositing temperature was required before the bulk absorption characteristics (with an edge at 5.9 eV) were observed. Later experimentation with a low pressure triode sputtering arrangement yielded films with the bulk properties in the as-deposited state.

Although the films seemed unsuitable as semiconductors, dielectric measurements indicated possible use as a refractory dielectric. Both the dielectric constant and dissipation factor showed less variation with temperature (25° to 350°C) than for the bulk ceramic material, indicating fewer conductive impurities. Observations of electrical breakdown and conduction behavior showed that films, less than 1500 A thick, demonstrated erratic behavior under applied voltage. This effect

was attributed to leakage at grain boundaries. Films of greater thickness showed no instability until fields greater than 9×10^6 V/cm were applied. The main features of the I-V characteristic at low fields were reversible and consistent with a space-charge limited mechanism. However, at higher fields the characteristics became unstable and changed irreversibly. Studies of MIS structures using oriented AlN films on a silicon substrate revealed that the films appeared polarizable, an effect assumed due to the piezoelectric character of AlN.

In order to reduce the electrical instabilities brought on by grain boundary leakage, an effort was made to induce an amorphous-like character to the deposits by the addition of an amorphous nitride component, viz., Si_3N_4. Films of the mixture were co-sputtered from cathodes with nominal Al:Si ratios of 6:1 and 1:1. The former differed only slightly from the pure AlN films showing similar optical and electrical behavior. Films prepared from the latter cathode, however, assumed an almost amorphous structure and completely reversible I-V characteristics which displayed the trap influenced space-charge limited behavior. Dielectric properties were more erratic and demonstrated an added dispersion with frequency.

A further effort, to prepare a mixed film with another stable component, viz. BN, is in progress. Films of BN alone have been reactively sputtered so that the properties of mixed AlN-BN may be compared to those of the undiluted nitrides.

1. INTRODUCTION

The objectives of this program are to study the feasibility of preparing thin films of the aluminum class of III-V compounds viz. AlN, AlSb, AlAs and AlP, by evaporation and sputtering and to correlate the structural, electrical and optical properties of the resulting films with their conditions of deposition.

This particular family of III-V compounds is an interesting one because of the broad range of electrical and optical properties which are covered by its members. AlSb, for example, possesses an energy gap comparable to that of Si and a spectral response which is an almost theoretical match to the solar spectrum. Light emissive junctions, radiating in the visible and ultraviolet may be possible with AlP. AlN with a band gap greater than SiC seems suitable as an insulating coating for integrated circuitry where high bond strength can provide both mechanical and environmental protection and perhaps improved radiation resistance. Other collected properties are given in Table I.

The compounds in bulk form, with the exception of AlN, however, suffer from serious chemical instabilities especially in the presence of water vapor. AlP reacts readily in moist air and is a known generator of phosphine (Ref. 2). Both AlAs (Ref. 3) and AlSb (Ref. 4) deteriorate rapidly on exposure. A literature survey notes that protective environments, viz., alcohol sheaths or vacua, are useful while electrical and optical studies are conducted.

In general, only AlN and AlSb have been studied extensively. Since, however, all of the compounds melt only in an overpressure of

Table I Aluminum-V Compounds Collected Properties

	E_g (300°K)	μ, w^2/v-sec	m^*	dE/dt	n	ε	Lattice parameter	m.p.
AlN	5.9	μ_p=14 290°K		-3.5×10^{-4} at 0°K	∥2.18 ⊥2.00	8.5	a_o=3.104 c_o=4.965 a_o=3.111 c=4.980	2200°C at 2 atm
AlP	2.45 2.42	μ_n=3500		5.8×10^{-4}	3.4		5.43 5.4625	
AlAs	2.16 (indirect) 2.9 (direct)	μ_n=100 for $n=6\times10^{17}$ μ_n=1200 μ_p=200					5.63	1600°
AlSb	1.60	μ_p=400(300°K) =5000(50°K)	m_n^*=0.3 m_p =0.4		3.4 3.18	10.3 static 9.0 optic	6.1355	1060°C

the Group V element, making both melt-growth and zone-refining techniques difficult to apply, such studies have mainly been restricted to polycrystalline materials or at best to small, fragmentary, platelike crystals prepared by sublimation or vapor phase techniques. Some success has been achieved by use of chemical transport methods, viz., the preparations of AlN and AlP. These transport methods utilize the heterogeneous reaction of a volatile Group III halide with Group V vapors at the surfaces of heated substrates. The halides may be chlorides or iodides. Reid, et. al. (Ref. 5) found that the iodide is to be preferred in the epitaxial growth of AlP on Si or GaAs since the transport of the Al may be effected at lower temperatures than by use of the chloride carrier. The lower source temperatures are preferred to prevent contamination via reaction of the vapor with the walls of the silica reaction chamber. Pastrnak, et. al. (Ref. 6) utilizes the chloride in the preparation of AlN reacting it with N_2 in a gas discharge. This technique, however, favors the formation of whisker-like growth, at thicknesses greater than 1000 A, due presumably to a tendency toward homogeneous nucleation in the gas phase. Work by Chu, et al. (Ref. 7), have shown that the ammonolysis of $AlCl_3$ and NH_3 yields highly oriented films of AlN to thicknesses of several microns.

Another compound of the series, viz., AlSb, has been prepared in thin film form by vacuum evaporation techniques (Ref. 8, 9, 10, 11). Co-evaporation of the separate elements is by far the most favored method since direct evaporation of a powdered charge tends to decompose, the volatile Group V element evaporating or subliming at a more rapid rate.

The present study describes the use of sputtering and evaporation techniques for the preparation of thin films of the Al-V family of compounds. The three-temperature evaporation method has been used in the growth of AlSb films and has been extended for the first time to the synthesis of AlAs and AlP films. The high decomposition temperatures of the AlAs and AlP compounds raises special preparative problems not previously encountered in the growth of other III-V compound films. Methods of overcoming these problems are discussed.

Major emphasis has been placed upon the preparation and properties of AlN films and their solid solutions with Si_3N_4 and BN. Interest in the nitrides was stimulated early during the contract when it became evident that thin-film AlN was not only the most chemically stable of the compound family, but also possessed very promising dielectric properties. In addition to presenting results of studies on the structural, electrical and optical properties of the nitride films the anticipated direction to be followed in the preparation of films potentially useful in MIS type structures and in piezoelectric transducers will be discussed.

The authors wish to thank Dr. J. E. Johnson of these Laboratories for his constructive assistance during the early stages of this study.

2. EVAPORATED FILMS

2.1 Aluminum Antimonide (AlSb)

2.1.1 Preparation - Essentially the same approach was used to prepare films of AlSb as that described by Johnson (Ref.10) and by David et.al. (Ref.11). However, the geometry of the deposition system was modified in order to obtain more film samples in a single pump-down. An aluminum metal charge (99.998%) was contained in a BN crucible which was mounted in a resistively heated tantalum holder (Fig. 1A). The antimony, in the form of small lumps, was distributed uniformly around a resistively heated circular V-shaped trough made from 5 mil tantalum sheet. Quartz shields were provided so that the antimony source was shielded from the aluminum and the vapor mixture could exit primarily through an aperture at the top of the reaction chamber. Substrates, contained in resistively heated tantalum envelopes were mounted on a sectored wheel (Fig. 1B) which could be rotated externally so as to bring them sequentially over the aperture. Excess vapor which bypassed the substrates was collected in a tantalum canopy clamped to a liquid nitrogen trap above the reaction chamber. Views of the complete system are shown in Figs. 2 and 3.

Calibration curves of substrate temperature (measured at the front face of quartz substrates) vs. heater current were plotted for substrates heated in the tantalum envelopes. The antimony and aluminum source temperatures were measured directly during each run with a thermocouple and optical pyrometer, respectively. The substrate temperatures

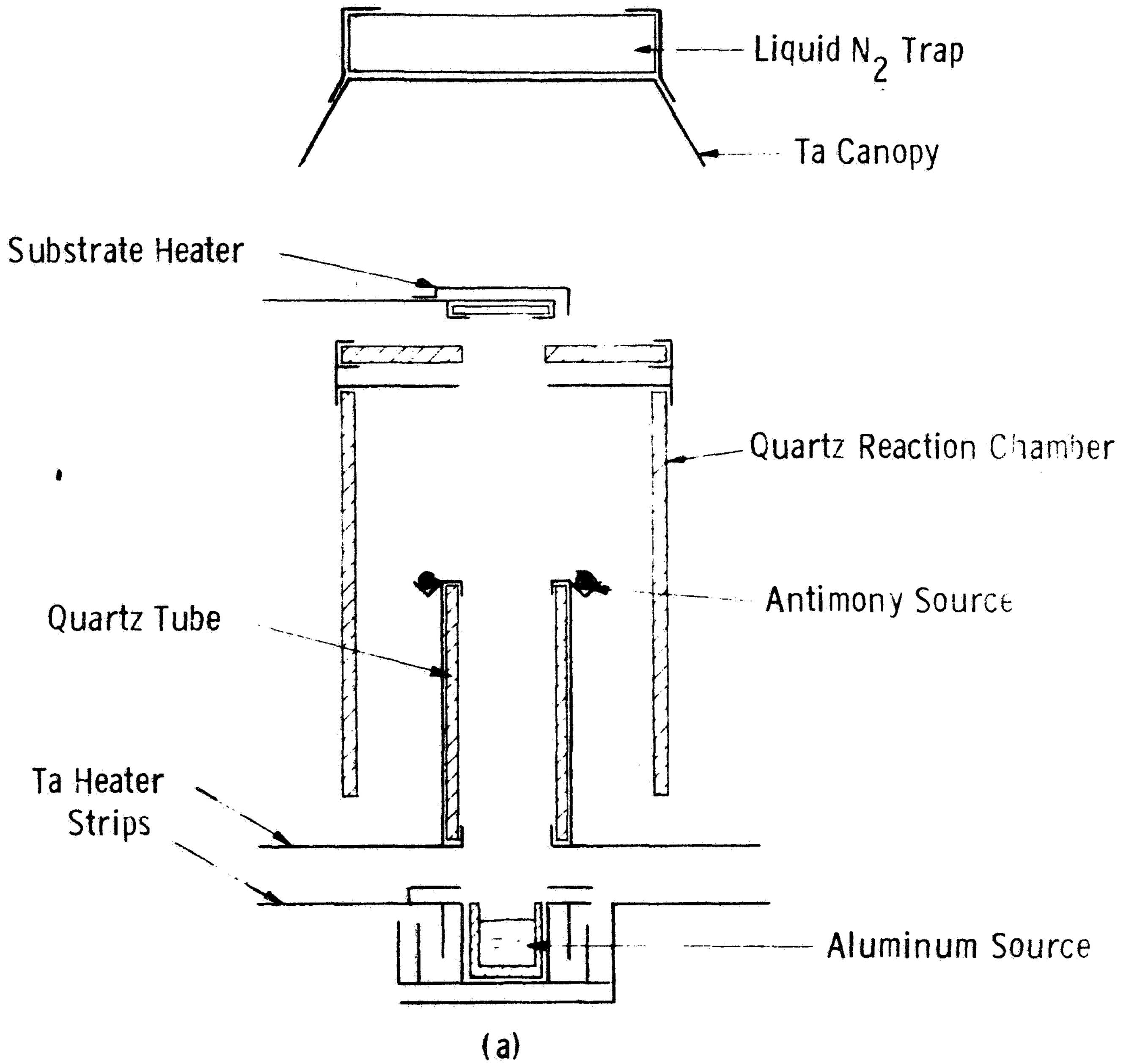

Fig. 1A – Schematic of system for co-evaporation of AlSb films, (a) front elevation of reaction chamber

Dwg. 854A430

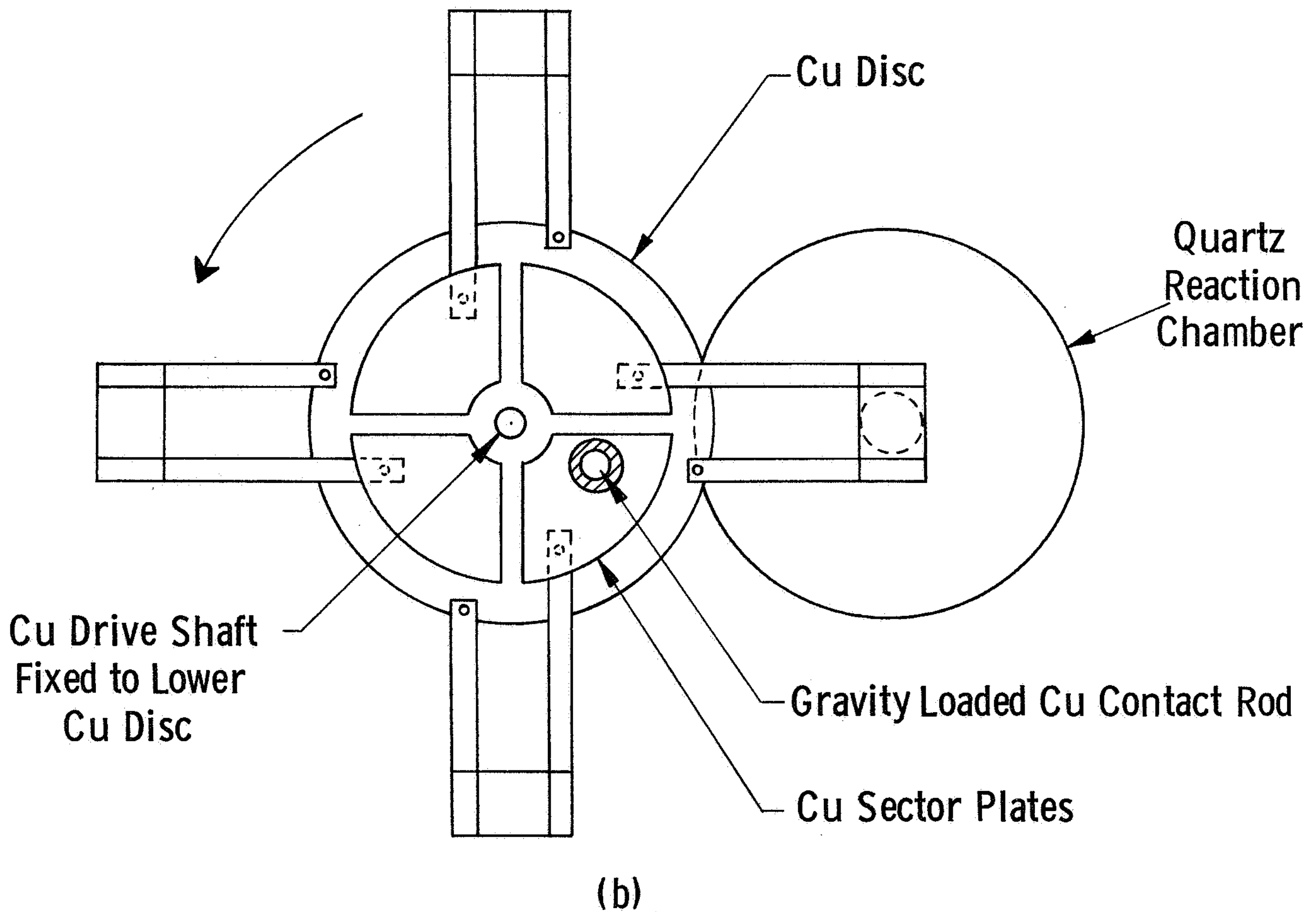

Fig. 1B—(cont'd) (b) plan view of mounting system used for sequential exposure of four substrates

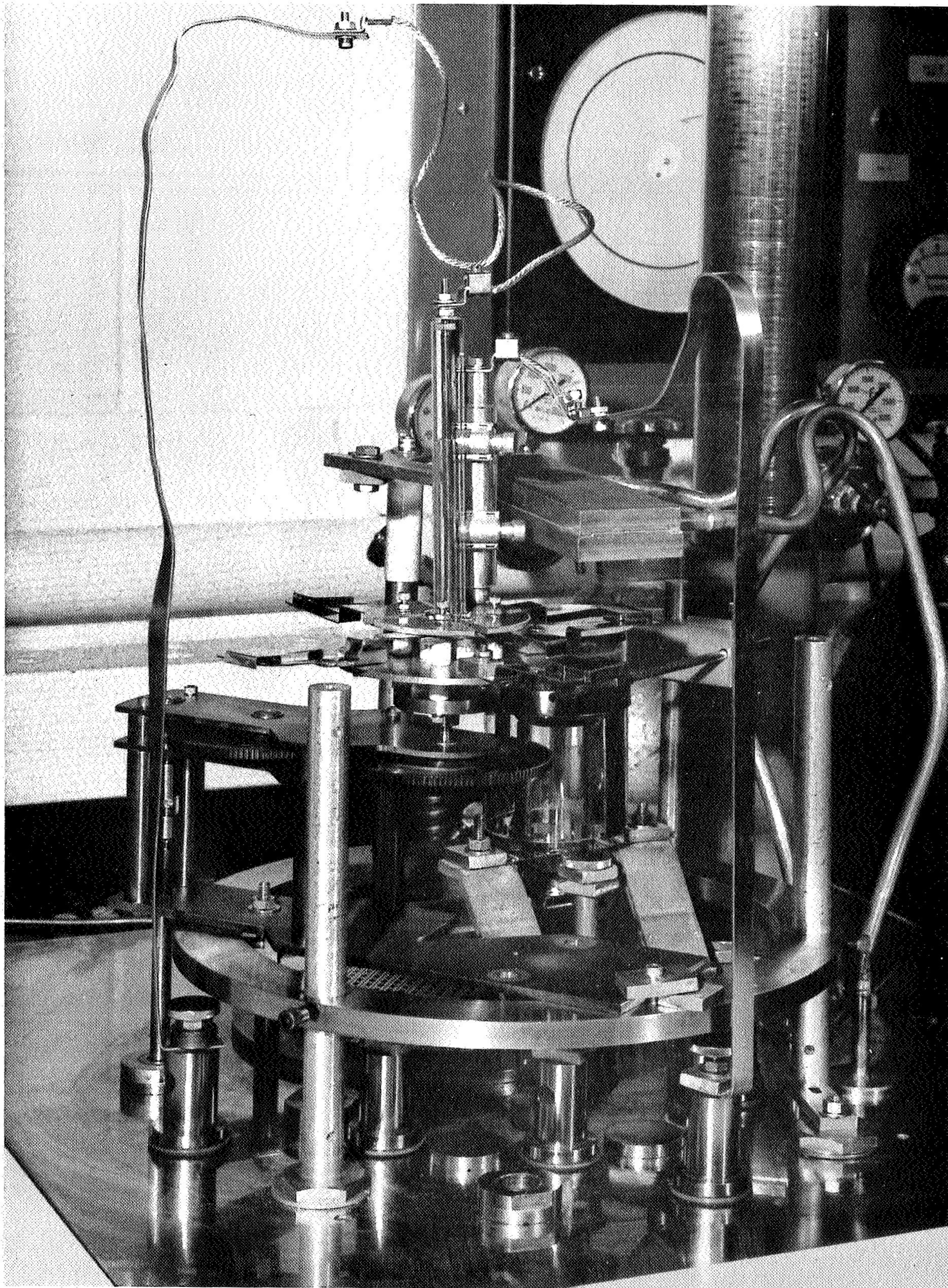

Fig. 2 —System for growth of AlSb films by three-temperature evaporation method

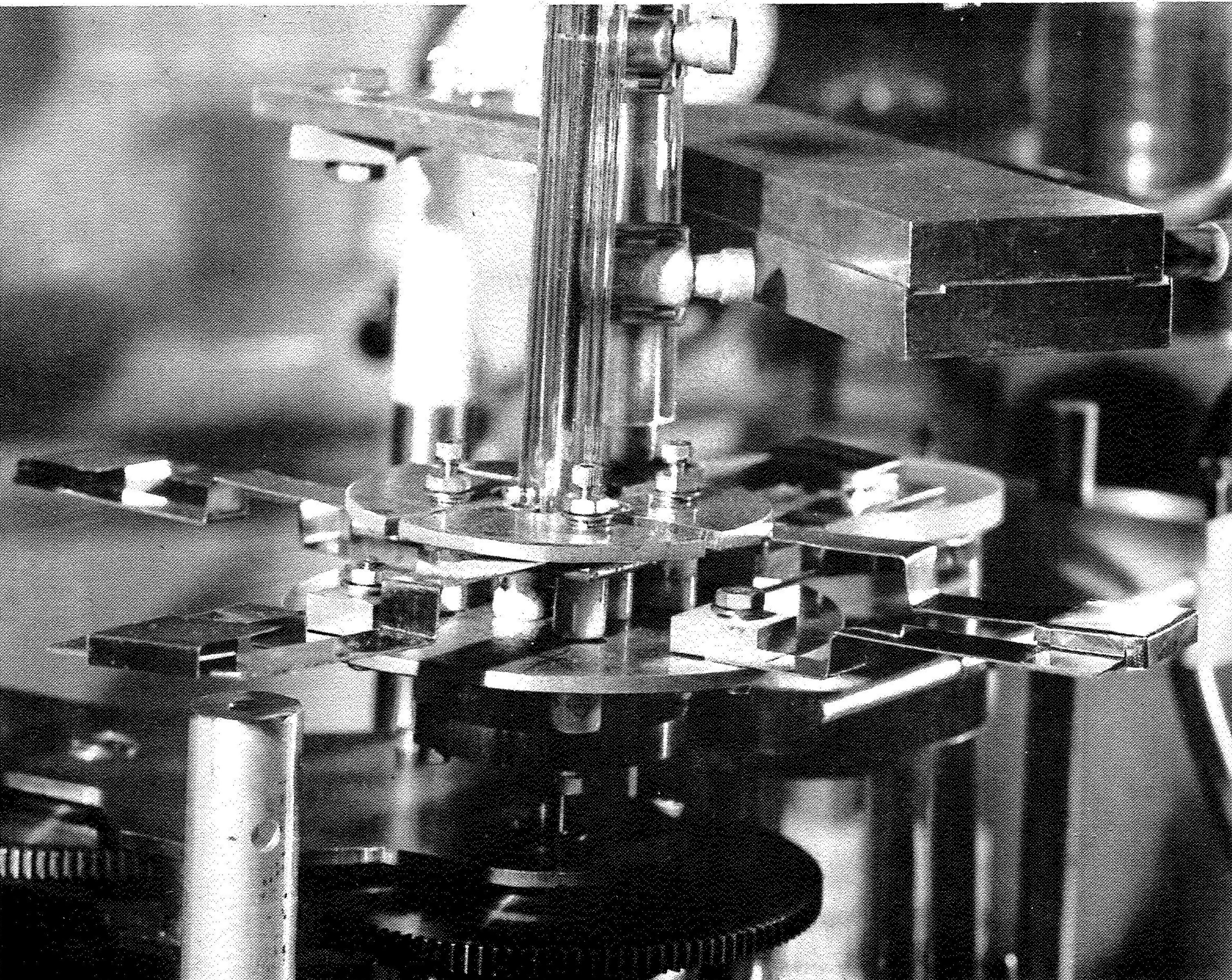

Fig. 3 –System for three-temperature evaporation of Al Sb films showing close-up of substrate assembly

RM-40127

ranged from 500 to 750°C, antimony source temperature from 495°C (V.P. 2×10^{-3} torr) to 540°C (V.P. 10^{-2} torr), and the aluminum temperature was held constant at 1200°C. A simple calculation based on these vapor pressure values and on the geometry of the system indicates that this range of Sb source temperatures should correspond to an ideal range of Sb/Al vapor flux ratios of 1 to 4. Typically, with an Sb source temperature of 520°C and substrate temperature of 600°C, a growth rate of about 300 A per minute was obtained. Substrates used included (111) crystals of CaF_2, (0001) oriented sapphire (Al_2O_3) crystals, (111) silicon wafers and vitreous silica (often coated with sputtered Ta to facilitate electrical measurement).

2.1.2 Structural Properties - When efforts were made to examine the crystallinity and orientation of the AlSb films using reflection electron diffraction, meaningful results were not obtained since the patterns yielded only diffuse diffraction features consistent with an amorphous surface structure. To obtain a more representative characterization of the entire film, the deposits were studied by glancing-angle X-ray diffraction using a Philips powder camera. The results showed that in each case, despite the amorphous surface layer, the films immediately after preparation possessed well-crystallized, and in many cases, strongly oriented structures.

Most of the samples examined were single-phase with the cubic zinc blende type structure of AlSb. In those cases where a second phase was present, this was identified as Al and its appearance could be accounted for by the fact that the Sb source was depleted or that its

temperature had fallen during the run. In contradiction to the claims of David et. al. (Ref.11) who reported free Sb in films deposited at temperatures below 650°C, no uncombined Sb was detected in the present study even at 550°C. This is consistent both with the earlier work of Johnson (Ref.10) in these laboratories and with the findings of Gunther (Ref.12) who reports 400°C as the lowest condensation temperature for Sb on InSb.

Structures varying from randomly oriented to almost completely epitaxial were obtained on the (111) face of CaF_2. Very strong (111) and (110) fiber orientations were produced on amorphous quartz substrates and, as shown in Table II, these appear to vary markedly in type with the temperature of deposition. Similar effects are found in both evaporated Ge films (Ref.13) and in sputtered (Ref.14) and co-evaporated (Ref.15) GaAs films deposited on vitreous silica.

2.1.3 Optical Studies - Absorption spectra for AlSb films deposited at from 600 to 700°C onto CaF_2 or sapphire were also studied. Measurements were made with a Cary spectrophotometer over a wavelength range 1900 A to 20,000 A. No significant difference in the spectra was noted for the various preparations, except for anticipated thickness dependences. Portions of the spectra from several films are plotted in Fig. 4. Data in this figure have been plotted only for those regions where the transmission is less than 10%, for which effects due to surface contamination and oxidation are least significant (Ref.16). Results from those samples exhibiting strong interference patterns near the 1.6 eV edge were not included.

Table II X-Ray Diffraction Data for Evaporated AlSb Films

Sample No.	Substrate	T_s (°C)	T_{Sb} (°C)	Thickness (Å)	Remarks
195-1	(111) CaF_2	550°	495	8,000	AlSb with weak Al phase
195-2	"	"	513	10,500	AlSb only, strong (110) texture
195-3	"	"	536	"	AlSb only, (110) texture
195-4	"	"	540	9,000	Epitaxial AlSb, weak Al phase
196-1	SiO_2	550°	520	∿10,000	AlSb only, strong (111) texture
196-2	"	600	520	∿10,000	AlSb only, strong (110) texture
196-3	"	700	520	∿10,000	AlSb only, weak (110) texture
196-4	"	750	520	∿10,000	AlSb only, weak (100) texture
197-1	(111) CaF_2	650	520	∿50,000	AlSb, weak Al phase
197-2	(0001) Al_2O_3	650	520	∿50,000	AlSb, strong (110) texture, very weak Al phase
199-2	(111) CaF_2	600	540	∿40,000	AlSb only, imperfectly epitaxed.

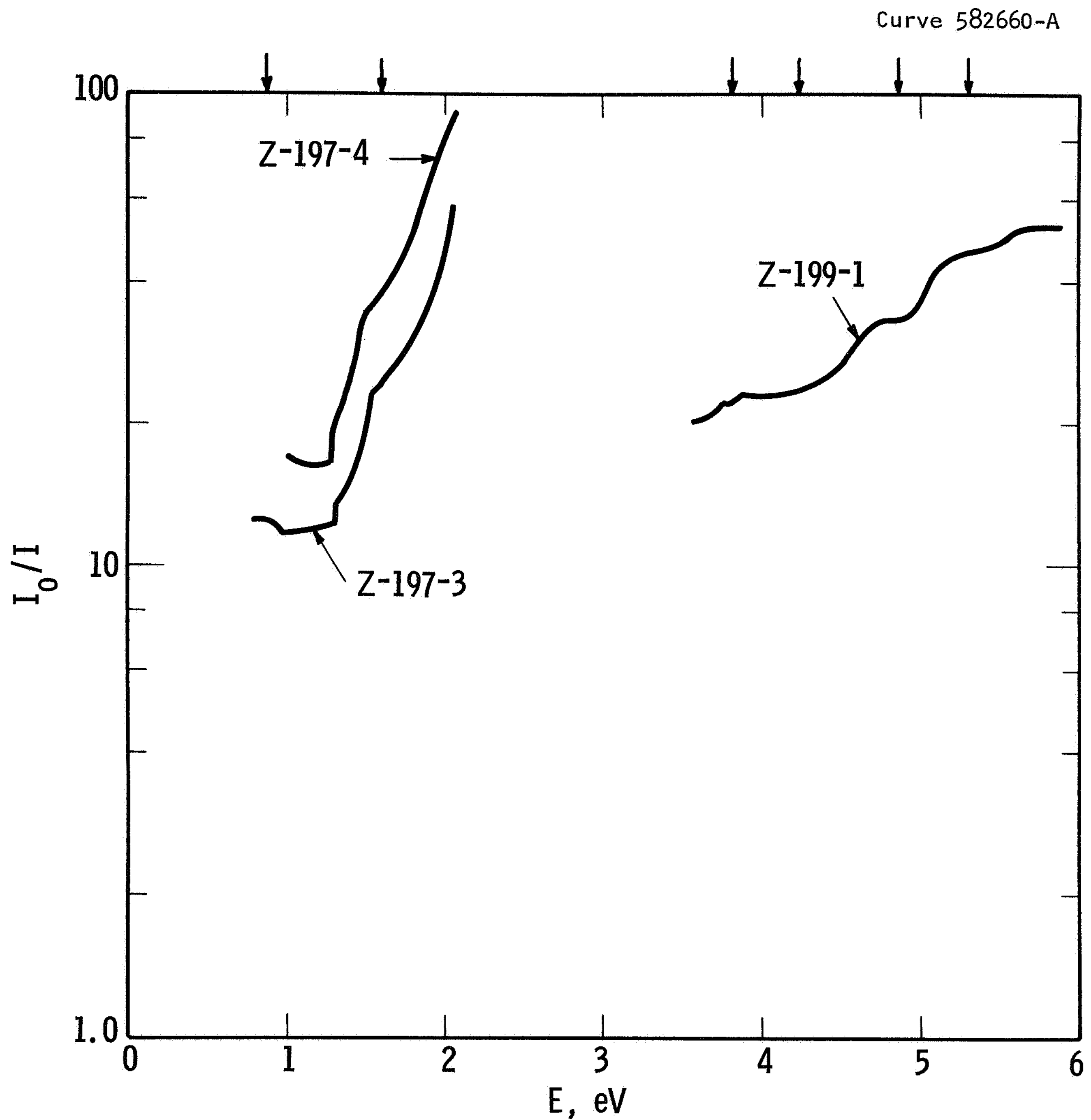

Fig. 4—Absorption spectra of AlSb films (significant structural features found by reflectance spectra are indicated by the arrows, including the band-gap value of 1.6 eV. Samples Z-197-3 and Z-199-1 are on CaF_2 Z-197-4 is on sapphire)

The single feature most prominent in the several regions of the spectra is that the several peaks observable at energies greater than the 1.6 eV absorption edge are all at energies less by about 0.1 eV than those tabulated from reflectance measurements on single crystals. This difference could be due in part to the difference in absorption versus reflection measurements and also, in part, due to the effects of impurities and structural disorder on the band structure of the material (Ref. 16). The absorption at energies just below the fundamental 1.6 eV edge also show added components which are due to states within the forbidden gap.

When AlSb films were allowed to age, they soon became visibly darker and more opaque. In this state, some were re-measured. A typical observation was that made on sample Z-197-4, the original absorption spectrum of which is given in Fig. 4. After several months storage in a nitrogen box, the spectrum was similar but a 1% transmission screen was required in the reference compartment of the spectrophotometer. Thus, a reduction in transmission to ∿1% of the earlier value had occurred.

2.1.4 Chemical Stability - As shown by the change in optical properties referred to above, the AlSb films, even when grown at thicknesses up to several microns, are highly unstable; Sorokin (Ref. 9) reports notable changes in resistivity and photoconductivity on removal from the vacuum chamber. Efforts were made to determine the character of the chemical and structural changes involved but these met with limited success.

Glancing angle X-ray diffraction patterns were obtained from films prepared on cleaved CaF_2 and on vitreous silica substrates at times varying from a few hours to several weeks after the samples had

been prepared. The results obtained differed widely and showed that complete structural degradation could occur in times varying from about three days to two weeks depending upon the substrate material and growth temperature used. The effect observed involved the transformation from a well-crystallized single AlSb phase to an amorphous product which could not be identified by X-ray diffraction. Low temperature annealing at 250°C of the amorphous films in an argon (1% H_2) ambient caused severe peeling and resulted in the development of a crystalline Sb phase, some amorphous material still remaining. It was concluded that this amorphous component was probably an anhydrous, or possibly hydrated, oxide of Al.

The wide differences found in the rate at which the film structures deteriorated may be attributed to differences in the morphology of the films. In general, those deposits prepared at higher temperatures were more granular and rougher and showed a tendency to degenerate more rapidly due presumably to their larger effective surface area.

2.1.5 Electrical Studies - AlSb film samples co-evaporated at a temperature of 600°C, a nominal Sb:Al flux ratio of 5:1, and a total deposition rate of 300 A/min onto vitreous silica substrates carrying metal film electrodes were used to investigate some electrical properties. Initially, measurements were made under vacuum on a film, 4 microns thick, deposited on sputtered Ta stripes. Resistances measured between stripes were very high, $> 10^{10}$ ohms, and showed a small and unsystematic dependence on temperature. It appeared that the high resistance was probably due to a barrier layer at the Ta/AlSb contact.

Curve 583675-A

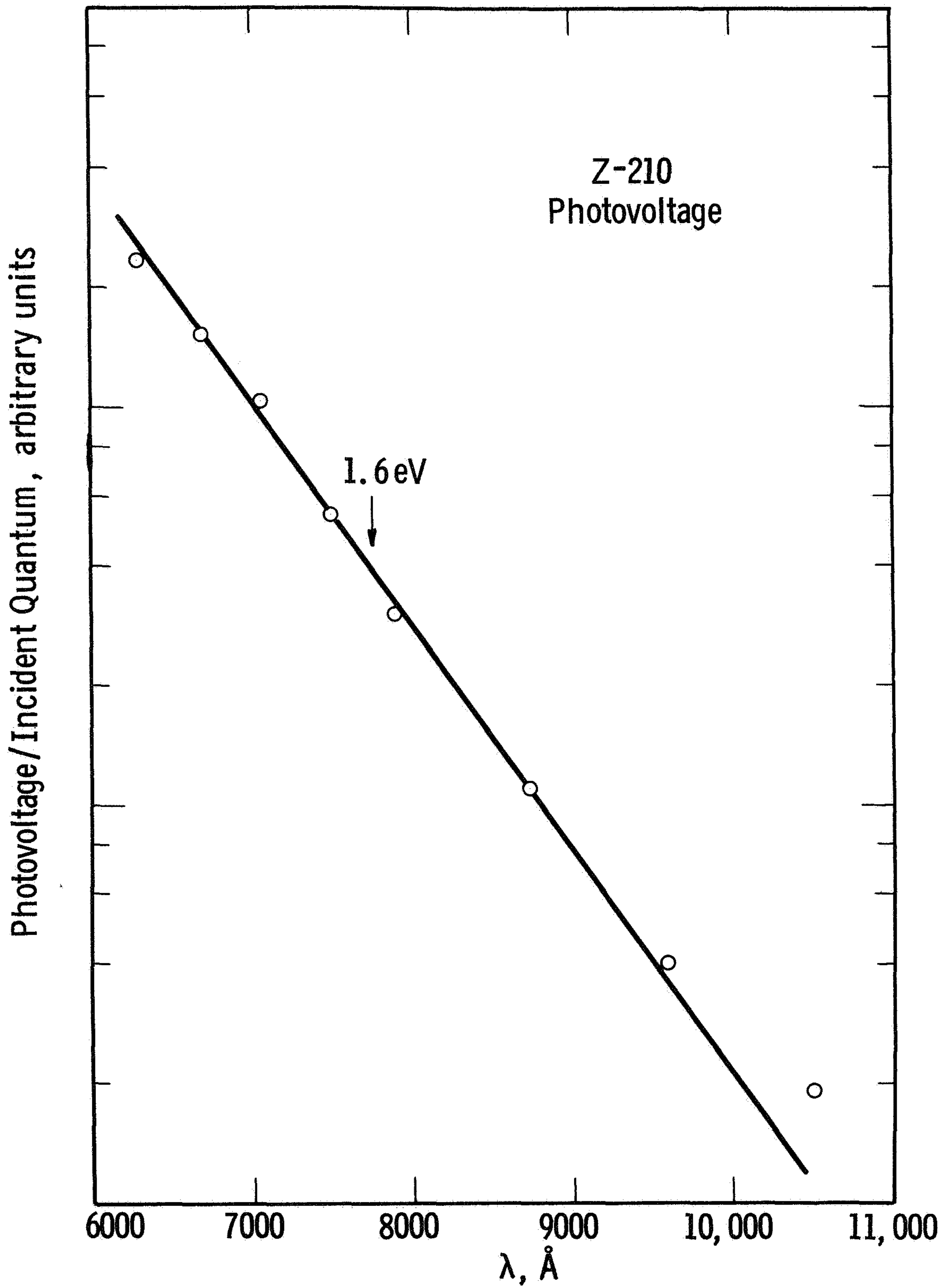

Fig. 5—Spectral variation of photovoltaic effect in AlSb film evaporated on Ta contacts

This hypothesis was confirmed when it was found that a photovoltage of several millivolts (open circuit) could be developed by shining a microscope illuminator on the sample. The strongest photoresponse came when the light was shone onto the AlSb directly over one of the electrodes.

The light energy dependence of the photovoltaic effect was determined by placing the sample in the beam from a monochromator, and measuring the short-circuit photocurrent, of the order of 10 pico amperes, with a Keithley 153 millimicroammeter. The intensity of illumination of the sample varied with wavelength as a quartz-iodine tungsten light source operated at constant voltage was used to illuminate the monochromator entrance slit. The relative energy of the beam as a function of wavelength was determined with a thermopile detector.

In Fig. 5, the relative photoresponse per incident quantum is plotted against the wavelength of the light and a reasonably linear correlation is seen, similar to that found by Abraham (Ref.17).

Mead and Spitzer (Ref.18) have also obtained similar data using single crystals of AlSb and other semiconductors that were fitted with evaporated gold electrodes under conditions such that no impurity layer was present between the AlSb and the gold film. By plotting the square root of the photoresponse of the Au/AlSb photocell vs the light energy, Mead and Spitzer were able to determine both the indirect and the direct band-gap of AlSb. The procedure involved decomposing the $(\text{photo-response})^{1/2}$ vs energy data into a series of straight lines by a graphical procedure.

In Fig. 6, we have similarly treated our photoresponse data. The square points are the raw data. A straight line was drawn through the points at lowest energy. Then, the $(\text{photoresponse})^{1/2}$ value of this extrapolated straight line was subtracted at each energy from the raw data points. The result is the sequence of circular points, which show another straight line behavior that extrapolates to zero at $h\nu = 1.6$ eV, the indirect edge of AlSb.

It is interesting to note also that the present low energy data extrapolate to zero at 1.03 eV while the low energy data of Mead and Spitzer extrapolate to zero at 0.90 eV. The difference, 0.13 eV, is in excellent agreement with the difference between the "recommended values" for the work functions of Au, 4.3 eV, and Ta, 4.12 eV which is 0.18 eV (Ref. 19). The implication of this result is that a metal-semiconductor contact of high quality has been obtained comparable to those obtained by the sophisticated cleavage technique of Mead and Spitzer.

The measurements described above, however, do not provide information on the electrical resistivity of the AlSb film itself since the metal-semiconductor barrier dominates the measurements. When the Ta stripes were over-coated with Ni, reasonable ohmic contact to the AlSb film was obtained. During growth of the AlSb film (to a thickness of 1 micron), the resistance decreased in a manner suggesting that bulk-type behavior (i.e. an absence of size effects) was obtained after the first 1500 A was deposited.

It was found that quite reproducible resistance-temperature behavior was obtained as a given film was cycled in vacuum over the range from the deposition temperature 600°C to ∿30°C, as shown in

Curve 583676-B

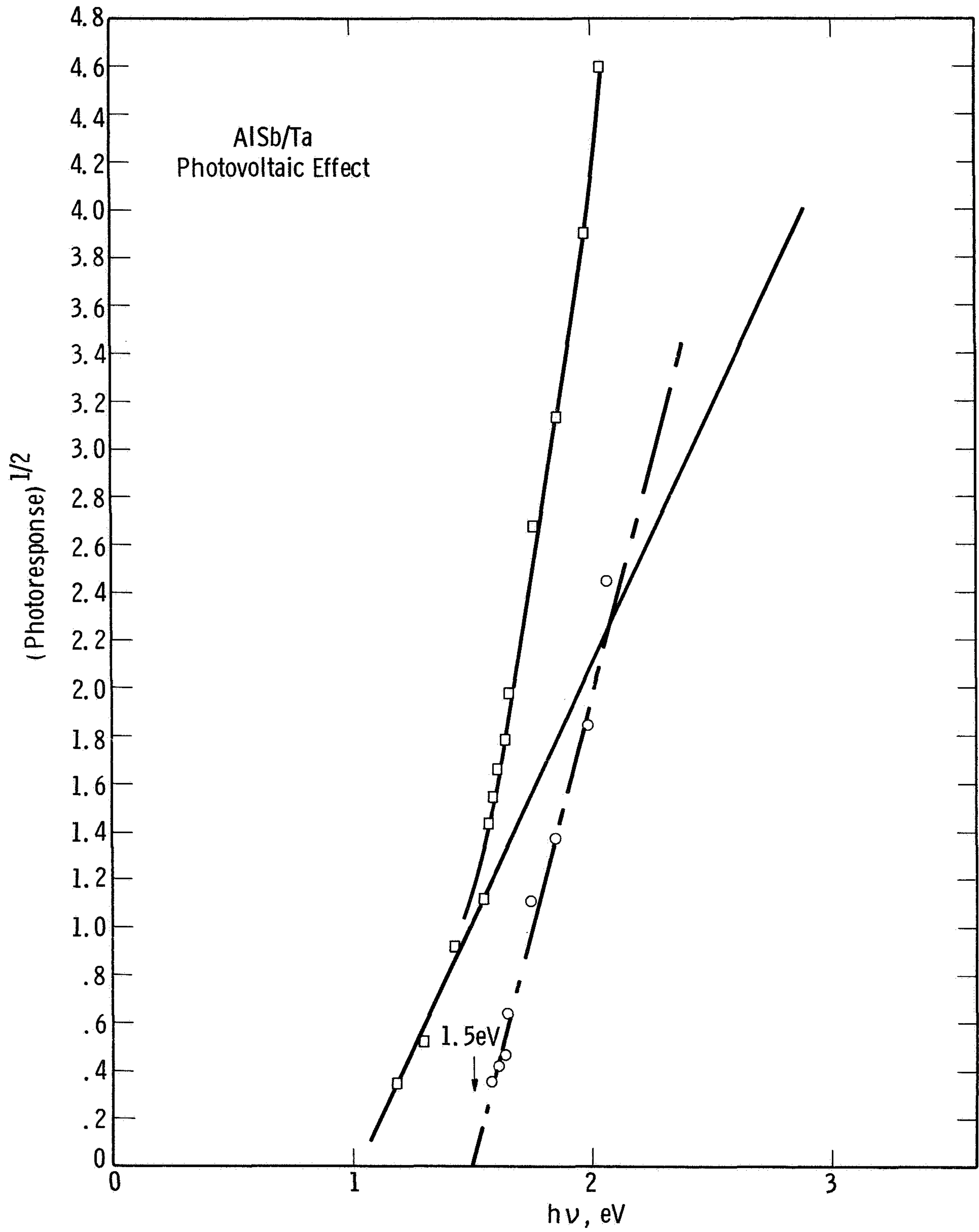

Fig. 6—Spectral variation of photoresponse from AlSb film

Fig. 7. Over this temperature range, the film resistivity varied from about 2×10^5 ohm-cm at 30°C to 50 ohm-cm at 600°C.

Data from two runs are plotted in Fig. 7. It can be seen that for each film the data lie on two linear segments with a transition at about 300°C. The activation energies derivable from these data are not the same for the two films although the high temperature range is dominated for each film by a level at near mid-gap, 0.8 eV.

At lower temperatures, values of 0.23 and 0.32 eV were found. It is not clear why these low temperature values differ but it is conceivable that the difference is mainly a matter of the stoichiometry achieved in the film deposition, since Kover (Ref. 20) has attributed a donor level at 0.3 eV to Sb vacancies. It should be noted that Shaw and McKell (Ref. 21) have reported a level at 0.8 eV in high resistivity single crystals.

The resistivity of a semiconductor can be expressed as

$$\rho = \frac{1}{ne\mu_n + pe\mu_p} \tag{1}$$

where n and p are the electron and hole concentrations and μ_n and μ_p are their respective mobilities, while e is the electronic charge. The concentrations, n and p, can in turn be expressed as

$$n = N_c \exp(-E_{fn}/kT) \tag{2}$$

and

$$p = N_v \exp(-E_{fp}/kT) \tag{3}$$

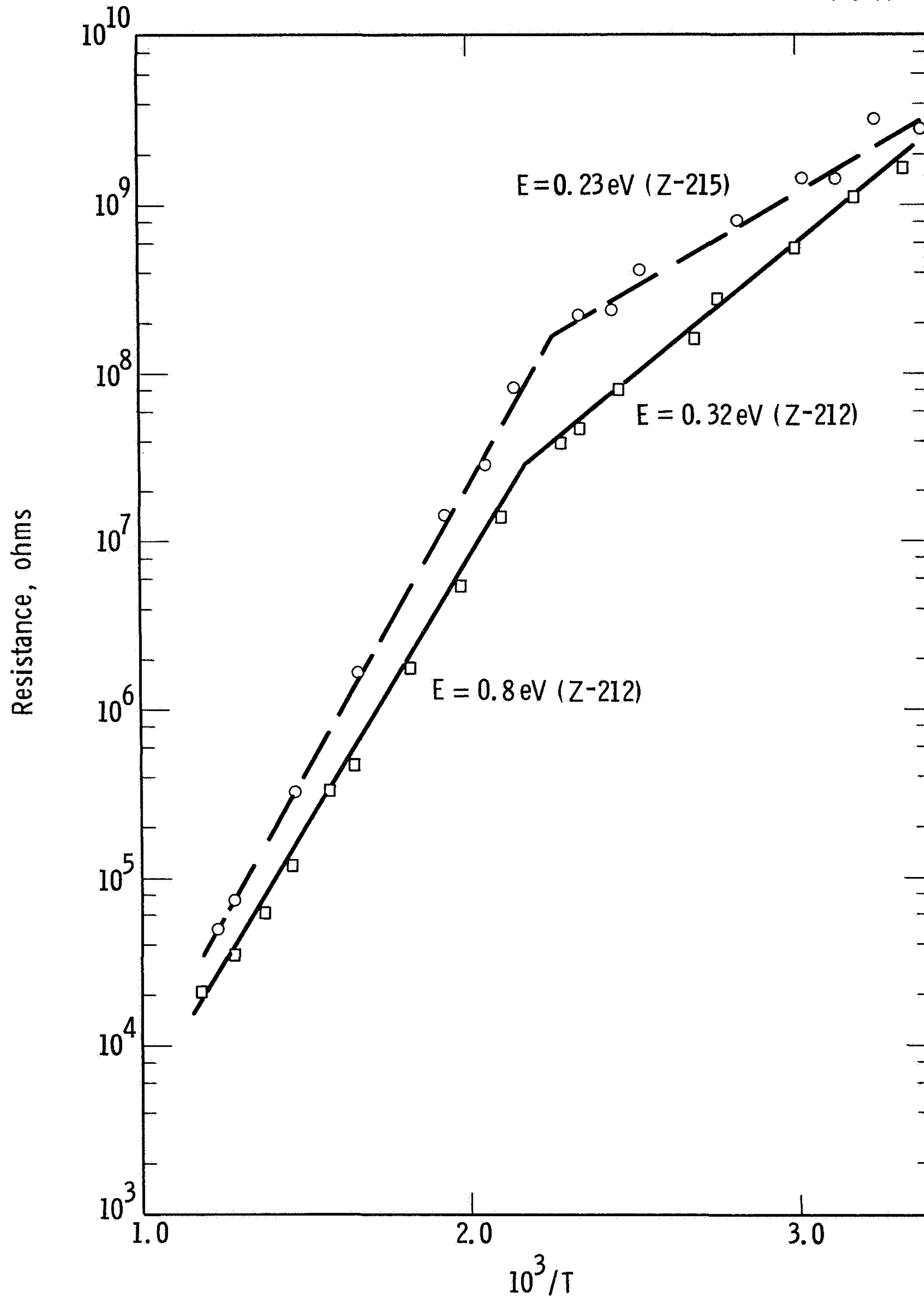

Fig. 7—Temperature dependence of resistance measured in Situ on AlSb films deposited at 600°C; (Z-212) thickness 1μ, (Z-215) thickness 2μ

where N_c and N_v are the conduction and valence band densities of states. The sum of the electron and hole Fermi energies, E_{fn} and E_{fp} are equal to the value of the energy gap, E_g (= 1.6 eV) when the sample is at thermal equilibrium.

From Eqs. (1), (2), and (3) it can be deduced that the resistivities at two temperatures should be in the ratio

$$\frac{\rho_{T_2}}{\rho_{T_1}} = \frac{n_{T_1} e\mu_{T_1}}{n_{T_2} e\mu_{T_2}} = \frac{\mu_{T_1}}{\mu_{T_2}} \left[\frac{\exp\left(-E_{fn}^{T_1}/kT_1\right)}{\exp\left(-E_{fn}^{T_2}/kT_2\right)} \right] \tag{4}$$

if only one carrier dominates the conductivity at a given temperature.

If an attempt is made to compute the resistivity ratio from Eq. (4), the result is comparable to experiment only if the mobility ratio is given an impossibly large value, with the 0.8 eV portion of the curve having the larger μ. Small values of the ratio could be explained by a variety of phenomena but the ratio seems much too large if it is assumed, for example, that conduction occurs by both holes and electrons at higher temperatures and by electrons alone at lower temperatures.

It therefore appears that the data of Fig. 7 do not represent a "bulk" property of AlSb films. Explanation of the data probably lies in a "barrier" phenomenon, but it is not clear just what kind of barrier is involved. The governing phenomenon may be intergranular contacts, micro-cracks, or metal-semiconductor barriers.

2.2 Aluminum Antimonide - Reactively Sputtered

The preparation of AlSb by an alternate technique, viz., reactive sputtering was also achieved during the course of the present studies. Essentially the method is similar to that described for AlN in Sec. 3.1.1, the Al substrate, substrate holders, experimental chamber and conditions for deposition being virtually identical. The scheme differs only in the means of injecting the group V element, in this case Sb, into the discharge in a gaseous or vapor form.

2.2.1 Preparation - An Al cathode designed to hold a number of solid Sb pieces was fabricated, as shown in Fig. 8. It was expected that the heat generated in the cathode by the discharge would provide a sufficient vapor pressure of Sb. A thermocouple was installed to monitor the temperature of the cathode during sputtering. With operating conditions approximating those of the AlN experiments, an equilibrium cathode temperature of 435°C was reached. The corresponding Sb vapor pressure was 10^{-4} torr, which should provide an arrival rate of Sb at the substrate surface of approximately 750 A/min.

Films were deposited on CaF_2 (111) substrates heated in the range 400 to 700°C; the temperature was confined to this range to prevent both condensation of excess Sb and thermal etching of substrates. Thicknesses of deposited films indicated growth rates of less than 50 A/min. This relatively slow rate together with the blackened appearance of the cathode surface implied that an Al-Sb reaction had occurred at the cathode surface, and that subsequent sputtering of the compound was impeded by the high resistivity of the layer.

Dwg. 854A621

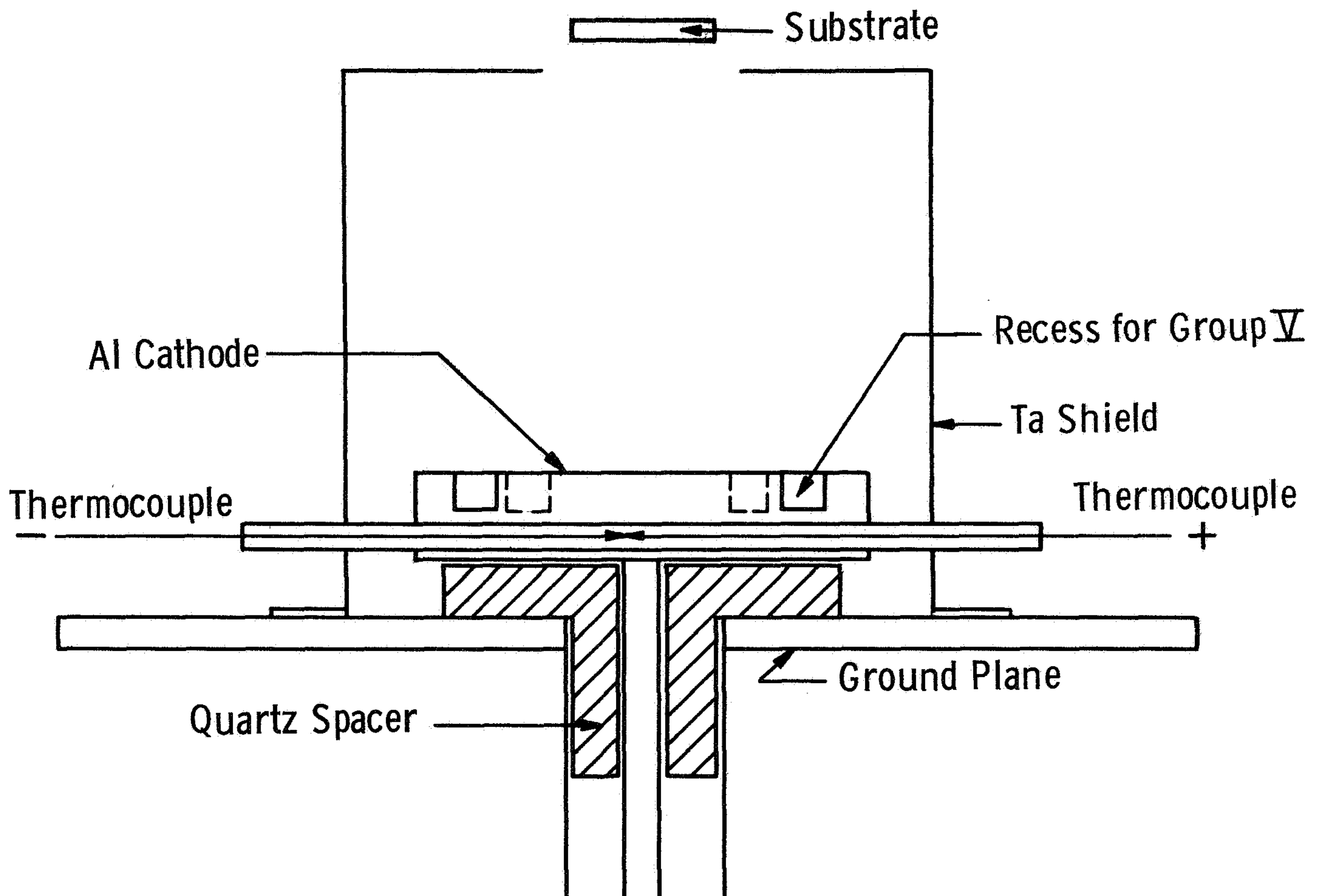

Fig. 8—Schematic of arrangement for diode reactive sputtering of AlSb films; recesses in cathode contain the Group V element (Sb)

In an effort to confine the reaction between the Sb vapor and Al to the substrate surface the arrangement was modified so that the Sb was supplied from a source external to the system (Fig. 9). During the bake-out cycle this source was kept cool by interposing a water-cooled flange between it and the main chamber. The films obtained by this method were Al-rich due apparently to insufficient transport of Sb from the external source.

2.2.2 Structural and Optical Properties

Transmission electron diffraction patterns obtained for films sputtered via the scheme illustrated in Fig. 8 are shown in Fig. 10. Deposits on (111) CaF_2 surfaces at 400°C show polycrystalline ring patterns. Films deposited on substrates at 650°C were highly oriented. The orientation relationship between the high temperature deposits and the substrate are as follows:

$$(111)_{AlSb} \,//\, (111)_{CaF_2},$$

$$[1\bar{1}0]_{AlSb} \,//\, [1\bar{1}0]_{CaF_2}.$$

Data from the absorption spectra of deposited films indicate band-gap values corresponding to measured values for bulk AlSb, viz. 1.55 to 1.6 eV. However, the very thin nature of the films made it difficult to obtain detail in the spectra.

2.3 Aluminum Arsenide (AlAs)

2.3.1 Preparation - In earlier temperature calibration experiments performed with the three-temperature evaporation system used for the

Dwg. 855A037

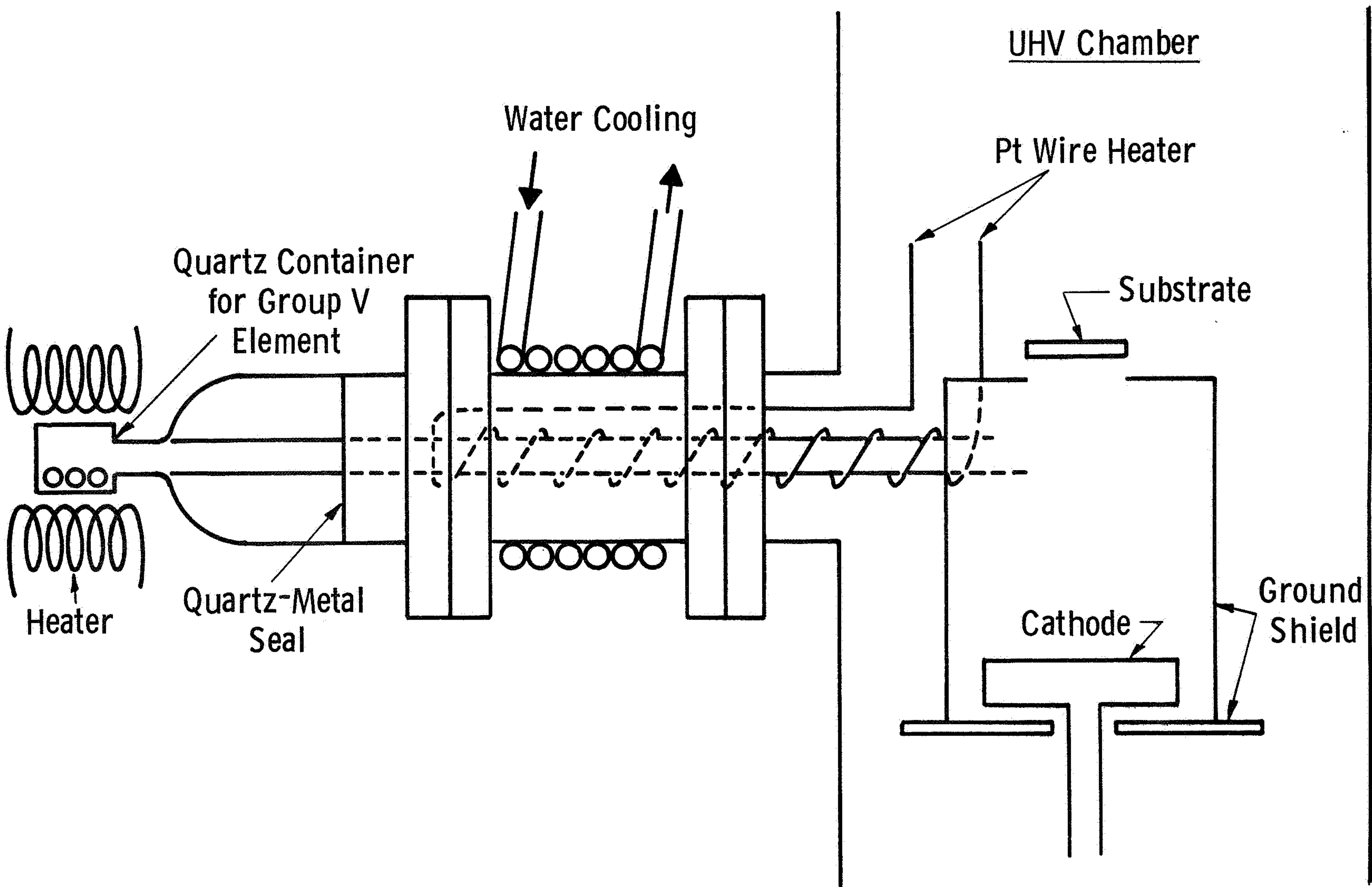

Fig. 9—Schematic of alternate sputtering system with external Sb source

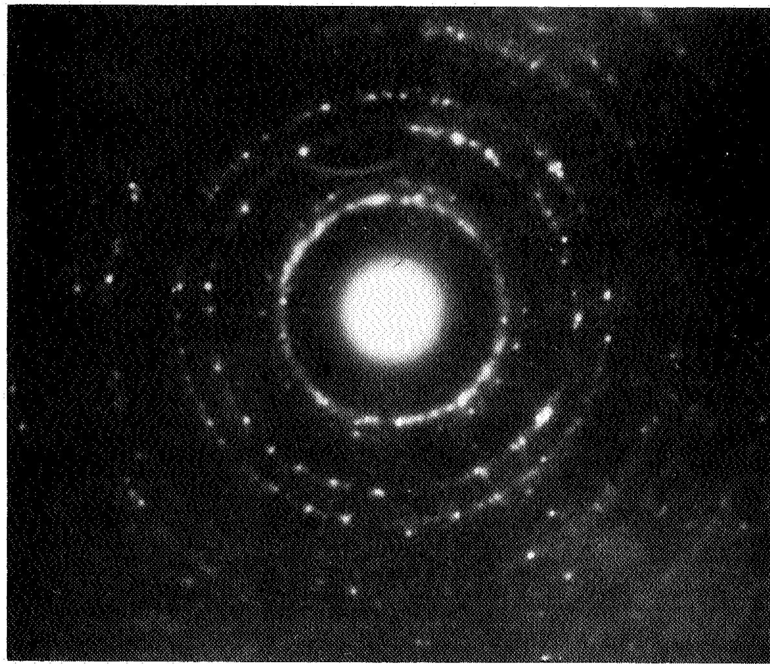

(a)

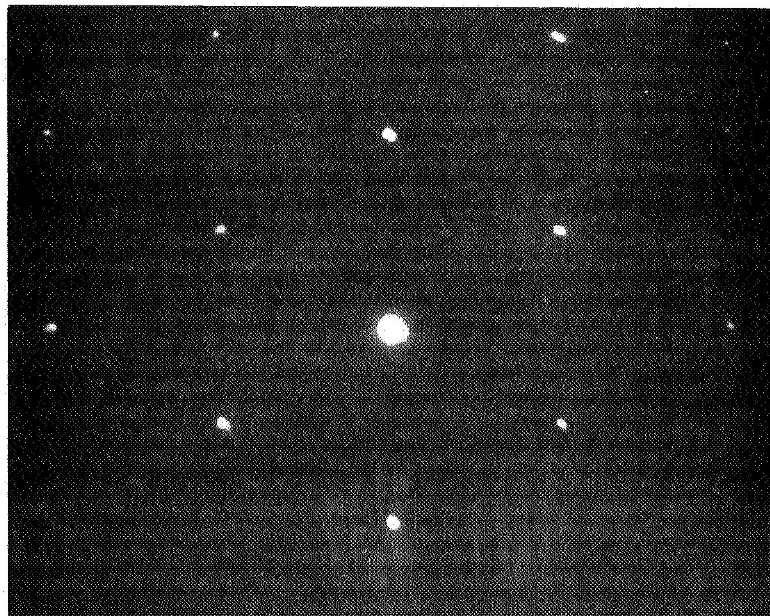

(b)

Fig. 10—Transmission electron diffraction patterns from sputtered AlSb films deposited on cleaved CaF_2 at (a) 400°C, approximate thickness 1500A and (b) 650°C, approximate thickness 1000A

RM-40681

preparation of AlSb films, it was found that when both the Al source and the substrate were at temperature the Ta ring source containing the Sb could achieve temperatures, due to radiation, ranging from about 150°C to 280°C. The equilibrium vapor pressures for As at the higher temperature is 4×10^{-2} torr corresponding theoretically to an approximate deposition rate of 800 A/min. Since this value appeared to impose a rather large lower limit to the As flux, efforts were made to provide a greater degree of control by isolating the As source in a separately heated pyrex extension to the reaction chamber as shown in Fig. 11. The remaining features of the system were essentially the same as those used for the deposition of AlSb films, except that a large liquid-nitrogen cooled Meissner trap was also added to collect unreacted As.

Several experiments were carried out with the modified system using As source temperatures ranging from 200 to 380°C, substrate temperatures from 500 to 700°C, and with the Al source operating at 1150°C. At As source temperatures below about 320°C, the film products obtained were found, by X-ray analysis, to comprise a mixture of AlAs and free Al. At higher As temperatures, no deposit was obtained. Inspection of the Al source after these experiments showed it to be covered with a yellow layer of AlAs crystallites. It was concluded that this surface reaction product had prevented further evaporation of the Al despite the high operating temperature of the metal melt. This interpretation is consistent with the high temperatures reported for the decomposition of the compound (Ref. 22).

The results achieved with lower As source temperatures indicated that despite the large amount of As vaporized (the cold traps in

Dwg. 855A035

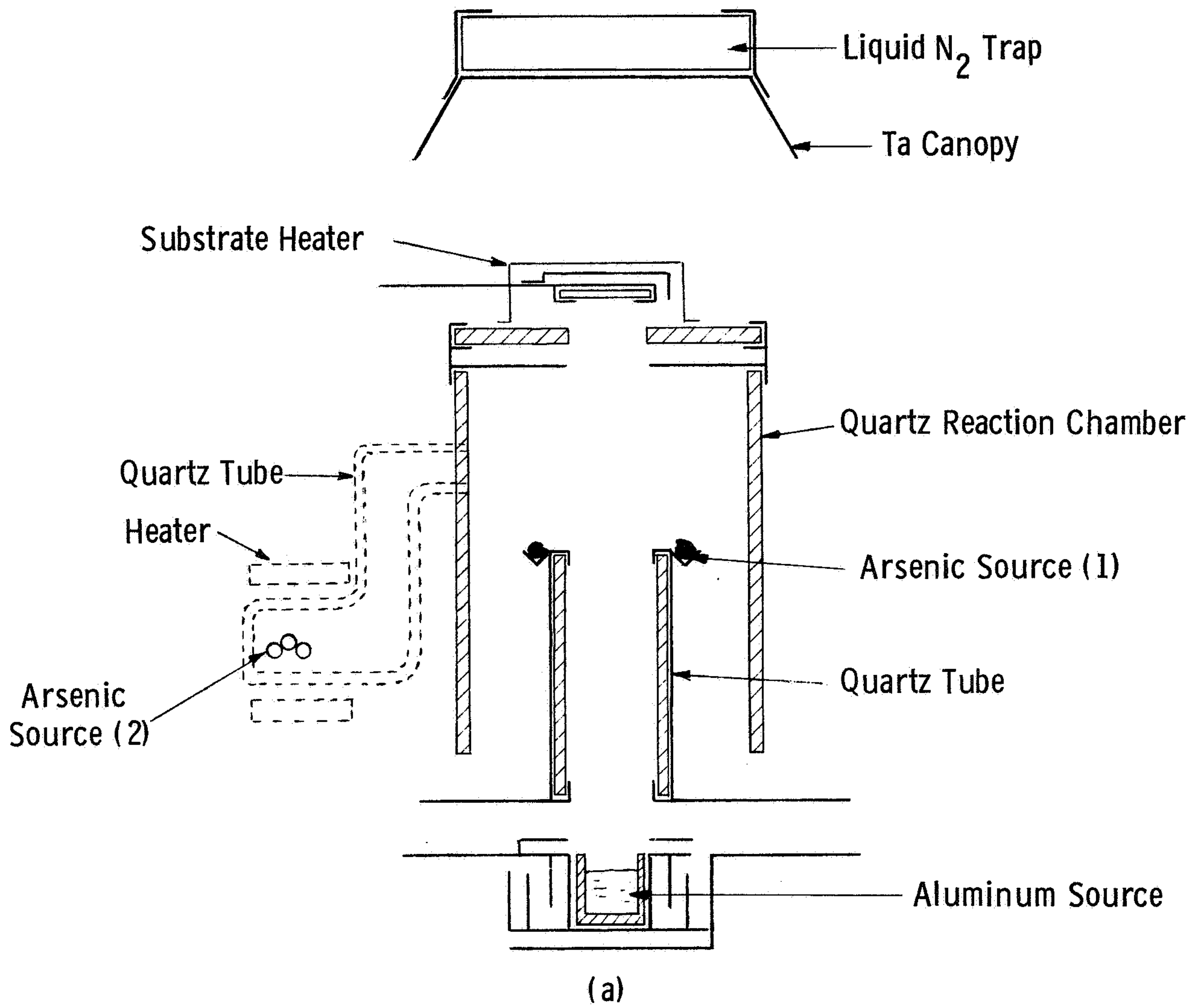

Fig.11—Modified system for co-evaporation of AlAs films

the chamber were found to be liberally coated with condensed As) transfer to the substrate surface with the arrangement shown in Fig. 11 was inefficient. It was reasoned that despite the poorer control in varying the As vaporization rate the non-equilibrium line-of-sight evaporation afforded by a Ta ring source arrangement might prove more effective. Thus, the modified system was abandoned.

With substrates held at temperatures below about 680°C, the following observations were made on varying the As (ring source) temperature. For As temperatures lower than 350°C, dark yellow opaque deposits were produced. When the As source temperature was increased above 360°C, the deposits obtained changed to a transparent yellow in appearance but were very thin. At higher As temperature (> 420°C), no visible deposit was obtained. In these runs the Al source was found to be again covered completely with a layer of yellow polycrystalline AlAs.

With substrates held at temperatures higher than 700°C, it was observed that if the Al source alone was operated, no condensation of Al occurred. Under these conditions, the deposit structure varied with the As source temperature in the following manner. When the As temperature was increased up to near 400°C, the deposition rate increased to a maximum of approximately 650 A per minute -- the film products in each case possessing the pale yellow transparent appearance characteristic of pure AlAs. For higher As temperatures, reaction at the Al melt occurred, inhibiting evaporation of the metal. Some selected results for AlAs films grown under near-optimum conditions are presented in Table III.

It is interesting to compare the conditions described here for producing stoichiometric films with those normally used for other III-V

Tabke III Summary of Selected Results for Co-evaporated AlAs Films Deposited on Vitreous Silica

Sample No.	T_S (°C)	T_{As} (°C)	Thickness (A)	Remarks*
Z-225	710	400	$\sim$ 12,000	Clear yellow film.
Z-227-2	705	399	$\sim$ 10,000	Film discolored, peeled after few hours' exposure to atmosphere.
Z-227-4	700	381	$\sim$ 12,000	Clear yellow film.
Z-231-2	750	384	< 1,000	Nominal doping of 0.1% Te. Very low deposition rate. Films metallic yellow.
Z-231-4	750	394	< 1,000	
Z-234-4	740	364	$\sim$ 20,000	Clear yellow film. Resistivity $\sim$ 70 ohm-cm.
Z-235-4	750	386	$\sim$ 20,000	Clear yellow film. Resistivity $\sim$ 250 ohm-cm.

* Glancing-angle X-ray diffraction studies indicated that those films with a clear yellow color possessed the cubic zinc blende type structure of AlAs with a strong <111> fiber texture.

compounds such as InAs or GaAs. For these compounds, the melting point and critical condensation temperature of the Group III element is lower than the lowest temperature at which the Group V element alone condenses, and the upper end of the "stoichiometric temperature interval" is defined by the decomposition temperature of the compound (Ref. 23). For the Al class III-V films, the critical condensation temperature of the metal is much higher and lies between the condensation temperature for the Group V element and the decomposition temperature of the compound. Thus, by adjusting the ratio of the Al and Group V fluxes and depositing at temperatures above 700°C, it was possible to ensure stoichiometry for each of the Al compound films.

2.3.2 Structural Properties - The films which were grown using the As ring source were examined by electron (reflection) and glancing-angle X-ray diffraction. Films grown at lowest controllable As flux were found by X-ray diffraction to comprise mainly the cubic sphalerite form of AlAs (Ref. 24) together with a minor Al phase. However, the reflection electron diffraction patterns, although confirming the composition analysis indicated by the X-ray method, showed the AlAs phase to possess a highly oriented hexagonal wurtzite structure (Fig. 12). Subsequent re-examination of the X-ray data did in fact show a weak trace of reflections consistent with the hexagonal polymorph but suggested that the amount present was probably less than 1 or 2 percent of the cubic form. In summary, such a film consisted essentially of non-oriented cubic AlAs (together with some free Al), but possessed a thin surface region in which the AlAs phase had adopted a strongly fiber-textured wurtzite-type structure.

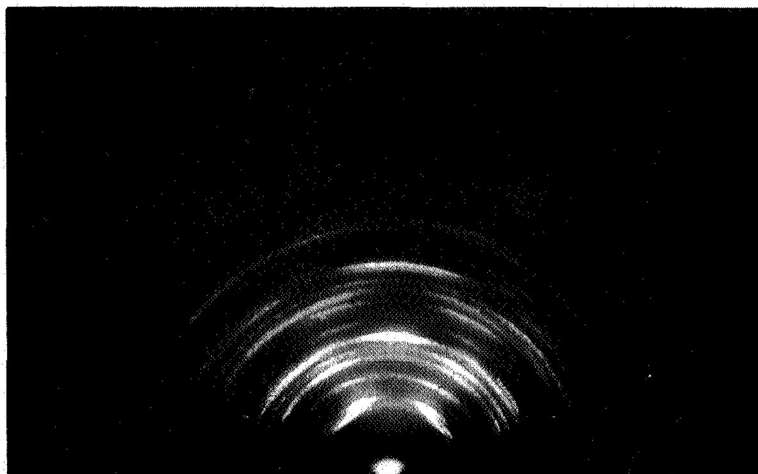

Fig. 12 -Electron diffraction pattern from evaporated aluminum-rich AlAs film showing Wurtzite structure

Films prepared at higher As flux densities and at higher substrate temperature, yielded no reflection electron diffraction patterns. X-ray diffraction, however, showed these to consist essentially of the cubic form of AlAs but with a strongly developed (111) fiber texture.

Towards the end of the structural investigations, a further AlAs film (KB59-1) grown by Dr. H. Kunig in these laboratories was submitted to us for structural and optical examination. This film has been deposited at 480°C by co-evaporation using the arrangement described previously by Johnson (Ref.10) for the preparation of AlSb films. In this system, the sources were arranged below and equi-distant from the substrate inside a thermally shielded enclosure in an effort to approach more closely equilibrium growth conditions at the substrate. The film comprised a poorly-crystallized, non-oriented, cubic AlAs phase but was appreciably thinner (∿ 1500 Å) than the nominal thickness (∿ 6000 Å) anticipated from the experimental conditions. In view of the fact that the Al source was observed to be covered extensively with a yellow layer of AlAs at the end of the run, it appears likely that the evaporation of Al was impeded or, more probably, stopped entirely before the experiment was completed.

2.3.3 Optical Studies and Chemical Stability - The optical absorption of several AlAs films was measured. Al-rich films were nearly opaque to visible light, and showed absorption thresholds at about one micron. The spectra of three later films, which were yellow to the eye, are shown in Fig. 13. Absorption features at the anticipated values of 2.1 eV (indirect edge) (Ref. 18) and 2.9 eV (direct edge)(Ref. 18) are clearly present.

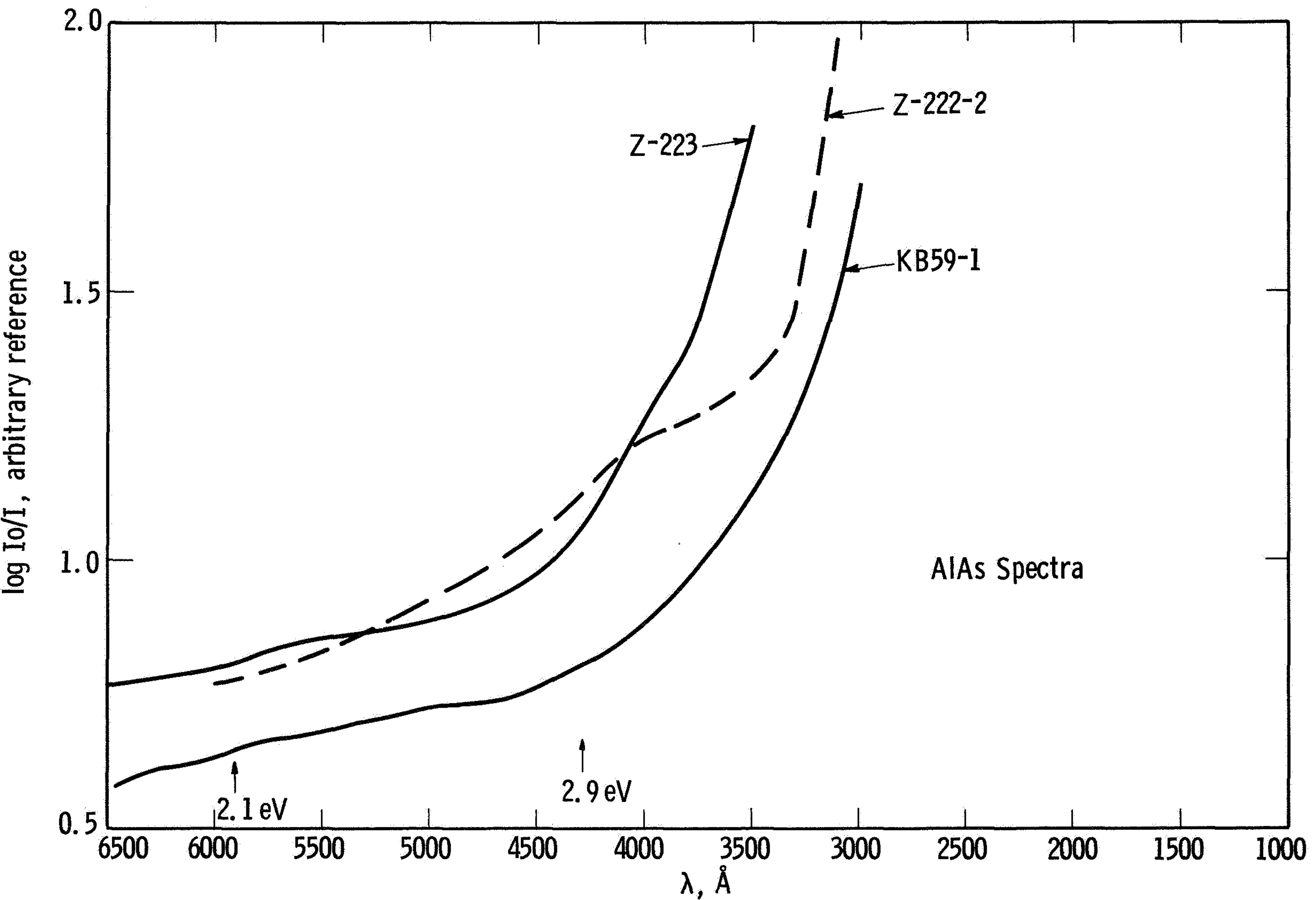

Fig. 13—Absorption spectra from evaporated AlAs films, (Z-222-2) 650°C, thickness 6000 Å, (Z-223) 750°C, thickness 3000 Å, (KB59-1) 480°C, thickness 1500 Å

The low temperature film KB59-1 seems to have a less developed set of absorption edges.

Measurements were made periodically to assess possible deterioration effects. One film stored in a dessicator between measurements, was measured each week for several weeks. An increase of the optical transmission of about 10% per week was observed. This is an opposite trend to that shown by the AlSb films.

A film of AlAs deposited onto a silica substrate previously coated with a set of Ta stripes and coated with MgF_2 in an attempt to protect the AlAs was examined electrically. The resistance from stripe to stripe was $\sim 10^9\ \Omega$ just after deposition and $> 10^{10}\ \Omega$ three days later, after storage in a N_2 flushed box. No photovoltaic or photoconductive effect could be observed in this film at this time, although a small photovoltaic effect had been observed three days earlier.

2.3.4 Electrical Studies - Resistivity measurements were made on film Z-234-4 referred to in Table III. To minimize chemical decomposition, this film was transferred rapidly from the evaporator to a vacuum system used for electrical measurements. A resistance vs $\frac{1}{T}$ plot (Fig. 14) was made for the range -190°C to 600°C and was found to be completely reversible. The log R vs. $\frac{1}{T}$ plot, however, was not linear suggesting that conductivity was dominated by a spread of shallow impurity levels which could not be characterized by a single activation energy. Similar results were later obtained on film Z-235-4 which was fitted with electrodes in a Hall bar configuration. This film was found to be p-type with a low mobility value in the range 0.5 cm^2/volt-sec. and an estimated carrier concentration of 10^{17} carriers/cm^3(measured at room temperature).

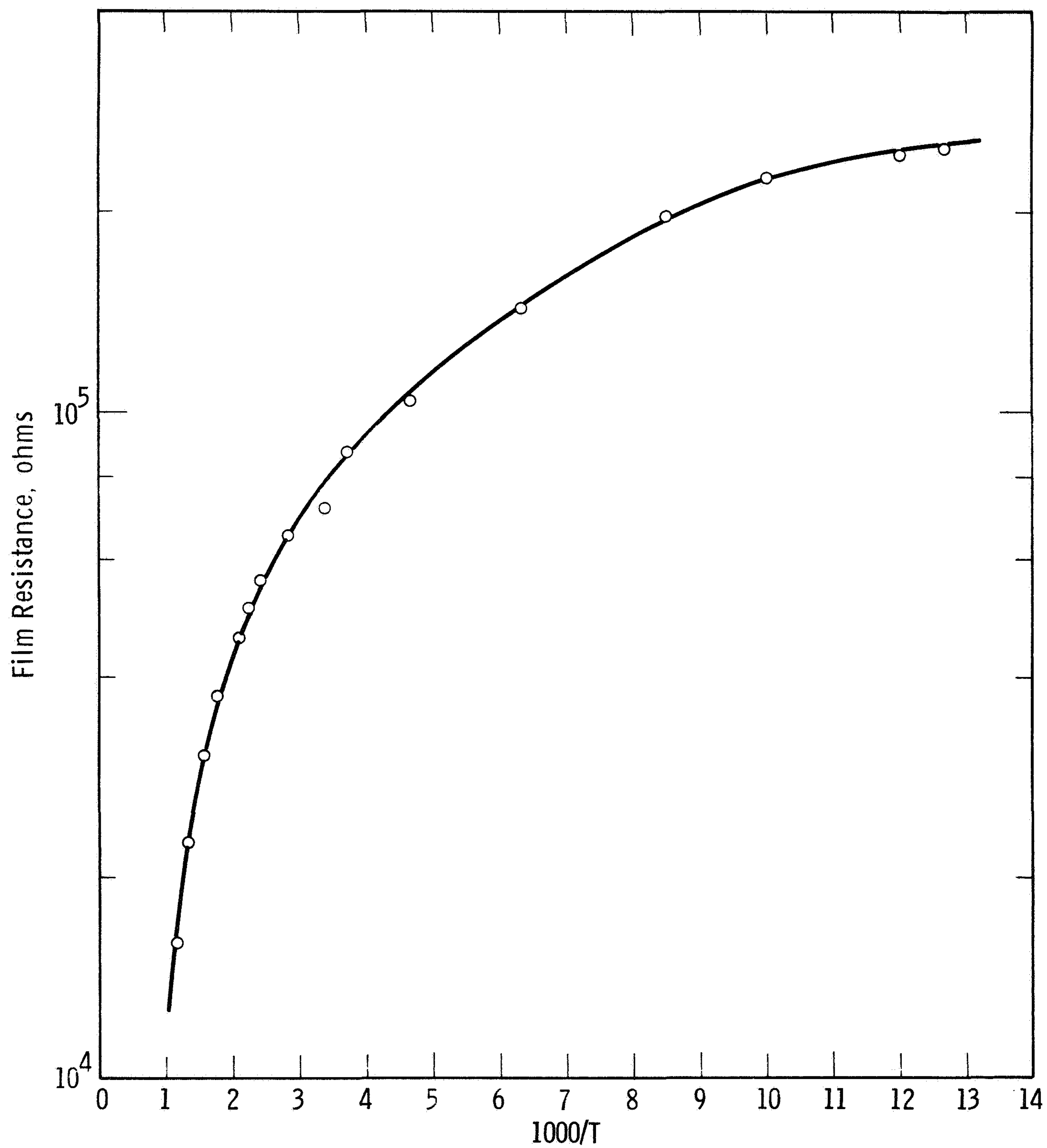

Fig. 14—Temperature dependence of resistance measured on AlAs film (Z-234) deposited at 720°C, thickness 2 microns

An attempt was made to observe thermally stimulated current behavior in Z-234-4 by irradiating it when cold (at -190°C with a 100 watt mercury vapor lamp) and then monitoring its dark resistance as the temperature was raised at a constant rate of about 2°C per minute. No TSC effects were observed, which was perhaps not surprising in view of the relatively low resistivity and presumably high carrier concentration of the film material.

Two AlAs film samples were prepared with nominal Te doping levels (based on the vapor pressure data for As and Te) of 0.1%. Actual conditions realized during growth, however, caused Te enrichment above this normal concentration due to a rise in the temperature of the Group V element source. Also, rather low deposition rates were obtained in these experiments, so that the approximate thicknesses of the films were only of the order of 1000 A. A resistance vs $\frac{1}{T}$ plot was made for one of these films, Z-231-2, in the temperature range from 25 to 450°C. An anomalous and irreversible drop in resistance occurred in the range above 200°C, evidently caused by major structural changes in the film, or by chemical decomposition.

2.4 Aluminum Phosphide (AlP)

2.4.1 Preparation - In the time set aside for the evaporation phase of the experimental study, it was possible to undertake only one attempt at synthesizing AlP in thin film form. Source and substrate conditions were adjusted so as to match approximately those which had proved successful in the preparation of AlAs films, i.e. with a nominal P/Al flux ratio of about 5 to 1, and with a substrate temperature of about 720°C. The

silica substrate was coated with Ta-stripe electrodes in a Hall bar configuration leaving the central area of the substrate uncovered to permit optical absorption studies.

At the completion of the run, which lasted 30 minutes, a transparent yellow deposit was visible both on the silica substrate and on those areas of the bell jar wall which had been exposed directly to the aluminum source. On admitting air to the chamber and raising the jar, a strong smell of phosphine (Ref. 2) developed. The chamber was closed again and evacuated immediately to avoid further reaction.

To extract the film sample safely from the vacuum system and to preserve it for subsequent measurement, a special handling procedure was employed. The entire bell jar was encased with a polythene bag large enough to extend to the base plate with the jar in the raised position. A plastic ampoule and a pair of forceps were enclosed inside the bag. Pure argon was bled into the chamber until it reached atmospheric pressure, whereupon the jar was raised and the forceps used (through the flexible polythene wall) to transfer the film to the ampoule. After the ampoule had been removed via a slit in the polythene wall, moist air was flushed through the chamber and into an exhaust system for several hours, until no further odor of phosphine could be detected with the jar open.

2.4.2 Structural, Optical and Electrical Studies - A rapid transfer from bell jar to the electron microscope was effected to limit possible deterioration. Examination via reflection electron diffraction confirmed the presence of AlP in its bulk sphalerite form, Fig. 15. The diffraction pattern also showed the film to possess a weak (110) fiber texture.

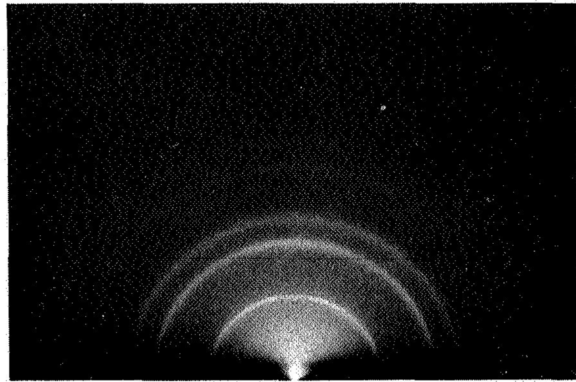

Fig. 15 —Electron diffraction pattern of AlP film deposited on silica at 720°C

RM-43692

To perform electrical resistivity studies the film was inserted into a second vacuum system and fitted with probes, precautions being taken to keep the film immersed completely in alcohol while the contacts were being adjusted. Similar precautions were observed while performing optical studies, the film being held in a large spectrophotometer cell filled with ethyl alcohol. Attempts were also made to measure the Hall effect with the film mounted in a tube containing flowing dry nitrogen.

The film resistivity, measured at room temperature by the four probe method via the Ta electrodes, was estimated to be 50 ohm-cm. Figure 16 shows the variation of film resistance with temperature between -180° and 600°C. The observed variation suggests that the conductivity is influenced by a spread of shallow impurity levels with activation energies ranging approximately between 0.04 and 0.15 eV. Attempts to determine the mobility for this film were unsuccessful, since the Hall voltage, for the small values of current which could be passed through the sample, was too low to be measured reliably.

Optical absorption was measured with the film immersed in ethyl alcohol. Figure 17 shows the spectrum obtained, together with a trace of the absorption of the spectrophotometer cell (containing alcohol) without the film. The absorption is seen to rise steadily at wavelengths less than 5000 A, as would be expected for a material with a 2.45 eV band gap (Ref. 25). Also evident is a set of interference fringes which, using the value 3.4 for the refractive index of AlP (Ref. 24), show the film to be 9100 A thick.

Curve 584732-A

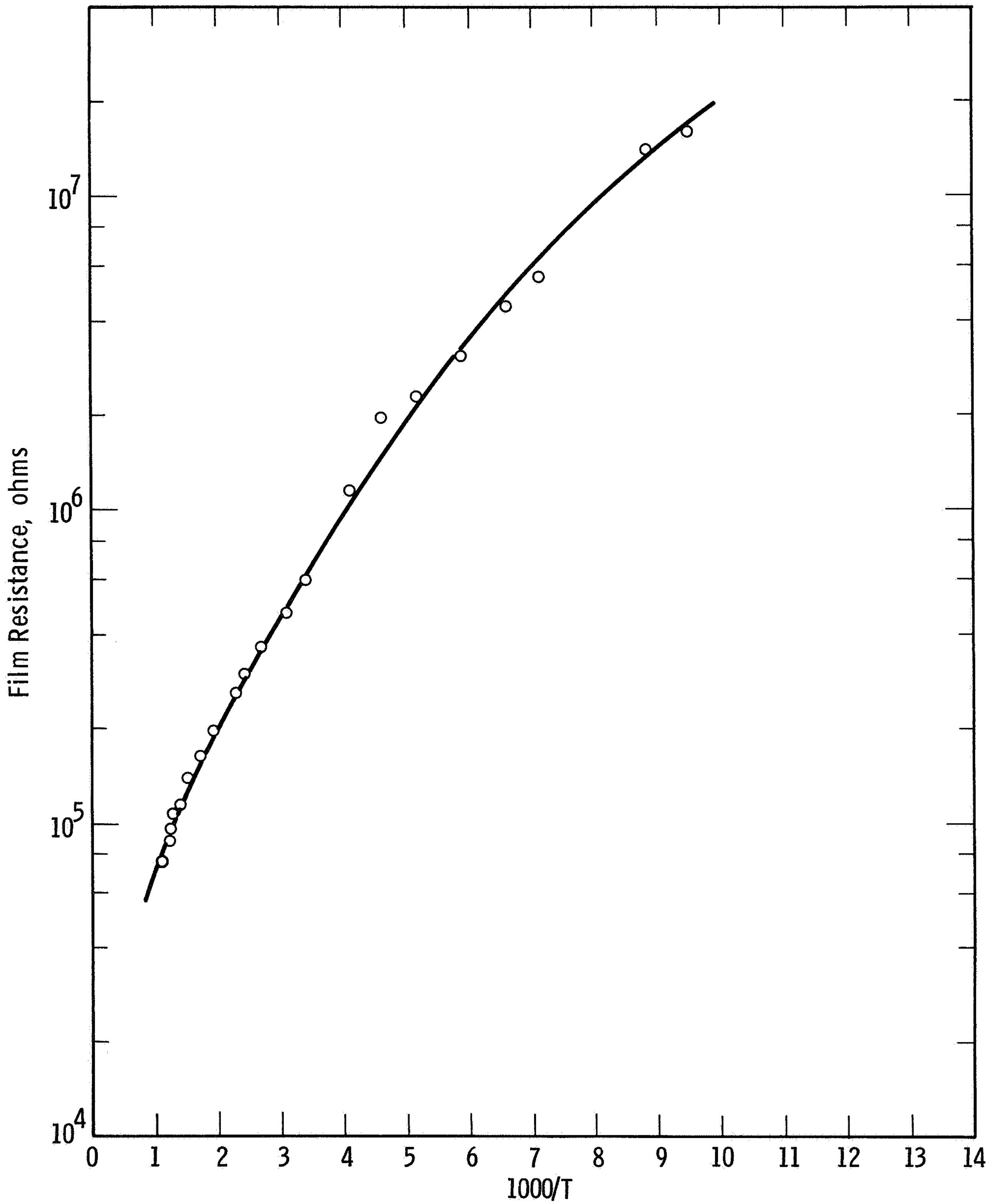

Fig. 16—Temperature dependence of resistance measured on AlP film (Z-237) deposited at 720°C, thickness 9100 Å

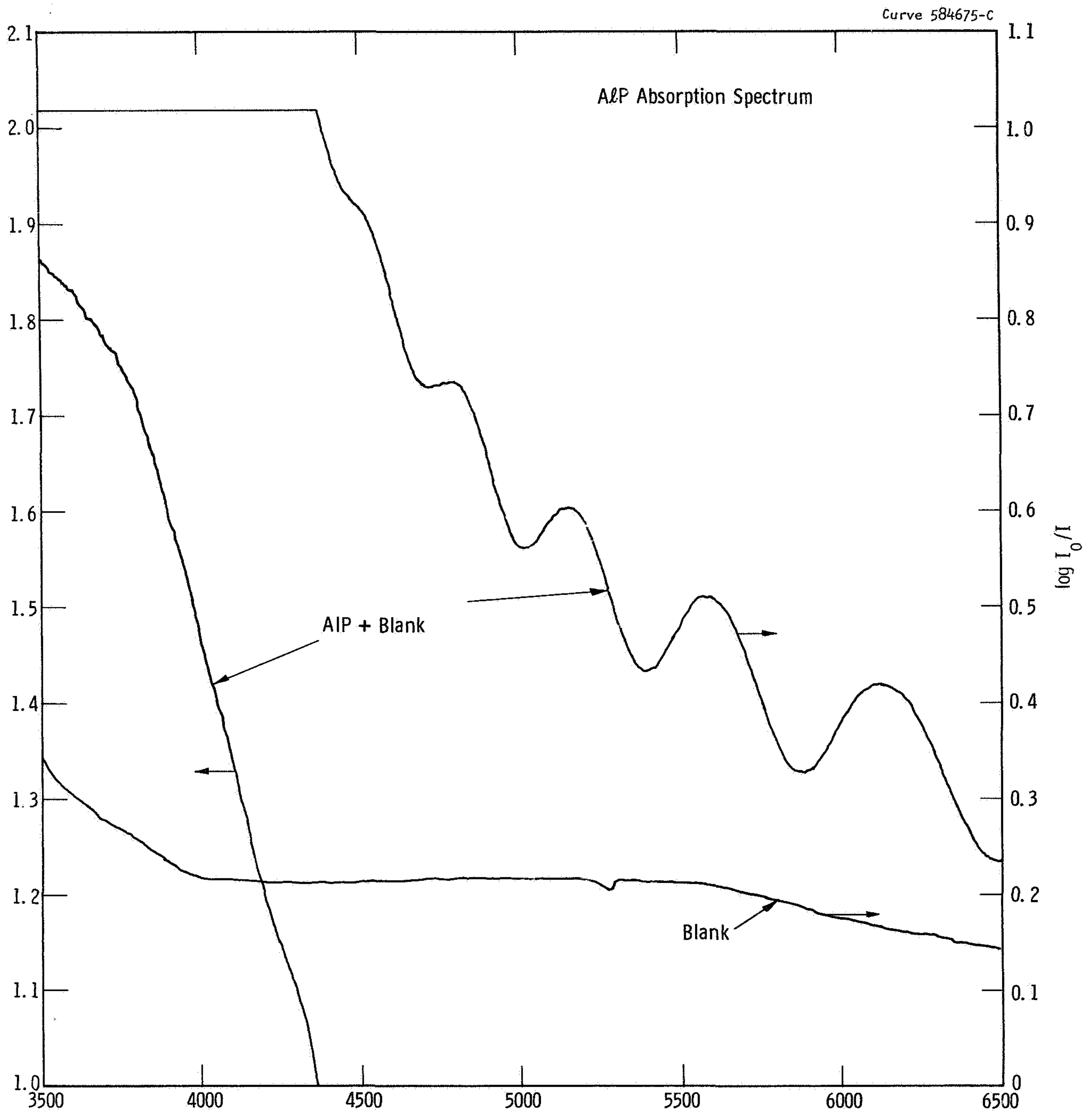

Fig. 17—Absorption spectrum of AℓP film, obtained with sample immersed in ethyl alcohol. (Absorption of cell and alcohol shown as "blank")

2.5 Discussion

The results reported in the preceding sections indicate that the reactive evaporation technique is not only well suited to the preparation of films of AlSb, in confirmation of other published data, but may also be used for the growth of AlAs and AlP films. Successful preparation of stoichiometric films of the latter compounds, achieved for the first time by this method, appears favored by using conditions such that the substrate temperature exceeds the critical condensation temperatures both of the Group V elements and of aluminum, and by maintaining the vapor flux of the Group V element low enough to avoid compound formation at the Al source. This last condition is especially critical since it is difficult to achieve Al source temperatures high enough ($\sim$ 1600°C) to ensure thermal decomposition of the arsenide and phosphide compounds which might form on the surface of the molten metal. High rates of deposition, approximately 300 to 600 A/min are attained with this method and there appears to be no difficulty in preparing films many microns in thickness.

The films, as a group, display bulk structural and optical properties. The main exception is the observation of a hexagonal wurtzite modification of AlAs in the surface layers of an Al rich deposit. Bulk type behavior is also shown in the relative chemical instabilities of AlSb, AlAs and AlP in moist air. These lead to changes in the structure and physical properties and to avoid this care must be taken immediately after preparation to protect the films prior to examination.

Ohmic contacts of good quality are achieved for the AlAs and AlP films using sputtered tantalum. The contacts to AlSb films, however, tend occasionally to be non-ohmic and electrical evaluation was complicated somewhat by the resulting barrier. The very rapid deterioration of these films makes it desirable that contacts be deposited "in situ" in order that the semiconducting properties can be observed.

Although relatively low resistivity film products were deposited, the carrier mobilities in the AlAs and AlP films were low; several orders of magnitude less than those recorded for bulk materials. The causes of low mobilities in the literature for films such as CdS, Si, Ge, GaAs, etc., are numerous; e.g., heavy compensation and attendant ionized impurity scattering (Ref. 26), grain boundary scattering (Ref. 26), dislocation scattering (Ref. 27), etc. In addition, the III-V compounds seem particularly prone to the formation of impurity bands at low impurity levels (Ref. 28). Both the observation of polycrystalline structures in the present films (with associated numerous boundaries) and the suggestion in the resistivity vs. temperature data of the presence of shallow impurity levels, seem consistent with this explanation.

3. SPUTTERED FILMS

3.1 Reactively Sputtered AlN - Diode System

3.1.1 Preparation - It is generally recognized that aluminum is one of the most difficult metals to sputter physically due to its highly resistive surface oxide which cannot easily be eliminated in the relatively high partial pressures of oxygen or water vapor encountered in conventional vacuo (10^{-5} - 10^{-6} torr). For this reason, although references to the physical and reactive sputtering of other metals abound in the literature, virtually none is available for aluminum and its compounds.

In the present studies, it was felt that since AlN possesses the highest insulation resistance of the compounds under investigation, reactive sputtering of Al in N_2 would provide an excellent test of the feasibility of extending this method to the other Al-V compositions. To avoid the oxide retardation problem referred to above, a Varian, ion-pumped, bakeable stainless steel uhv table top system (of the VI312 type), capable of base pressures in the low 10^{-9} torr range, was used for the experiments.

The sputtering arrangement was of the simple diode type, Fig. 18, the relative cathode-anode spacing being 4 cm. A 5 cm diameter disk of aluminum (purity 99.999%) served as cathode. The anode was a larger disk, 8 cm diameter, of Ta with a rectangular cut-out measuring 2 x 1 cm at its center. Four substrates were mounted in resistively heated Ta envelopes (Si substrates could alternatively be heated directly)

Dwg. 855A256

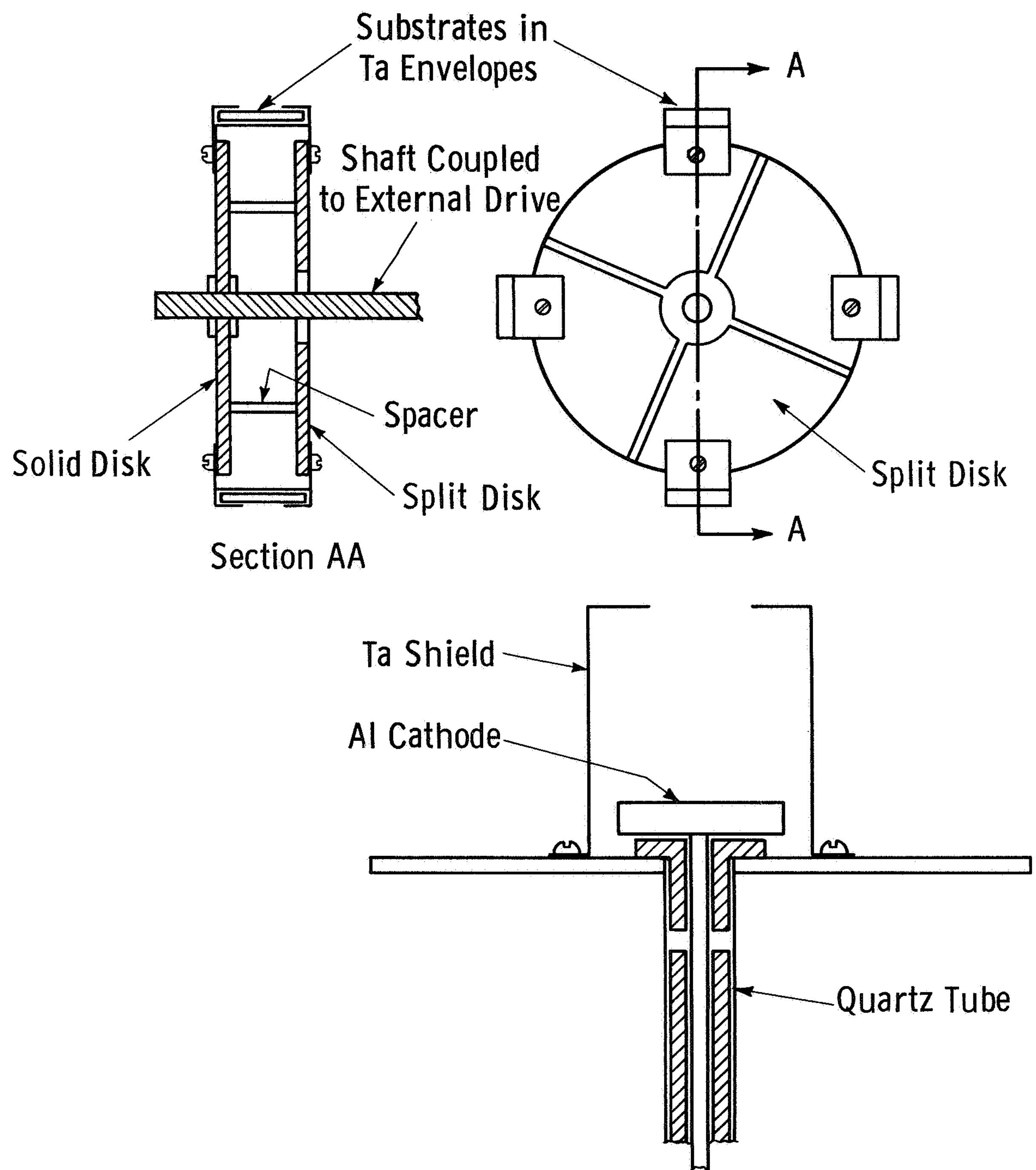

Fig. 18—Schematic of arrangement for diode reactive sputtering of AlN films. Resistive heating of substrates in Ta envelopes via the solid and split disks of the substrate holder

and could be positioned directly above the aperture in the anode by a rotatable holder externally driven. A number of different substrates were used among which were single-crystal Si, SiC, Al_2O_3 (sapphire) and vitreous SiO_2. Where possible, substrate dimensions were 10 mm x 8 mm x 2 mm. Both the sapphire and silica substrates could be used when both optical and electrical measurements were required.

When a pressure of 10^{-9} torr had been attained, the experimental chamber was isolated from the ion pump and "Research Grade" argon (impurity conc. < 5 p.p.m.) was admitted until a discharge was established. Using a static argon pressure of 80×10^{-3} torr, an anode-cathode potential of 2500v and a current density of 1 ma/cm^2, the cathode was sputtered until Al was observed to be deposited on a monitor silica slide. A partial pressure of about 5×10^{-3} torr of nitrogen (impurity conc. < 1 p.p.m.) was admitted through a needle valve, and with the discharge intact, the leak rate was adjusted until the total chamber pressure remained constant. Under these conditions, the rate of consumption of N_2 in the discharge was balanced by its rate of replacement via the needle valve.

It was reasoned that optimum stoichiometry in the films would be achieved by using substrate conditions favoring condensation only of the AlN composition. In this case, since N_2 is a permanent gas, it was necessary simply to use a chemically inert substrate and to maintain its temperature high enough to prevent the aluminum condensing alone. Most depositions were carried, therefore, at temperatures higher than 550°C which from Rhodin's (Ref. 29) earlier data on "critical temperatures" for aluminum might be expected to ensure at worst only a very small condensation rate for the metal.

Substrates were heated prior to positioning above the anode aperture. Thicknesses of deposited AlN films were measured interferometrically. Some additional test data indicated that, with the voltage, current density and argon pressure values used for reactive sputtering, pure Al could be deposited on unheated substrates at rates in excess of 200 A/min. However, the AlN growth rates under comparable conditions were only 50 - 100 A/min. At high temperatures rates ranged between 10 - 30 A/min.

3.1.2 Structural Studies - Structural studies of the AlN films were carried out in most cases by means of reflection electron diffraction using the high-resolution diffraction attachment of a JEM 7 electron microscope. The data obtained from these studies are summarized in Table IV and examples of the electron diffraction patterns are shown in Figs. 19A, 19B, and 20. Deposits sputtered onto unheated substrates appear to comprise of single-phase hexagonal AlN form (Ref. 30) but show no evidence of preferred orientation. No significant change in structure is observed until the substrate temperature is raised above 800°C, when a (0001) fiber texture develops. This texture gradually strengthens with increasing temperature until at 950°C signs of azimuthal alignment consistent with epitaxy are apparent. At 1000°C, a considerable part of the film possesses a well-developed epitaxial structure with the relationship to the Si substrate:

$$(00.1)_{AlN} \,//\, (111)_{Si} \quad ,$$

$$[11.0]_{AlN} \,//\, [1\bar{1}0]_{Si} \quad .$$

Table IV Electron Diffraction Data for Reactively Sputtered AlN Films

Sample No.	Substrate	T_s (°C)	Thickness (A)	Remarks
184	Si(111)	27	5000	Crystalline but no orientation
185	Si(111)	27	2500	Crystalline but no orientation
186-1	Si(111)	800	600	(0001)-fiber texture
186-2	Si(111)	∿500	600	weak (0001)-fiber texture
188-2	Si(111)	800	5000	(0001)-fiber texture
188-3	Si(111)	1000	5000	epitaxial AlN(0001)
191-1	Si(111)	950	2500	strong (0001)-fiber texture (tending towards epitaxy)
191-2	Si(111)	900	2500	(0001)-fiber texture (Not epitaxial)
191-3	Si(111)	1000	2500	strong (0001)-fiber texture (tending towards epitaxy)
192-1	SiC(0001)	1300	1900	mostly epitaxial AlN(0001) --some ring component
192-2	CaF_2(111)	800	600	(0001)-fiber texture
192-3	CaF_2(111)	600	2500	(0001)-fiber texture

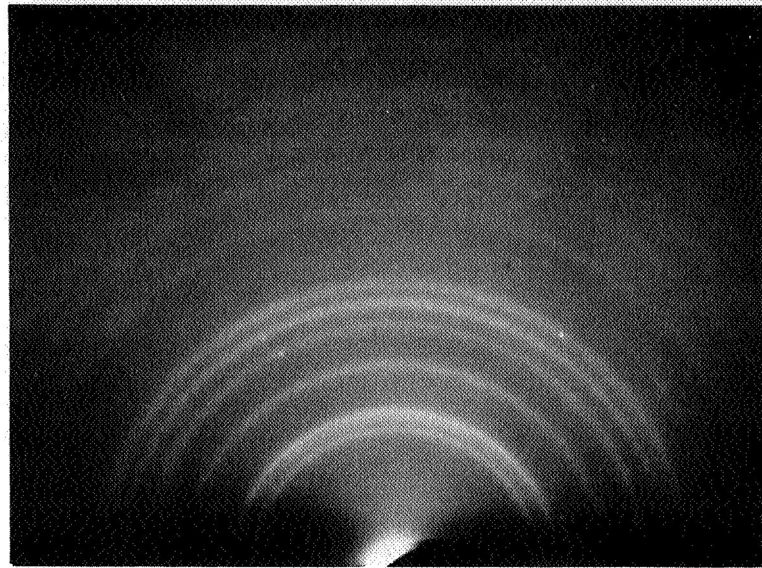

(a)

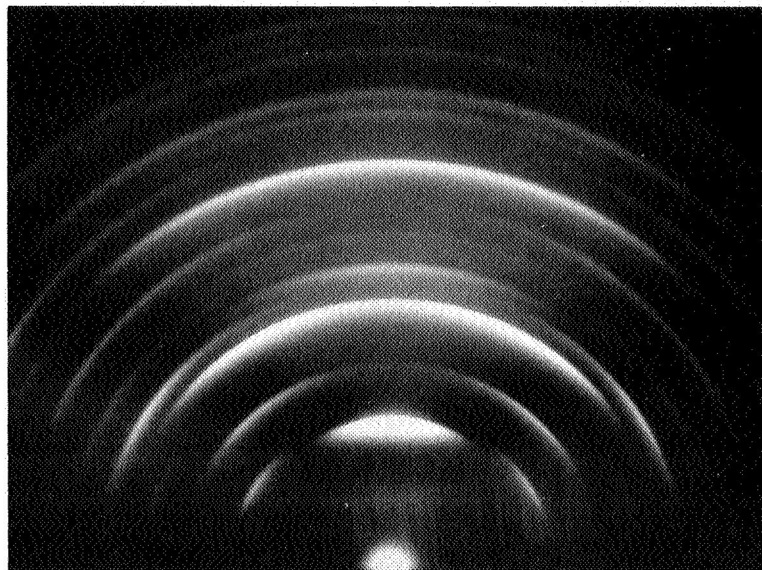

(b)

Fig. 19A—Electron diffraction patterns of AlN films reactively sputtered on (111) Si: (a) unheated substrate; (b) substrate temperature 900°C

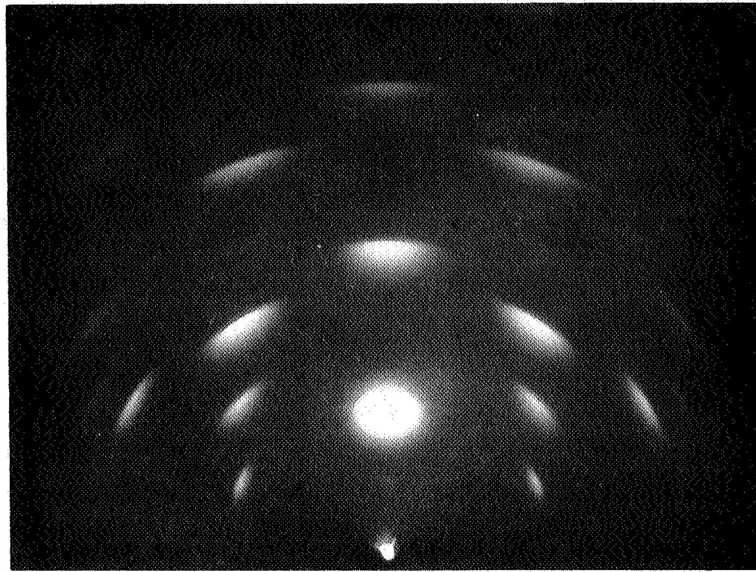

(c)

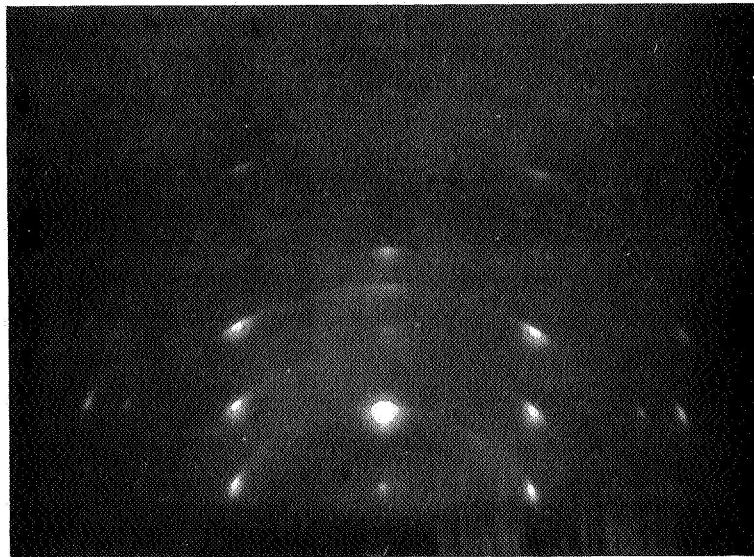

(d)

Fig. 19B—Electron diffraction patterns of AlN films reactively sputtered on (111) Si: (c) substrate temperature 950°C; (d) substrate temperature 1000°C

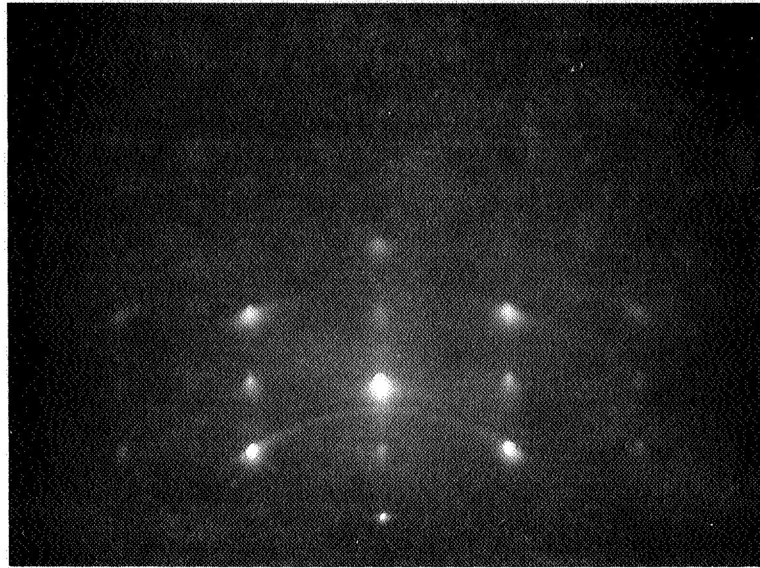

(a)

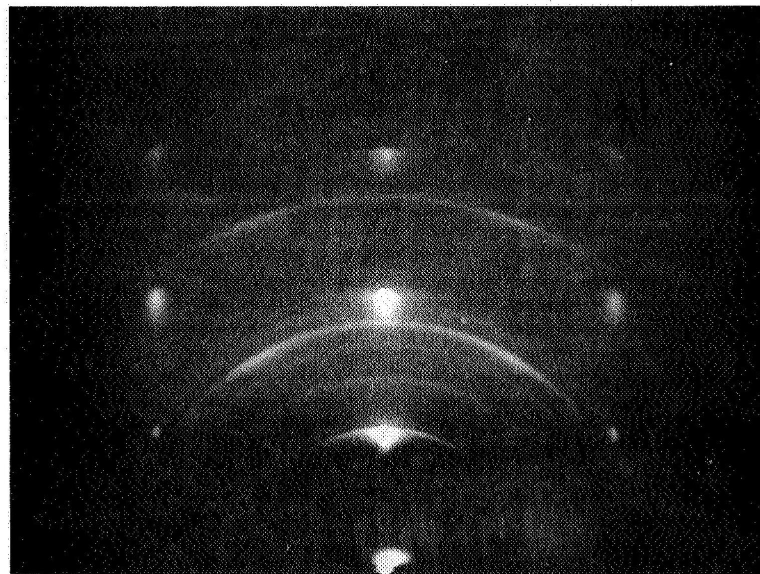

(b)

Fig. 20 —Electron diffraction patterns of AlN films reactively sputtered on (0001) faces of 6H-type SiC crystals: electron beam along (a) [11.0] and (b) [10.0]

Similar results were obtained in the growth of AlN films on SiC crystals, although in this case the epitaxy temperature appears to be somewhat higher than for Si. Epitaxy is incomplete even at 1300°C (Fig. 20), the orientation of the epitaxial component being:

$$(00.1)_{AlN} \,//\, (001)_{SiC}$$

$$[11.0]_{AlN} \,//\, [11.0]_{SiC}$$

Evaluation of grain size based on AlN films deposited on Si showed the films to be composed of arrays of small crystallites with average diameters of 600 A (Fig. 21).

3.1.3 Chemical Stability - In view of the rapid deterioration observed in the structure and optical properties of the AlSb films on exposure to the atmosphere, it was decided to check on the chemical resistance of AlN films to high temperature oxidation. Film samples prepared on Si substrates were allowed to age for several weeks then were re-examined by reflection electron diffraction and by glancing-angle X-ray diffraction. They were found still to display well-crystallized and oriented single-phase structures. The films were then heated in air for periods typically between 15 and 30 minutes at temperatures ranging from 250°C to 750°C. No change in the electron or X-ray diffraction patterns was observed until the temperature exceeded 700°C, when the electron diffraction pattern showed an increase in the diffuse background scattering. The structure change appeared to have been confined to the film surface, however, since the X-ray pattern showed only slight broadening in the diffraction lines. Moreover, the X-ray pattern was essentially unchanged even after oxidizing for several hours at 750°C.

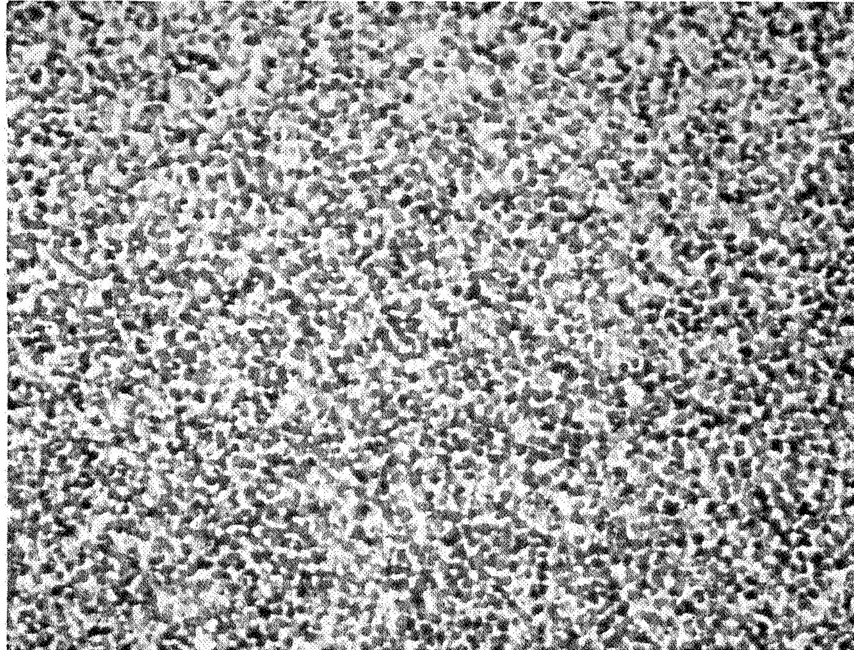

Fig. 21—Transmission electron micrograph of reactively sputtered AlN film (1000A thick) deposited on (111) Si at 900°C

RM-44305

AlN films thus possess a far higher resistance to chemical attack than do the other Al-V species.

3.1.4 Optical Studies - In general, qualitative examination of the optical spectra confirmed that the films were AlN. Quantitative comparisons, however, indicated that certain prominent features of the spectra were influenced by effects due to impurities or structural disorder in the films.

One AlN sample which was examined, viz., Z-192-3, was prepared on a CaF_2 substrate held at about 600°C. The data are presented in Fig. 22. The absorption is seen to rise monotonically as a function of energy. Various values for the energy gap could be obtained for this film, depending on the energy function plotted. More meaningful, however, is a comparison to the data of Cox et.al. (Ref. 1) who measured the absorption spectra for thin AlN single crystal platelets. Their data, shown in Fig. 23, give the absorption spectra for an as-grown AlN single crystal together with an optical scan for the same crystal after annealing for 2 hours at 1100° in argon. The data in Fig. 22 when normalized to the same value as that of Cox et.al. at wavelengths greater than 3600 A, show an increasing absorption that closely parallels that of their Ar-annealed crystal, although the correspondence is not exact. Cox et.al. (Ref. 1) interpret the absorption-increase caused by argon annealing as being due to nitrogen vacancy formation. In Fig. 23, we also show the absorption spectra of two films of reactively sputtered AlN which had been prepared to nearly identical thicknesses on silica, after which one was annealed in nitrogen at 900°C for 2 hours. The spectra

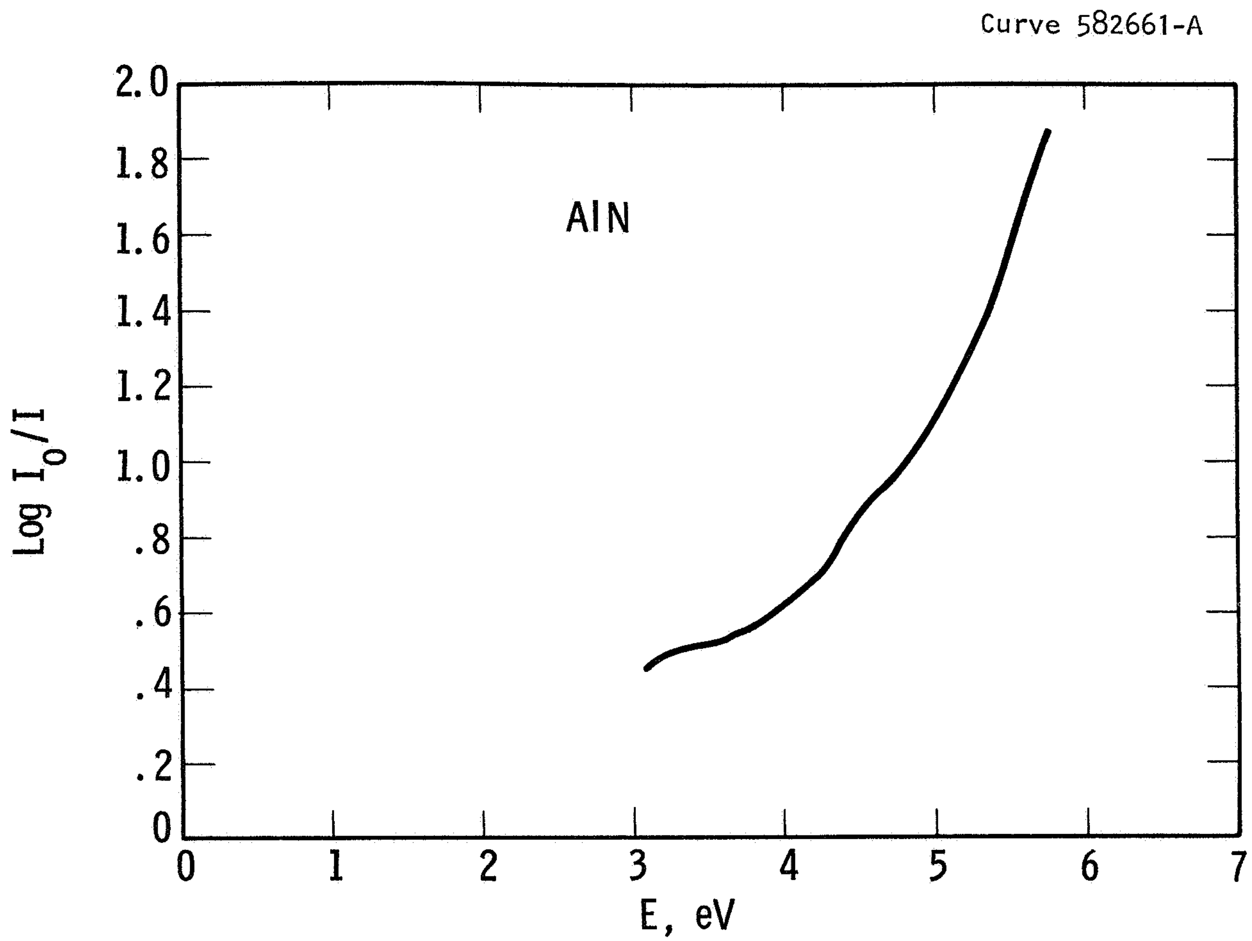

Fig. 22—Absorption spectrum of AlN film on CaF_2

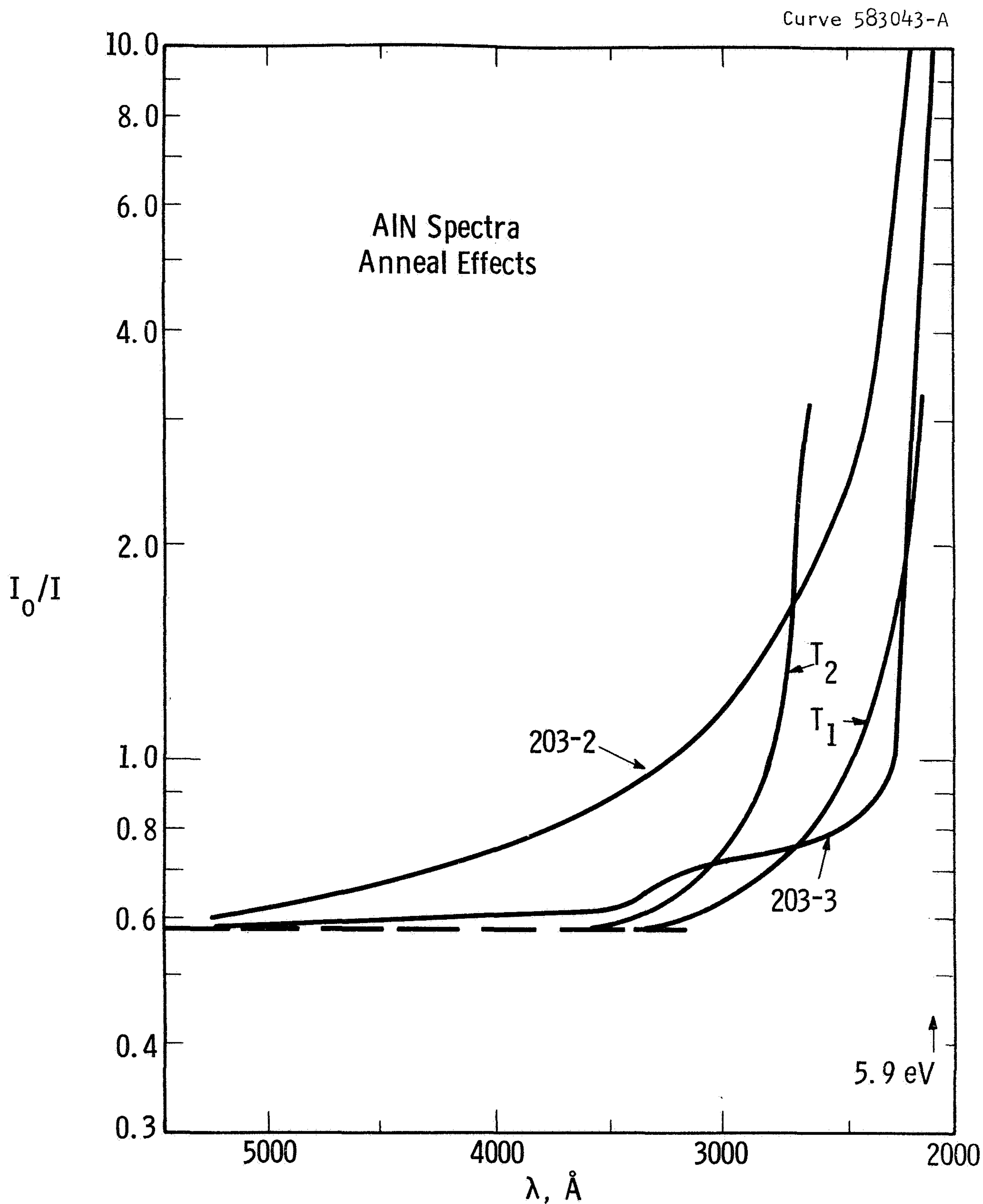

Fig. 23 Optical absorption data comparing properties of reactively sputtered AlN to bulk single crystals. Film Z-203-2 is an as-grown film; film Z-203-3 has been similarly deposited but has been annealed at 900°C in N_2. T_1 is an as-grown crystal (Cox, et al.). T_2 is a crystal annealed in Argon.

showed that, after annealing the absorption at energies < E_g is decreased and that it then closely resembles that for as-grown bulk crystals.

Changes in the spectra were emphasized by running a spectrum with the N_2 annealed film in the reference compartment of the Cary, and the unannealed film in the regular sample compartment, Fig. 24. It can be seen that there are significant changes at 4.42, 3.75, and 2.8 eV. The feature of 5.05 eV may be an instrumental artifact, since the slits are opening rapidly in this wavelength region.

These absorption spectra show that the number of mid-gap states is significantly reduced by the nitrogen anneal. They also show that a significant ordering of the structure takes place. The reduction in state density is indicated by the reduction of the absorption, while the ordering is indicated by the appearance of discrete absorption thresholds rather than the monotonically increasing absorption found in the as-grown films.

To insure that the shift of band-edge position in the N_2 annealed films was not due to an effect generated by a particular type of substrate a set of four AlN films were deposited to a thickness of 8000 A at about 1000°C, two on the (0001) face of sapphire (Al_2O_3) and two on vitreous silica, and examined optically in annealed and unannealed states. The results are shown in Fig. 25, and indicate that the substrate material has no effect on the change in absorption edge nor in the general details of the absorption curves. We thus conclude that the shift is associated with a built-in surplus of Ar due to the nature of the ambient during deposition. The Ar occlusion presumably leads to a

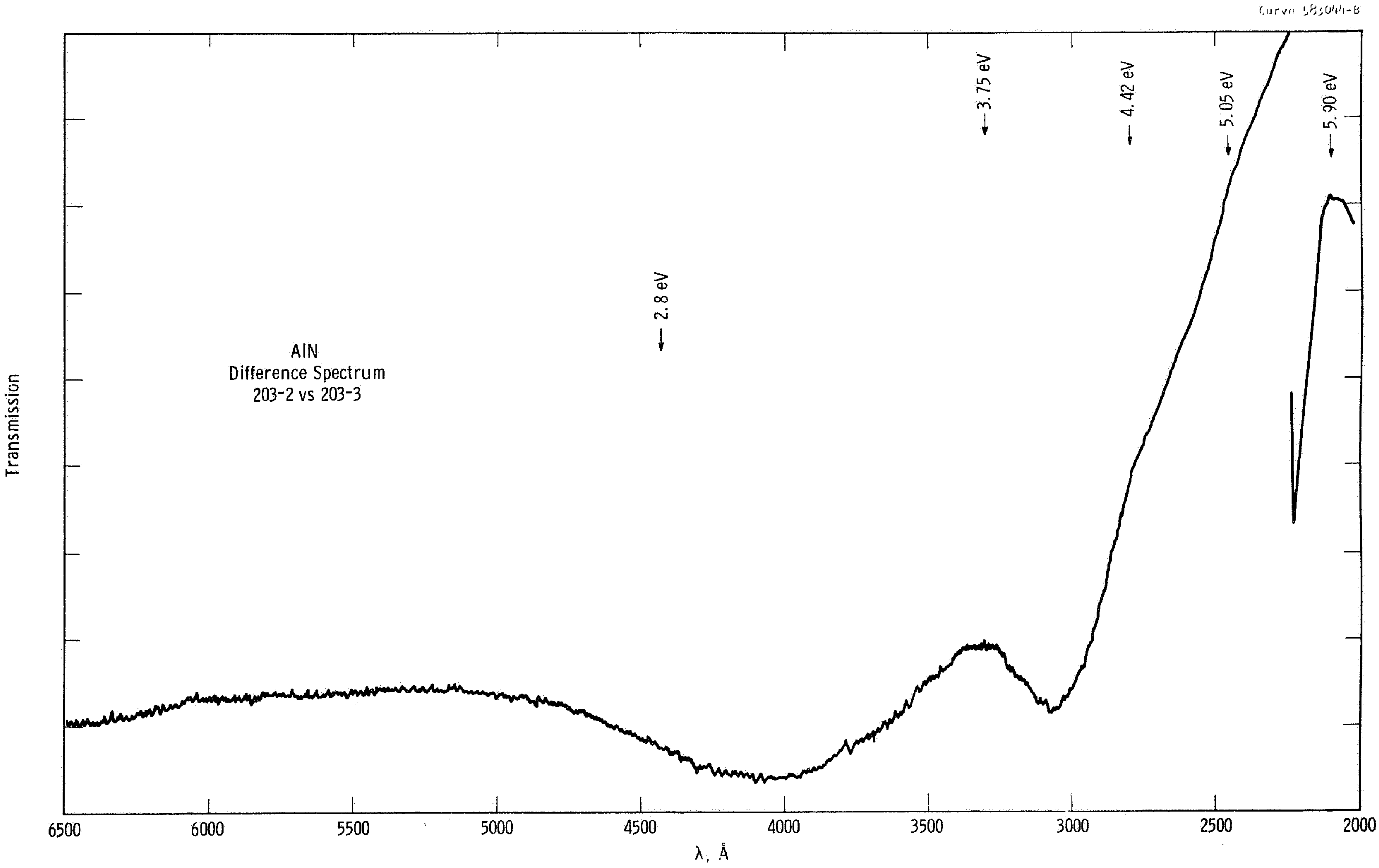

Fig. 24—Absorption difference spectrum obtained from nitrogen anneal of sputtered AlN film

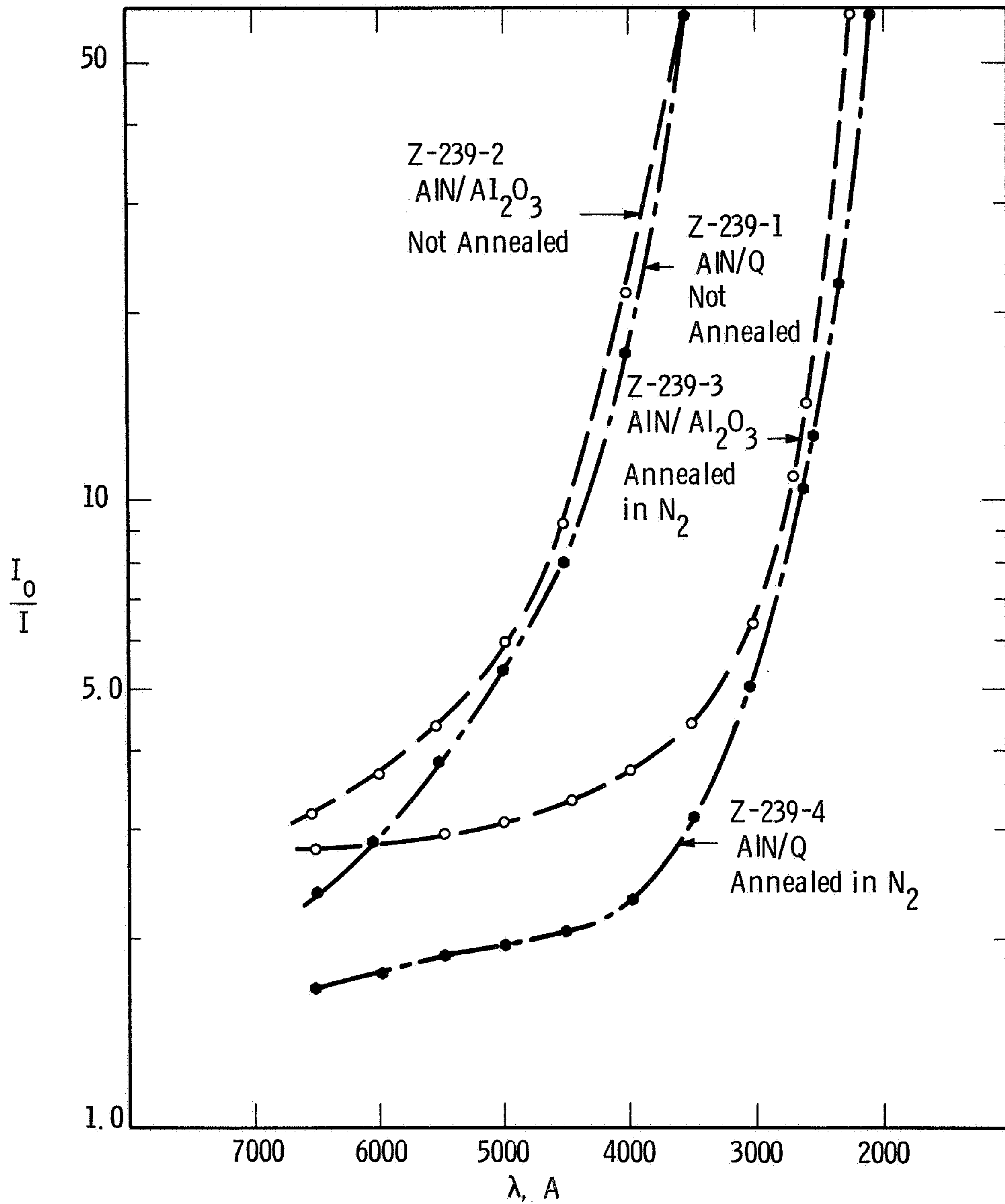

Fig. 25—Optical absorption in four AlN films, thickness 8000 A, deposited on vitreous silica and sapphire under same sputtering conditions. One film on each substrate was given standard annealing treatment in nitrogen

nitrogen deficiency or a nitrogen vacancy condition similar to that reported for Ar annealed bulk crystals (Ref. 1).

3.1.5 Dielectric Properties - A comparison was made of the capacitive properties of reactively sputtered AlN films with those of the bulk material. To obtain a representative result for given deposition conditions, capacitor structures based on a metal-nitride-metal sandwich arrangement were constructed. These consisted of base electrodes, those in immediate contact with the substrate, of sputtered Ta, 2500 A thick. Such films either covered the entire substrate or only part of it, the latter configuration being chosen to permit optical evaluation. After an AlN film was deposited, counter-electrodes of evaporated Au and Al or of sputtered Ta were deposited. No intentional heating of substrates was attempted during the electroding schedules. The counter-electrode configuration was an hexagonal array of 0.3 mm dots on 0.5 mm centers, thus approximately 200 individual test samples were available on a given substrate.

Capacitance measurements were made over a frequency range between 1 and 100 kHz with an impedance bridge (General Radio Type 1608-A.) When Ta/AlN/Ta sandwiches were examined the effects of temperature change could be observed between 25° and 500°C, heating taking place in a 10^{-5} torr vacuum to prevent oxidation of the electrodes. Attempts to use gold or aluminum electroded sandwich structures in similar experiments were unsuccessful, the main difficulty being caused by peeling of the counter-electrode as the temperature was raised. Room temperature measurements were also made using the Au/AlN/Ta and Al/AlN/Ta sandwiches and were in excellent agreement with those using the Ta electrodes.

Reproducible measurements were obtained from films in the thickness range 0.15 to 5 microns. Films with thicknesses less than 0.15 micron demonstrated an erratic behavior under applied voltages, the breakdown being attributed to leakage at grain boundaries. The following dielectric data thus are based on the properties of the thicker films.

At 25°C and 1 kHz, measurements of capacitance yielded a dielectric constant, $\varepsilon/\varepsilon_o$, of about 8.5 in good agreement with that for the bulk. The film dielectric proved to have a slight frequency dependence and variations of $\varepsilon/\varepsilon_o$ with temperature up to 500°C for several frequencies are shown in Fig. 26. Some comparative selected bulk data (Ref. 31) are also shown. The temperature dependence of $\varepsilon/\varepsilon_o$ for the films differed from that for the bulk, the former being insensitive to temperature up to 350°C and at this limit still retaining a room temperature value. The dielectric constant for the bulk material at 350°C and 1 kHz shows a three-fold increase over the room temperature value.

The dissipation factor, D, as a function of temperature is shown in Fig. 27. Again, there is little temperature variation up to 350°C whereas the bulk data (Ref. 31) indicate approximately two orders of magnitude change, referred to the room temperature value, when measured at 350°C and 10 kHz.

It is noteworthy, that the thin film configurations using the Ta electrodes are structurally stable even after thermally cycling several times to 500°C. This stability implies that no significant

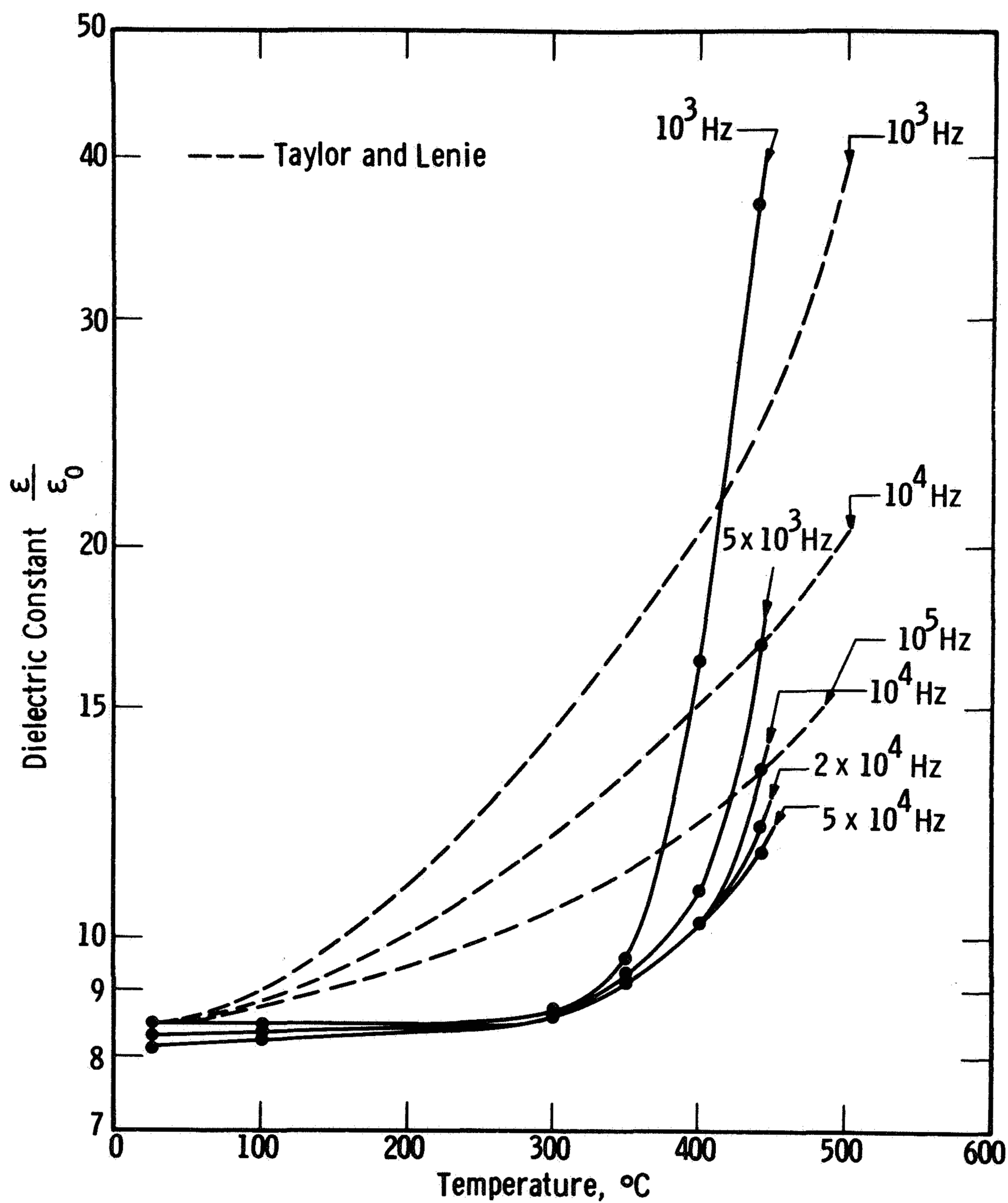

Fig. 26—Variation of dielectric constant, $\varepsilon/\varepsilon_0$, with temperature at several frequencies

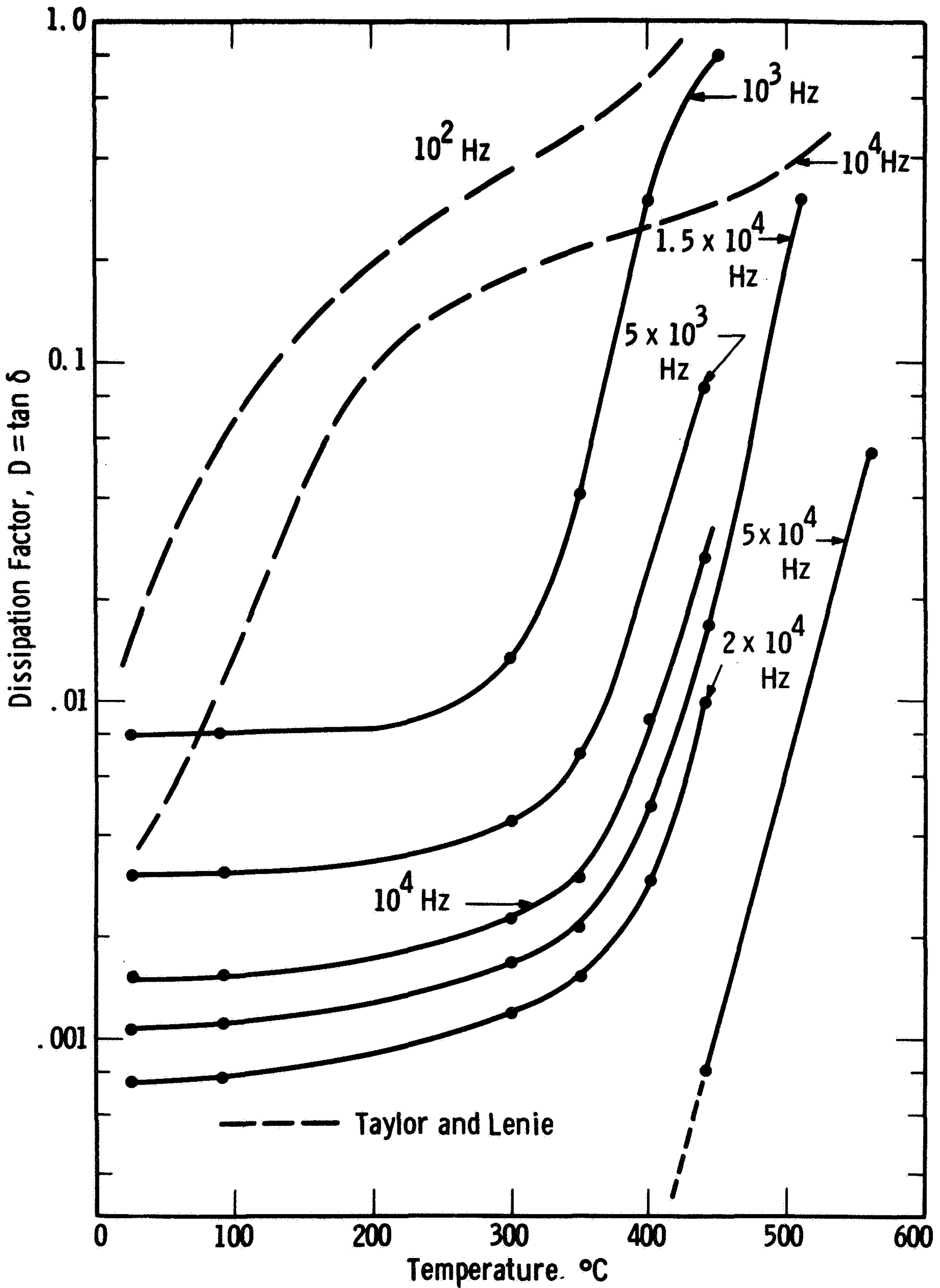

Fig. 27—Variation of dissipation factor, D, with temperature at several frequencies

diffusion of the electrode material has occurred. The thermal insensitivity of capacitance and loss data also appears to suggest that the films contain fewer or less conductive impurities than the bulk ceramic.

Volume ac resistivities, as calculated from capacitance and loss values, were plotted as a function of temperature for several frequencies and are shown in Fig. 28. At frequencies less than 10 kHz, the resistivities of both the AlN films and the bulk material decrease for a corresponding increase in frequency, the effect in the bulk being more pronounced. The resistivity-frequency dependence for the bulk ceramic is also retained at frequencies greater than 10 kHz. The resistivity trend in the films, however, in the higher frequency range is reversed, resistivity increasing with frequency. No satisfactory explanation is as yet available to account for the differing resistivity-frequency relationships. It is probable, however, that more than one polarization and conduction phenomenon is operative and that the observed data, especially in the films, are due to a combination of superposed effects (Ref. 32).

The resistivity-temperature variations in both the films and the bulk show decreasing resistivities as temperatures are raised. However, at comparable frequencies, the film material exhibits higher resistivities in the temperature range below 400°C. Those for the films show an additional frequency dependence at temperatures near and above 350°C.

3.1.6 <u>Properties of Annealed Films</u> - In addition to the data referred to in Sec. 3.1.5, are results obtained during temperature

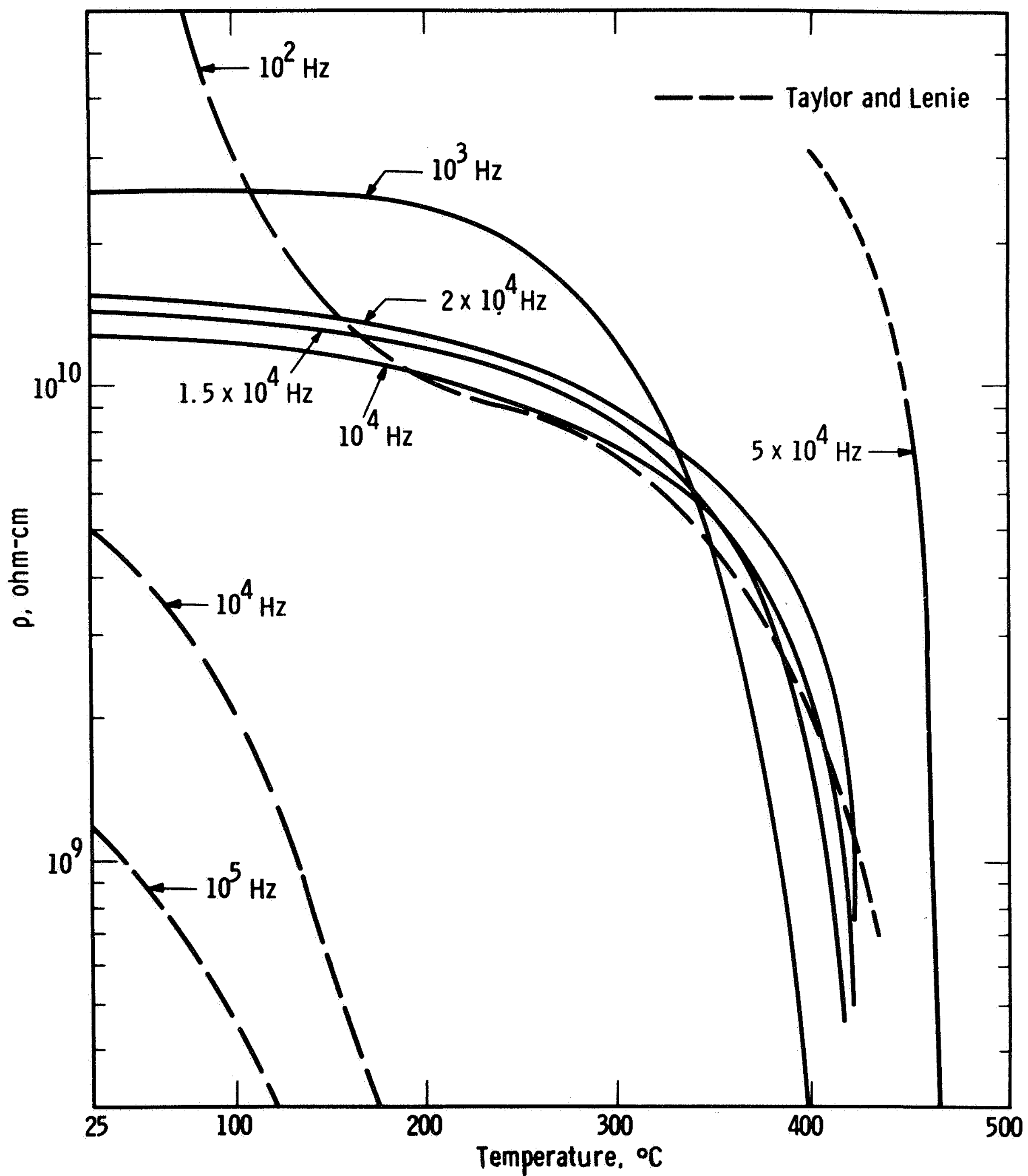

Fig. 28—Variation of ac resistivity with temperature at several frequencies

cycling of several test specimens. (The tests were coincident with I-V measurements which will be reported in Sec. 3.1.8). A typical result appears in Table V.

Table V

Frequency Variation of Capacitance and Loss Values
Of Some Annealed AlN Films

	before 220°C - 20 hr. anneal		after 200°C - 20 hr. anneal	
f(kHz)	C (F x 10^{-12})	D	C (F x 10^{-12})	D
1	8.6	.04	8.7	.025
2	8.6	.0175	8.6	.0045
5	8.45	.004	8.5	.0015
10	8.3	.0017	8.5	<.0001
15	8.1	.001	8.4	<.0001
20	7.9	.0005	8.4	<.0001
50	7.9	<.0001	8.3	<.0001
100	7.9	<.0001	8.1	<.0001

Measurements in the 1 to 100 kHz frequency range on annealed samples show no significant change in capacitance but display a marked reduction in loss. This suggests that the ac resistivity at frequencies above 1 kHz has been increased after annealing. At first sight, these results conflict with an increase in current (and therefore in the dc conductivity) found in the I-V data after annealing. The apparent disagreement can be resolved by considering the marked increase in the dispersion of the dissipation factor after anneal relative to that

in the as-grown films (see Fig. 29; these data are extracted from Table V). If the data in Fig. 29 are extrapolated to frequencies less than 1 kHz, one notes that the loss for annealed films soon becomes greater than for the unannealed films. Thus, low frequency loss characteristics would still be consistent with a lowered dc resistivity (the latter suggested by the I-V data of Fig. 34).

3.1.7 <u>I-V Measurements</u> - To assess the potential usefulness of the AlN films as dielectric layers in, for example, semiconductor field effect devices, it was desirable to study their behavior under applied fields. Since the high preparation temperatures used in these experiments had limited the choice of base electrodes, only films deposited on bulk Si or on to sputtered Ta films were investigated. Data were obtained using the sandwich arrangements described previously. In some cases, large area counterelectrodes were also used.

Figs. 30 to 33 illustrate some of the results. In general, with Au and Ta counterelectrodes, data are reproducible in form. This is illustrated in Fig. 30 which shows a plot based on measurements from four 0.5 mm diameter electrode areas on the same film. Each capacitor structure was measured up to about 70 V and one was taken to a maximum voltage of 115 V. The I-V characteristic up to about 60-70V was reversible. However, when the current was taken to high values a new characteristic was followed on reducing the voltage. This plot approximates to a square law; i.e., the observed dependence is

$$J = k\ (V)^{2.2} \quad . \qquad (5)$$

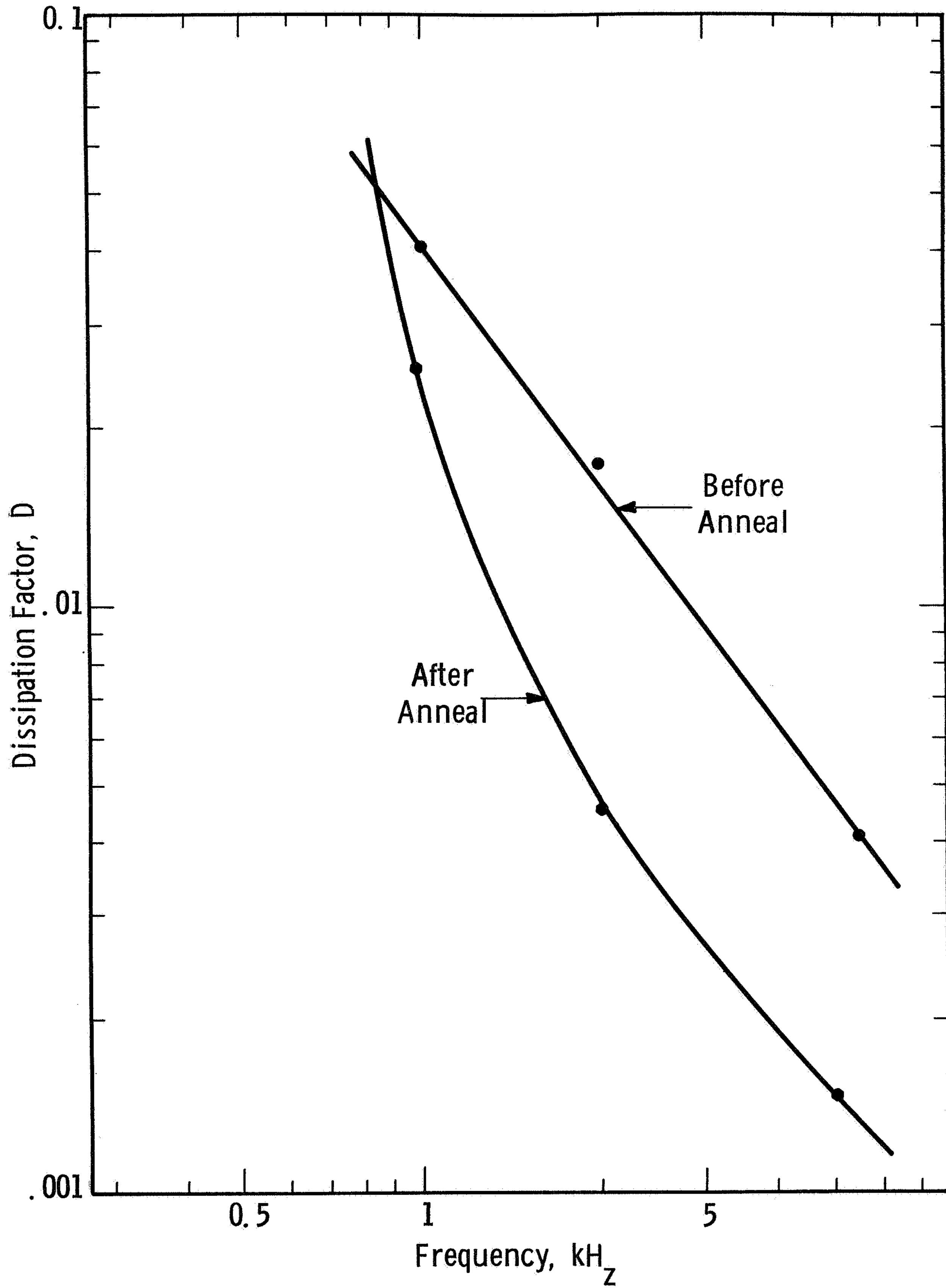

Fig. 29—Effects of thermal anneal on dissipation factor (loss) of reactively sputtered AlN films

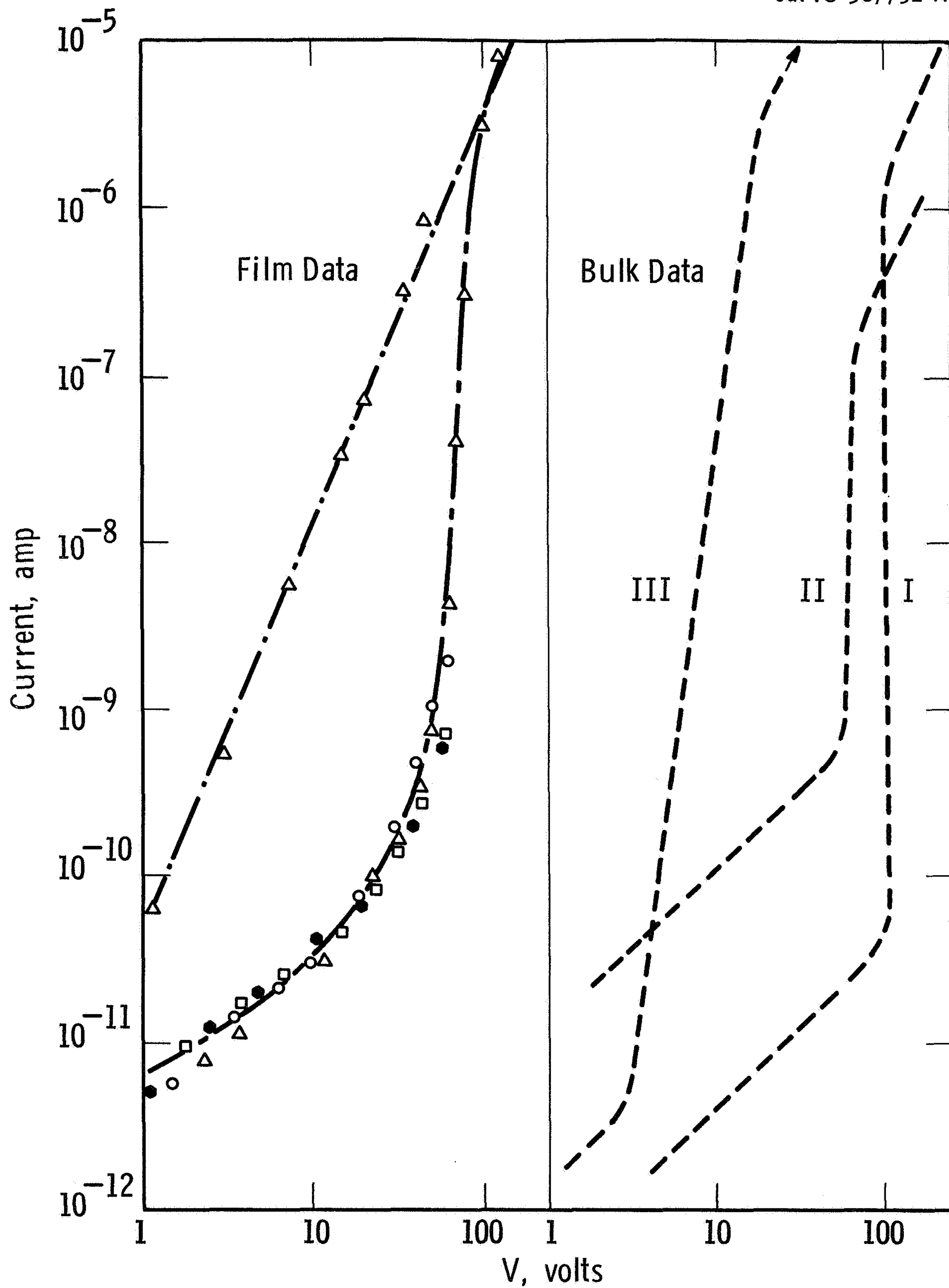

Fig. 30—Current-voltage data for Au/ AlN/Ta film sandwich structure, AlN film thickness 8000 A. Also shown are data of Kawabe et. al for single crystal AlN

The slope of the low voltage segment of the initial plot on all films tested is approximately unity indicating the Ohm's law is followed.

It is interesting to compare our results with the data of Kawabe (Ref. 33) et.al. for single crystal platelets of AlN fitted with Au electrodes on opposite faces. These workers explain their results on the basis of a space-charge limited current mechanism of the type outlined in the theory of Lampert (Ref. 34). At low applied voltages where any excess injected carriers are trapped, the carriers n normally present thermally will generate an ohmic current of the form

$$J = e\ n\ \mu\ V_a/d \qquad (6)$$

where V_a is the voltage applied to an insulator of thickness d, and μ is the carrier mobility. When the traps are filled at an applied voltage V_{TFL}, the injected carriers are available for conduction and a steep rise in current occurs until the I-V characteristic meets a line represented by Child's law, i.e.,

$$J = 9\ \theta\varepsilon\ \mu\ V_a^{\ 2}/8\ d^3, \qquad (7)$$

where θ is the fraction of the total charge available for conduction, and ε the dielectric constant of the insulator.

The results of Kawabe et.al. (Ref. 33) for Au electrodes are reproduced at the right of Fig. 30 and demonstrate the extreme sensitivity of the I-V characteristic to thermal history of the crystal, and presumably to a number of traps. Curve I is the result obtained initially, Curve II after the crystal has been heated to 160°C and cooled slowly, and Curve III after heating to 160°C and quenching. These treatments produce significant

changes in V_{TFL} and hence in the voltage ranges over which Ohm's law (equation (6)) and Child's law (equation (7)) are obeyed.

Our data for the Au electroded AlN film are not inconsistent with the space-charge limited model, although they are open to alternative interpretations. If this model is assumed, the approximate value of V_{TFL} can be used in the theoretical expression,

$$V_{TFL} = e\ d^2\ N_t/2\ \varepsilon \qquad (8)$$

to calculate the trap density N_t. Taking V_{TFL} as 75 V, from Fig. 30 d as 8×10^{-5} cm. and ε as 8.5, the value of N_T is about $10^{18}/cm^3$. This is about 5 orders of magnitude higher than Kawabe et.al. (Ref. 30) find for single crystals but is a reasonable estimate for a polycrystalline film. Incidentally this value of N_T corresponds very closely to the number of crystallites/cm^3 in the film (i.e., $2.5 \times 10^{17}/cm^3$) based on the micrographic data in Fig. 21.

Some results obtained with Al electrodes on the same AlN film are shown in Fig. 31. A much wider variation of the I-V characteristics from sample to sample was found in this case and the current was more erratic at lower voltages. This behavior could mean a variation in the number and energy of traps between samples, but in view of the consistency in the results with Au electrodes, it is more probable that the effect is spurious, and arises from a chemical interaction or perhaps an oxide film at the Al/AlN interface.

Rather strong photoconductivity effects were observed with the Al/AlN/Al sandwiches although none were observed when other electrode materials were used. Using visible radiation from a tungsten lamp,

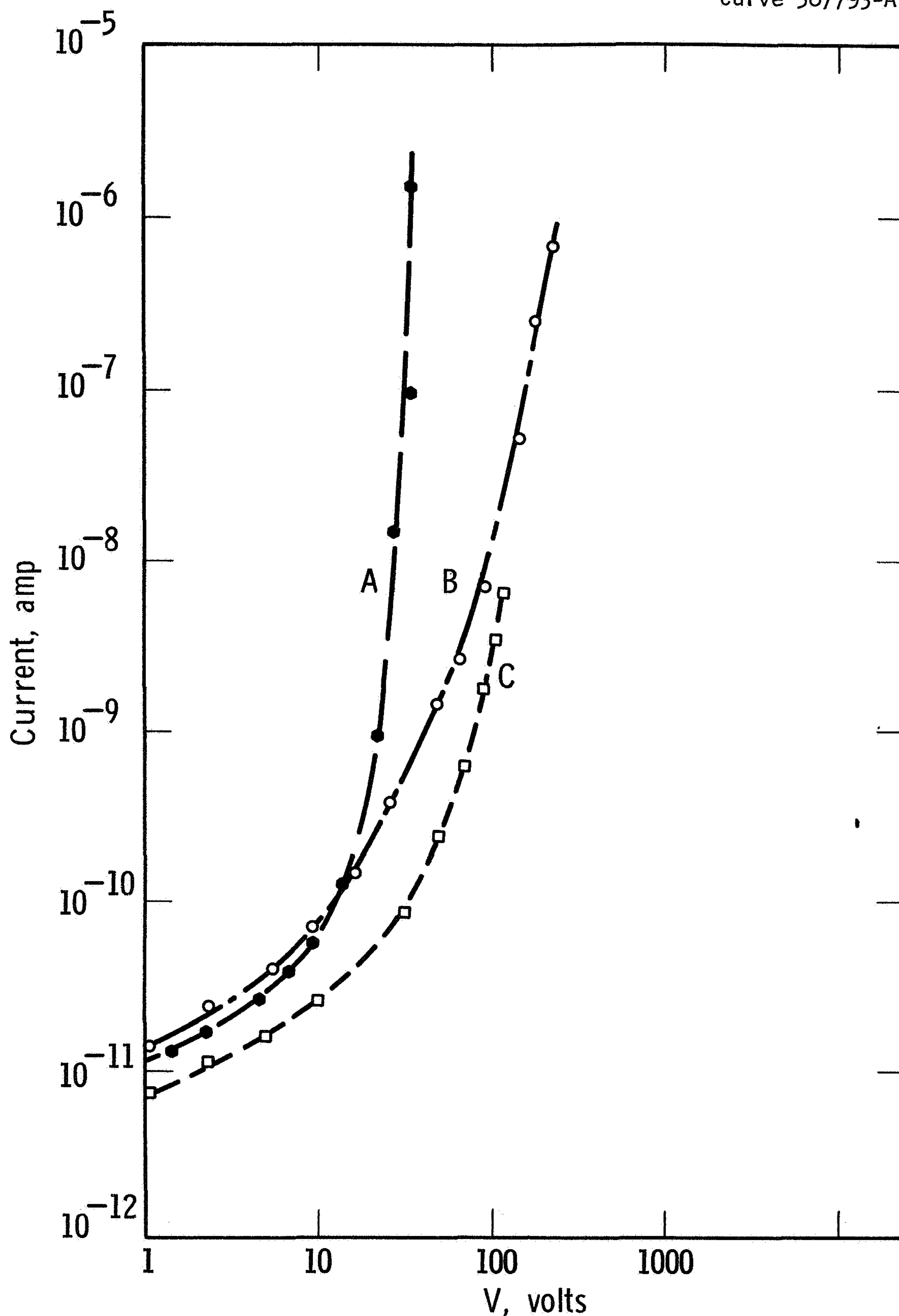

Fig. 31—Current-voltage data for Al/ AlN/Ta film sandwich structures, AlN film thickness 8000 A. Curves A, B and C obtained from adjacent test samples on same film

focused with an internal parabolic reflector, no photoconduction was detected. However, with a 2 watt mercury-argon lamp placed about one inch from the sample, the results shown in Fig. 32 were obtained. Although the spectral dependence of the effect was not measured, it seems probable that the photoconduction is a maximum at about 2.8 eV, which Cox, et.al. (Ref. 1) and Kawabe et.al. (Ref. 33) report for Al-doped AlN crystals.

Figure 33 shows a fairly typical I-V characteristic for a Ta/AlN/Ta sandwich. This result is somewhat different from those found with Al and Au electrodes. Thus, despite the fact that a thinner sample was used (approximately 4000 A) the current values are reduced compared with those for Al and Au, except at low applied voltages in the near-ohmic range. Also, the effective field for breakdown was relatively high, corresponding to a voltage of 350 V, giving a dielectric strength of about 9×10^6 V/cm.

3.1.8 I-V Data for Annealed Films - Because efforts to fully explore the complete I-V behavior were impeded by erratic behavior at high voltage, the currents in this region being strongly time dependent, several test specimens were examined at elevated temperatures. The purpose of an increased temperature was to possibly facilitate a complete filling of traps at lower voltage thus permitting observation of the trap-filled voltage limit before the onset of instability.

Some results from heated films appear in Fig. 34. The 25°C curve depicts typical behavior for an as-grown film. Data in this case were taken from Ta/AlN/Ta sandwiches in which the nitride thicknesses

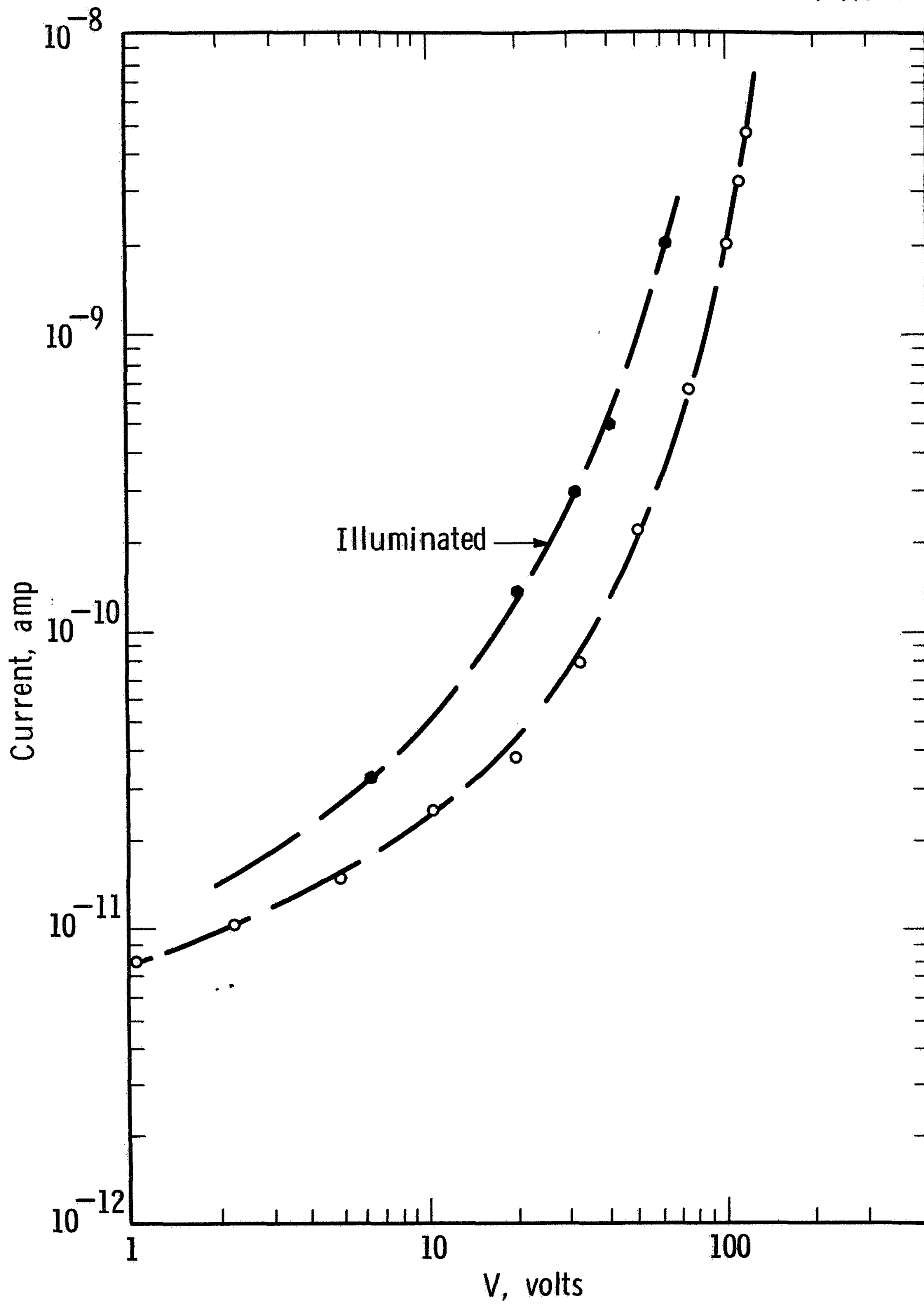

Fig. 32—Photoconductivity effect for Al/AlN/Ta film sandwich (sample illuminated with mercury-argon lamp)

Curve 587795-A

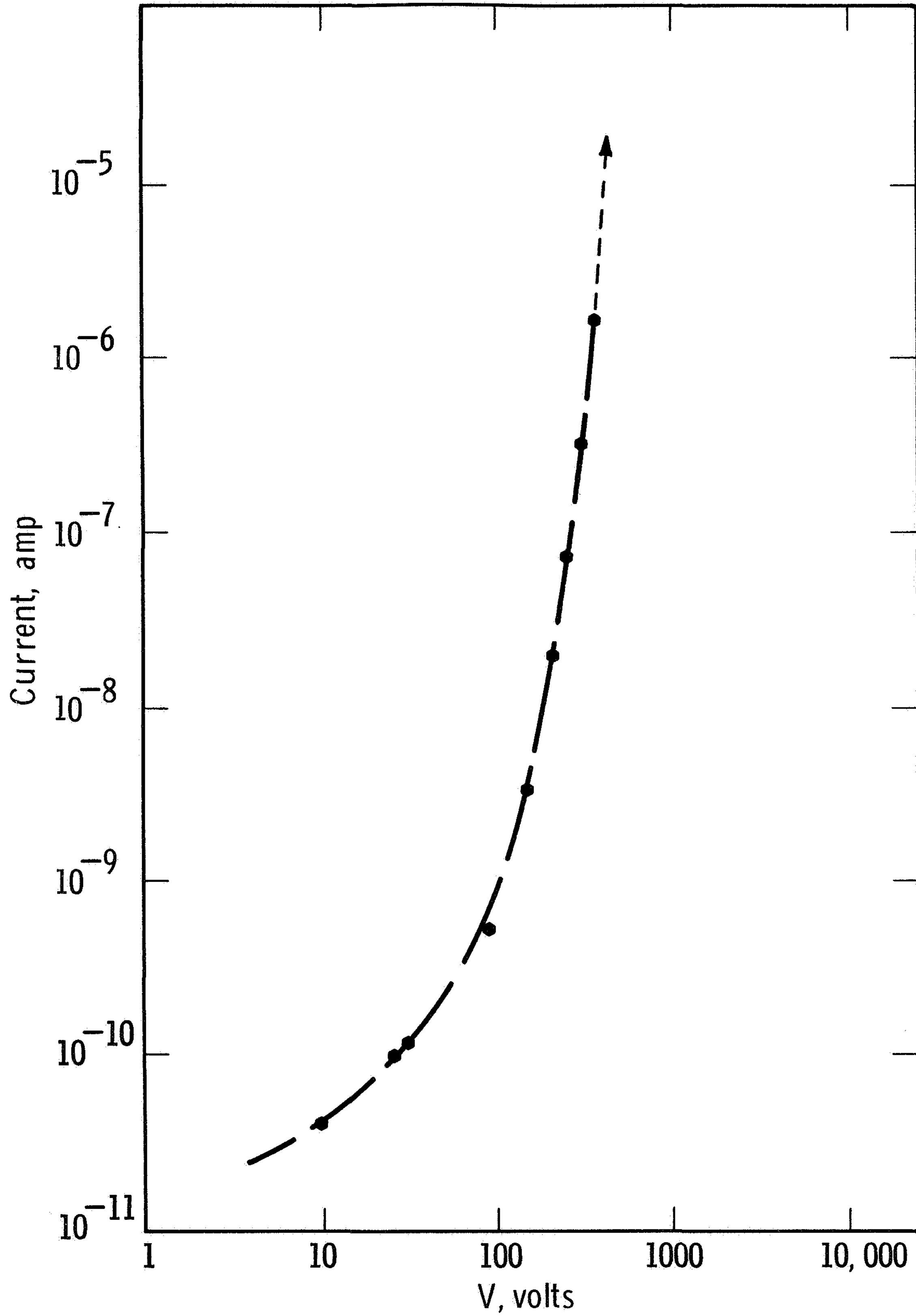

Fig. 33—Current-voltage data for Ta/AlN/Ta film sandwich structure, AlN film thickness 4000 A

Curve 587796-A

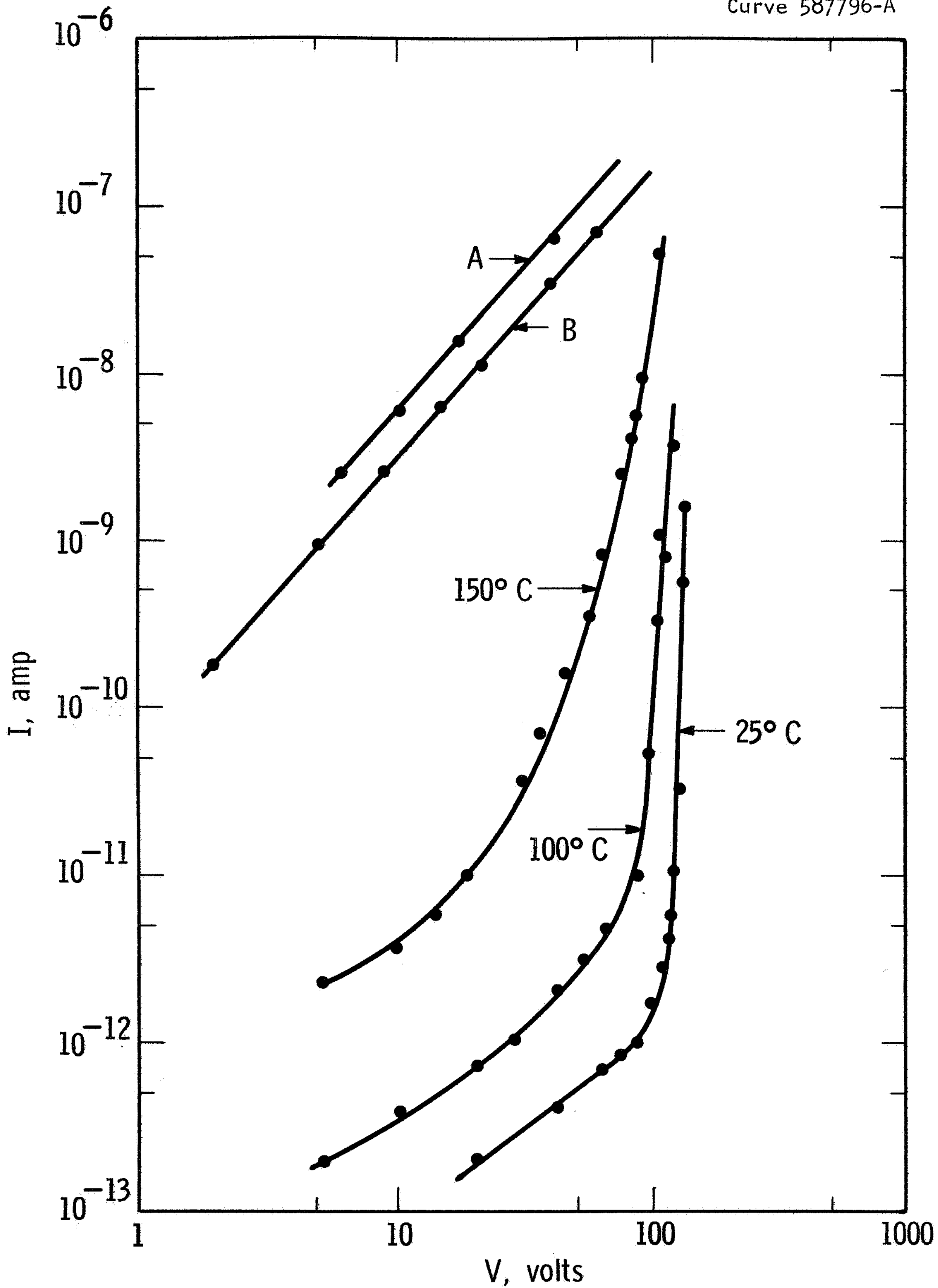

Fig. 34—I-V relationships of an AlN film at various temperatures. The dielectric is part of a Ta/AlN/Ta structure. AlN thickness is 4500 A

were approximately 4500 A. On raising the temperature, a progressive decrease in dc resistivity was observed. At 150°C, the rapidly rising current region is no longer prominent. The anticipated filling of traps and observance of reversible transition to a Child's type, square law I-V relationship, however, had not occurred even at an applied potential of 100 volts. At 150°C, and with 120 volts applied the square law dependence was finally observed but it had occurred irreversibly, Curve A, Fig. 34. Moreover, a 20 hr. anneal at 150°C of similar sandwiches with no applied voltage produced identical irreversible square law behaviors, Curve B, Fig. 34 (measured at room temperatures after anneal).

The mechanism which has produced the new I-V characteristic is, as yet, uncertain. In effect the behavior suggests that all traps are filled or no longer available. Diffusion of Ta from electrodes seems unlikely since the original deposition of AlN took place at 950°C (on one electrode). To test the possible effects of diffusion from a surface electrode, however, I-V measurements were made on several Al/AlN/Ta sandwiches, the Al being deposited on an unheated AlN film (thickness 6000 A). After a 20 hr., 220°C anneal, departure from the space-charge limited, trap-filled behavior was observed and is shown in Fig. 35. The curves, in fact, tend to resemble those produced by a 150°C anneal of the 4500 A Ta/AlN/Ta structure (Fig. 34). The specimens were then submitted to a further 60 hr., 220°C anneal. Both previously electroded and unelectroded regions were subsequently examined, the latter now receiving Al electrodes. These results are also incorporated in Fig. 35. The square law characteristic is not observed, possibly

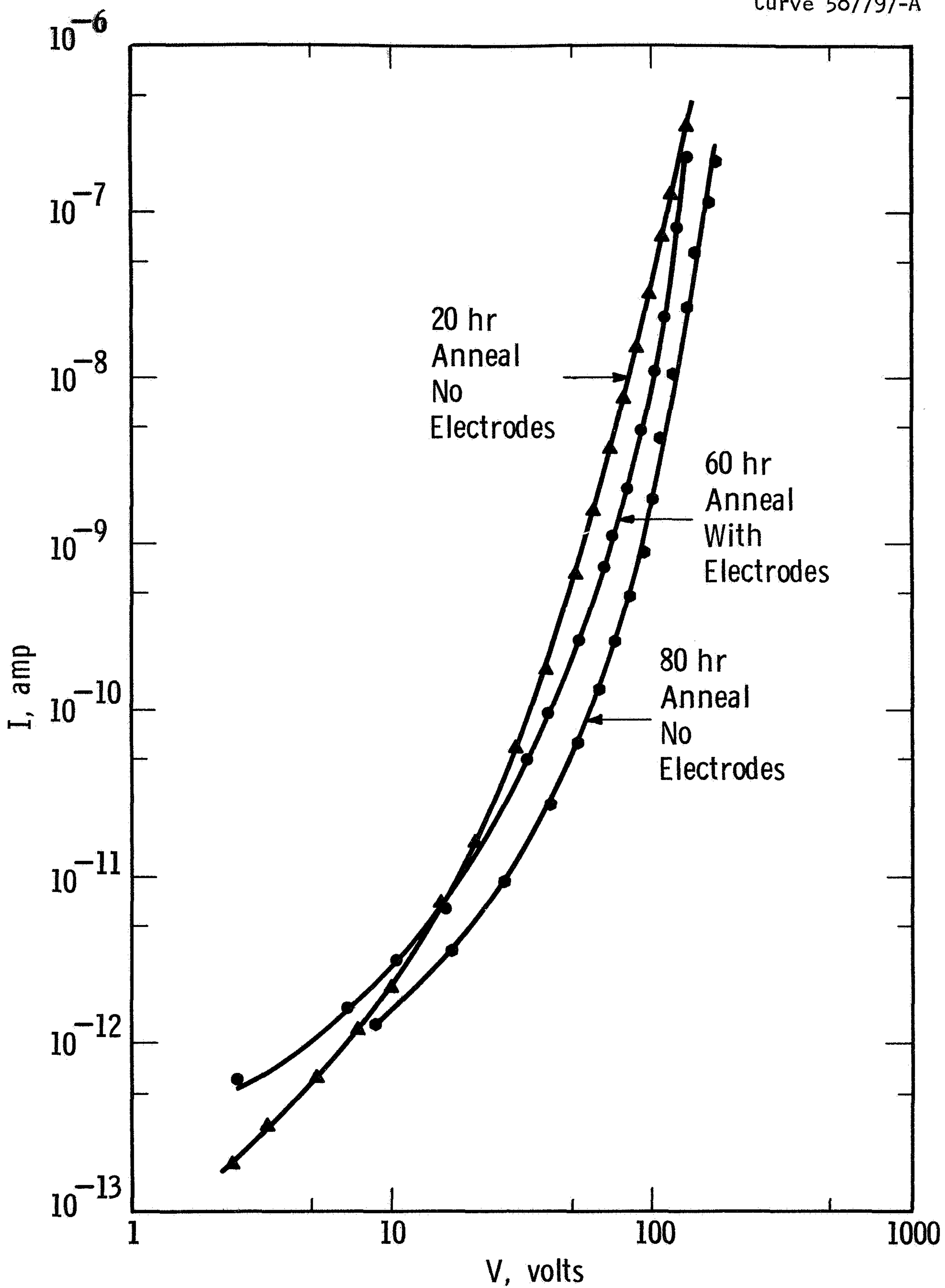

Fig. 35—I-V relationships of an AlN film for various annealing schedules. Annealing temperature is 220° C; AlN thickness is 6000 A

a higher temperature is required for the 6000 A AlN film. Diffusion seems even more unlikely, at this point, since unelectroded areas (during diffusion) showed similar behavior to previously electroded and annealed regions.

3.1.9 C-V Measurements - Capacitance-voltage studies, viz., those which relate some properties of MIS devices, were made on several AlN films sputtered onto silicon substrates.

The films fell into several categories, depending on the temperature at which they were deposited, and the technique used to heat them during the deposition. In an early series, in which substrates were heated resistively by passing current through the silicon, two films were prepared at 1000°C and 800°C respectively. The 1000°C sample did not suffer dielectric breakdown for voltages < 100 volts and the C-V study of this film is described below. The other (800°C) film broke down at ~ 4 volts, obviating any study of its C-V characteristics. Later sets of films were prepared on silicon substrates heated inside tantalum envelopes. For films held in envelopes at a nominal 800°, 900° or 1000°C temperatures, breakdown was observed at 5 to 15 volts when film thicknesses were less than 1500 A. When thicknesses exceeded 1500-2000 A, results were reproducible and similar to those for a dilute mixed nitride as shown in Fig. 39 of Sec. 3.4.4.

For the resistively heated film on which C-V measurements were made, the substrate was p-type, and the accumulation mode capacitance at large negative potentials across the sample (silicon grounded) varied from 3.0 to 3.9 picofarads as the AlN film thickness varied from the

the center of the sample to its edges. The AlN film dielectric constant calculated from these values lies between 8.0 and 9.4, which numbers bracket the published values. The uncertainty arises from the method used to determine the film thickness, that is, counting the interference fringes observed under monochromatic light. Dielectric loss in these 1000 A films was negligible at 100 kHz.

In the tracing of a typical C-V plot (Fig. 36), the bias voltage was swept from zero to +60 volts, then from +60 to -60 volts and back by a 0.025 Hz saw-tooth sweep generator.

On the initial sweep, from 0 to +60 volts, the capacitance of a typical unit was 2.4 pF, its lowest value. The capacitance remained at 2.4 pF on the sweep from +60 volts to about -25 volts, when it rose to 3.3 pF. This value was maintained as the sweep continued to -60 volts, and back to +30 volts when a decrease to 2.4 pF was observed. On continued sweeping, the point of increase in capacitance shifted from -25 to -37 volts, while the point of decrease remained at +30 volts. In all, the mid-point of the capacitance change, that is the voltage at which $C = \frac{3.3 + 2.4}{2} = 2.9$ pF, shifts by 75 volts with each sweep to $\pm$ 60 volts. Using the relationship given by Grove, et.al. (Ref. 35) to calculate the charge induced in the semiconductor by the charges in the dielectric, viz.,

$$\frac{Q_s'}{q} = \frac{(-V_{FB} + \phi_{ms})\ C_0}{1.6 \times 10^{-19}\ A} \qquad (9)$$

where Q_s' is the number of induced charges per unit area, V_{FB} is the flat-band voltage, C_0/A is the capacitance per unit area and ϕ_{ms} is the

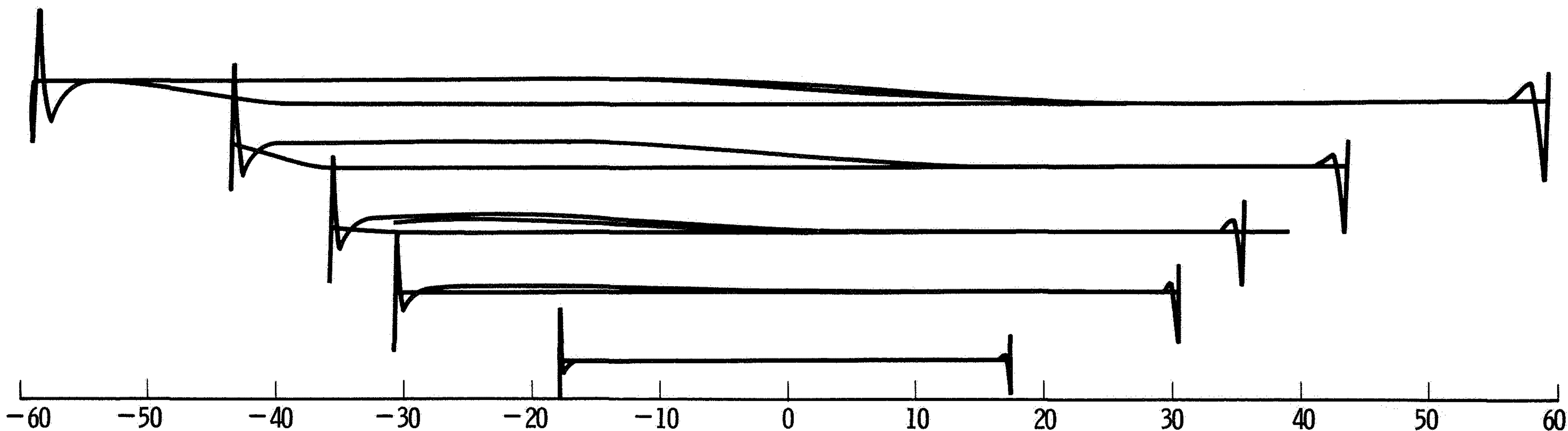

Fig. 36—Capacitance-voltage traces for Al-AlN-Si with varying sweep voltages. The transient at the end of the sweep is an instrumental artifact

metal-semiconductor work function difference (usually neglected), we note that a change of 7 x 10^{12} charges/cm^2 thus occurs in the surface state density with each sweep.

The sense of this hysteresis in the C-V behavior is that of ions moving in the oxide under the drive of the $\pm$ 60 volt sweep. Reduced sweep voltages generate smaller loops. Flat-band conditions occur at smaller voltages in both directions. Motion of ions of only a single charge type cannot account for the change of the flat-band voltage from large positive to large negative values: it is necessary that both positive and negative ions be present. An alternate explanation is that the AlN film is polarizable, and that the degree and direction of the polarization are determined by the sweep voltage.

In films prepared in heated Ta envelopes, deposits on p-type Si similarly display a charge associated movement with a change of bias. C-V data for films on n-type substrates are remarkably dissimilar showing no loop characteristic. A possible doping of the substrate surface, thus forming a p-type layer and junction, is believed influential in the suppressed characteristics of these films. Interposition of thin, thermally grown SiO_2 layers will be tried to alleviate the doping effect.

3.2 Reactively Sputtered AlN (Triode System)

During the course of the present investigation, it was noted that after a period of many hours the growth rate of AlN would decrease due presumably to the formation of a passivating layer of the compound

on the cathode. In a particular experiment, a drop in the N_2 partial pressure occurred inadvertently and was associated with a significant increase in the total sputtered AlN yield. The effective deposition rate in this experiment was, in fact, some five to six times greater than that normally observed.

Reference to an earlier work by Krikorian and Sneed (Ref. 36) on the reactive sputtering of Al_2O_3 suggested that both increased sputtering rates and a more highly oriented deposit might be obtained by using low partial pressures of oxygen (cited pressures necessary for epitaxy of stoichiometric films are between 10^{-5} and 2×10^{-5} torr). It is possible that similar effects might occur in the reactive sputtering of AlN. Exploration of such parameters in detail is a time consuming exercise in an ultra-high vacuum facility, however, since a wide range of growth temperatures of N_2 partial pressures should be studied. Therefore, it was decided that a systematic study of film structures and growth rates should be undertaken in a more flexible triode sputtering system capable of base pressures in the 10^{-7} torr range. Previous studies with such a system had indicated that both pure Al and AlN films could be deposited with this arrangement.

3.2.1 Preparation - The experimental arrangement basic to the supported discharge facility consists of a filament (tungsten wire), anode, target and grounded substrate support. The latter pair are positioned in a vertical plane parallel to one another. The target-substrate spacing is 4 cm. An axial magnetic field is applied parallel to the electron current which flows from the filament to the anode, and

helps to enhance the probability of ionizing collision in the target-substrate region. Sputtering is carried out by accelerating the ionized species, argon, onto a negatively biased (1500-2000 V) Al target.

Substrates are heated in Ta strip heater envelopes and the working arrangement permits sequential heating and exposure to the discharge of one of four substrates.

3.2.2 Composition and Growth Rate Evaluation - Some data obtained by electron and X-ray diffraction analyses which are representative of AlN films sputtered reactively in the triode sputtering facility are shown in Table VI. The sputtering voltage in all experiments except those marked with an asterisk was -1500 V. The marked values were prepared with the target at -2000 V.

Table VI Data for Triode Reactively Sputtered AlN Films

Temp. °C	N_2 Press. (torr)	Film Composition	Thickness (A)	Growth Rate (A/min)
300°C	5×10^{-5}	Al	3000 A	100
560°C	---	Al	1000 A	34
560°C	5×10^{-5}	Al	1000 A	34
560°C	10^{-5}	Al & AlN	1000 A	34
560°C	5×10^{-4}	AlN	3000 A	100
700°C	5×10^{-4}	AlN	2000 A	100
900°C	5×10^{-4}	AlN	3000 A	∿50
*800°C	5×10^{-4}	AlN	3000 A	100
*900°C	5×10^{-4}	AlN	1500 A	80

We assume that thickness and growth rates associated with deposition at 300°C reflect, to a fair approximation, the sputtering

rate of Al at -1500 V dc. Thus, the growth rates of AlN near 560°C seem to represent complete reaction of all incident Al atoms when the N_2 pressure exceeds 5 x 10^{-4} torr. At higher temperatures, a sticking factor correction must be accounted for.

Optical and electrical measurements were made on films deposited on vitreous silica substrates partly metallized with sputtered Ta electrodes (∿ 1000 A thick). The first set of four films (Z-270) were grown with target voltages of -1500 Vdc, a N_2 partial pressure of 5 x 10^{-4} torr and at temperatures which covered the range 600° to 900°C. For the second set (Z-271), the target voltage was altered, in this case being -2000 Vdc. Film thicknesses ranged from 1500 A to 3000 A. As judged from electron diffraction data, the film structures were, in all cases, consistent with that expected for pure AlN. No addition phase, e.g., Al, was detected. Both the degree of crystallinity and orientation, however, were observed to increase markedly as the substrate temperature was increased from 600° to 900°C.

3.2.3 Optical Properties - The optical absorption data for these films differed significantly from that obtained from AlN films prepared in a glow discharge environment. In the latter conditions, the partial pressures of Ar and N_2 were 80 x 10^{-3} and 5 x 10^{-3} torr, respectively. The triode sputtered films displayed a sharp absorption edge and irrespective of the substrate temperature (within the 600° to 900°C range) the position of the edge corresponded to an energy gap of 5.95 $\pm$ 0.5 ev (Fig. 37). It should be emphasized that these films were not subjected to a N_2 anneal yet displayed the bulk AlN optical spectrum in the

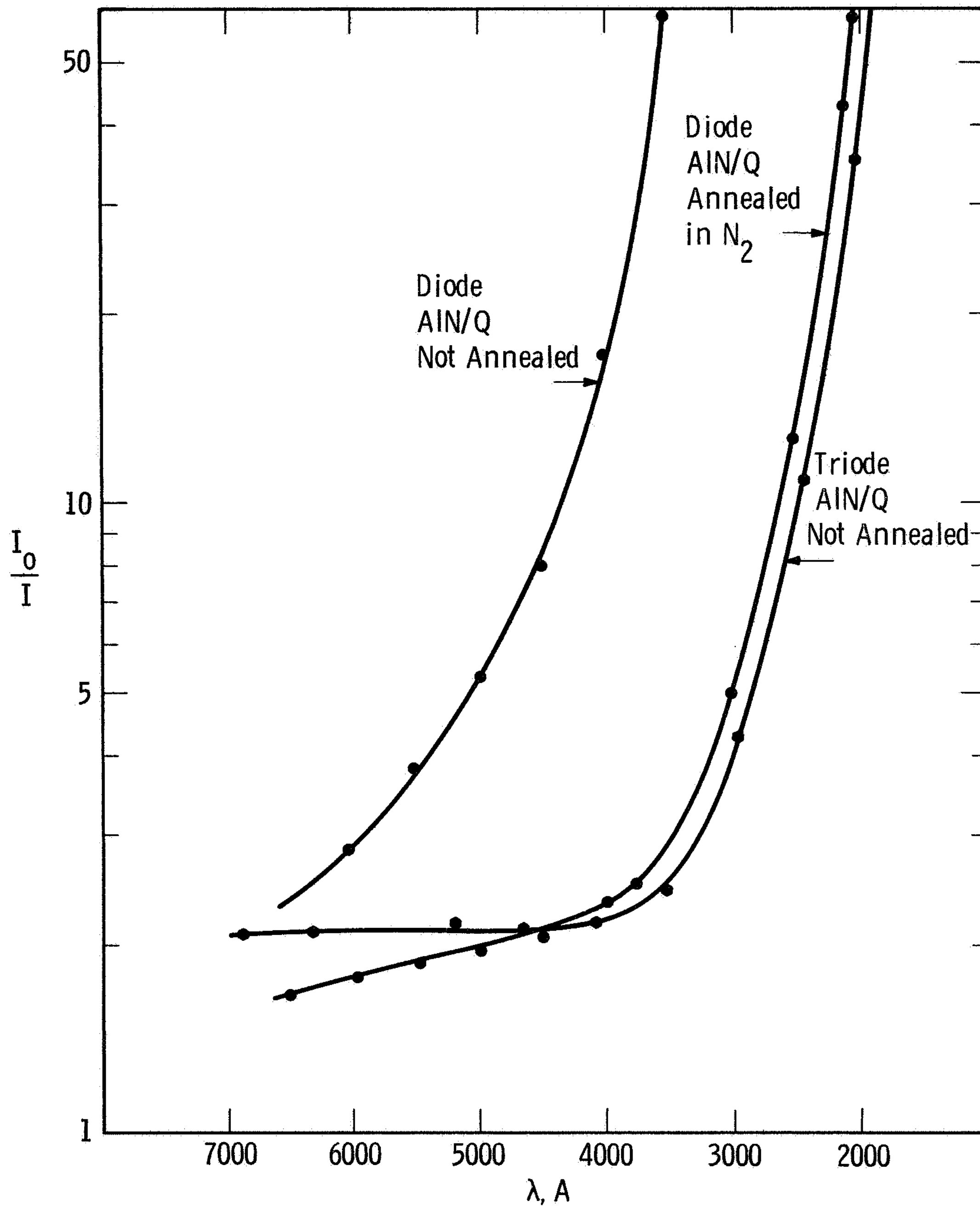

Fig. 37—Optical absorption in three AlN films deposited on vitreous silica, two having been prepared by diode reactive sputtering, the third by triode reactive sputtering. The shift toward higher wavelength for the unannealed diode-prepared film is likely due to a N_2 deficiency in the film. The triode prepared film does not suffer in a like manner

as-deposited condition. This behavior had not been evident in the glow discharge deposited films which, as-deposited, showed significant shifts of the absorption edge to lower energies.

3.2.4 Electrical Measurements - Test results from experimental capacitor configurations, i.e., films fitted with 0.3 mm evaporated Al counterelectrodes, indicated that even for films only 1400 A thick, the dielectric loss was low, lying typically at about .02 at 500 Hz, decreasing to .003 at 1 kHz and becoming less than .001 at frequencies greater than 5 kHz. The dielectric constant showed no perceptible dispersion with frequency and capacitances of 50 picofarads were measured.

The behavior of the very thin films on application of dc fields was far less erratic than for some of comparable thickness prepared by glow discharge sputtering. The I-V data showed conduction consistent with a space-charge limited mechanism with breakdown occurring at about 35 to 60 Vdc corresponding to breakdown fields greater than 3×10^6 v/cm. Room temperature, dc resistivities measured with an applied field of 3×10^5 v/cm were approximately 10^{13} ohm-cm.

Several AlN films of two thicknesses, $\sim$ 1000 A and 3000 A, were deposited on both n- and p-type Si substrates. MIS measurements (at 1 MHz) revealed that the former were leaky and suffered breakdown at applied fields of approximately 3×10^6 v/cm. The latter, however, exhibited a behavior not unlike that reported for nitride films prepared by diode reactive sputtering. The hysteretic behavior indicates the movement of charge in the dielectric on the p-type substrate. Measurements carried out for an identical film on an n-type substrate were, again similar to those for the diode sputtered nitride, apparently insensitive to any movement of charge.

3.3 Mixed Al-Si Nitrides

The dielectric properties of diode sputtered AlN films show them to be good, low loss insulators, at least in a thickness range which exceeds 1500 A. (The lower thickness limit for triode sputtered films is approximately 1000 A.) Use as an insulator at lower thicknesses is impeded presumably by grain boundary conduction phenomena since AlN, unlike several other insulating films used in electronic components, is deposited in a crystalline form. Suppression of this crystalline state by the lowering of substrate temperatures has not been successful.

Some effort, therefore, has been directed in bringing about a reduction in film crystallinity (an increase in atomic disorder) by attempting to prepare mixed nitrides of the form AlN-Si_3N_4, the latter component being known to adopt an amorphous film structure.

3.3.1 Preparation - Preparation of two sets of films, with nominal Al:Si ratios of 6:1 and 1:1, has been accomplished to date. The ratios cited are related to the target areas of the respective elements and do not necessarily indicate the true compositions of the films. Electron microprobe analyses of the films will be made as part of the continuing study. Films were deposited in the optimized conditions used for the diode sputtering of pure AlN (see Sec. 3.1.1). Substrates included Ta coated vitreous silica and n- and p-type Si wafers.

3.3.2 Structural and Optical Properties - When films prepared by sputtering a cathode with a 6:1::Al:Si area were examined by electron diffraction, it appeared to consist primarily of a polycrystalline AlN-type phase, Fig. 38. The diffraction data, however, showed some

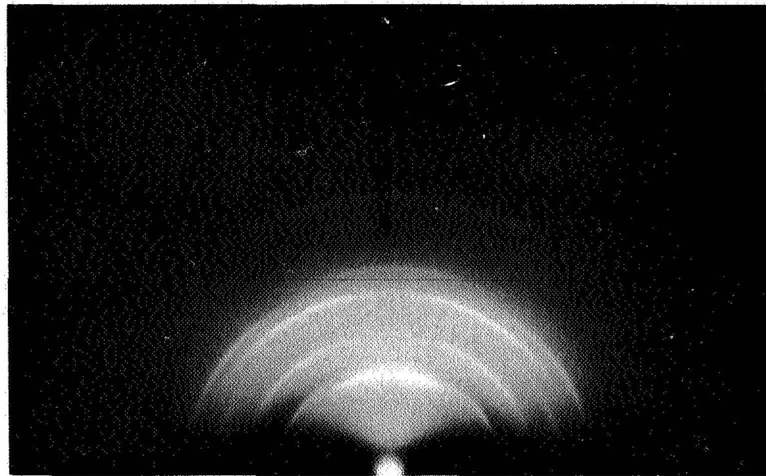

Fig. 38—Electron diffraction pattern of mixed $AlN\text{-}Si_3N_4$ film. Substrate temperature, 900°C; thickness 6000 A

evidence of an additional component, one which caused diffuse scattering of diffracted electrons. When the 1:1::Al:Si target was used, the diffuse diffraction component became far more prominent. The partly resolved diffraction rings which were measured, however, indicated that a phase consistent with poorly crystallized AlN was still present.

Optical absorption measurements were made on both sets of AlN-Si_3N_4 films. The as-deposited films showed a diffuse absorption edge occurring in the approximate wavelength range as for pure, as-deposited, AlN films. Annealing at 900°C in N_2 caused a sharpening of the edge and a shift to higher energies, again in a manner similar to that for annealed AlN films.

While the shift for the 6:1::Al:Si nitride films matched that for the pure form, the edge for the 1:1::Al:Si nitride films shifted to energies greater than 5.9 eV, viz., to an absorption edge value of approximately 6.35 eV. The effect is unexpected since the energy gap of the added component, Si_3N_4, is reported to be 4.35 eV (Ref. 37). Other studies, however, have recorded conflicting values, e.g., 5.0 eV (Ref. 38) and 6.35 eV (Ref. 39).

3.3.3 Electrical Measurements - The results of capacitance vs voltage measurements at 1 MHz made for deposits on the Si substrates are shown in Fig. 39. The sandwich configuration, after Al counterelectrodes have been deposited is that of a MIS (metal-insulator-semiconductor) structure.

The symmetrical shift of the C-V plot for films deposited on p-type substrates indicates that a polarization effect probably is generated within the dielectric by the application of a field; such an effect is observed in the pure AlN films (see Sec. 3.1.9) and has also

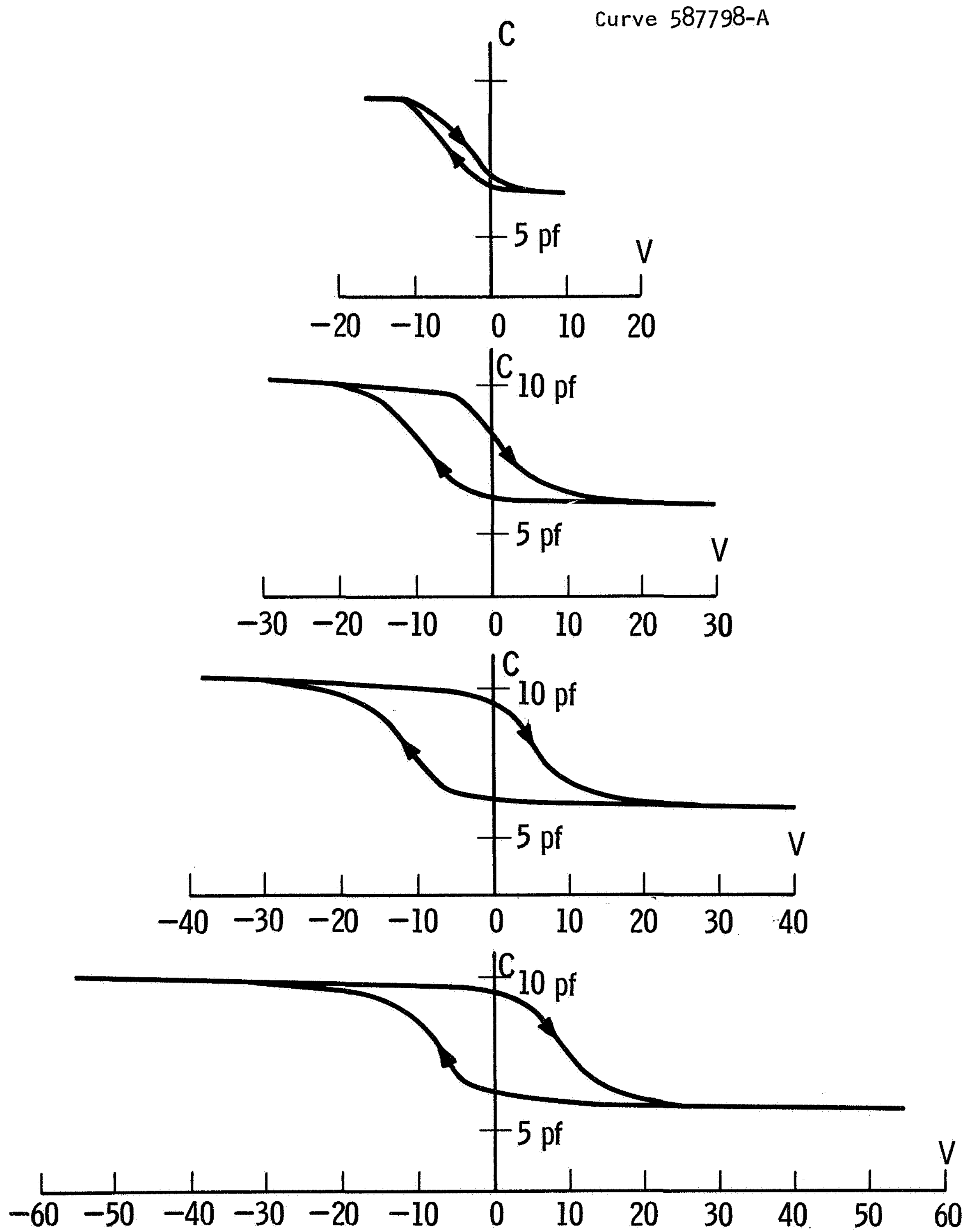

Fig. 39—Dielectric polarization effect observed in mixed AlN-Si_3N_4 films. Film thickness is approximately 4500 A

been observed in Si_3N_4 (Ref. 40). As for the pure AlN films, the polarization may be due to the orientation of dipoles in the AlN component by the applied field or by a stress-induced polarization inherent in it (AlN is strongly piezoelectric). The charge induced in the Si by the charges contained in the dielectric is $8.75 \times 10^{11}/cm^2$, a value intermediate between those reported for vapor deposited Si_3N_4 and SiO_2.

Deposits on n-type substrates showed no tendency to display loop-type characteristics, the flat band voltage exceeding 100 V.

Measurements relating current and voltage characteristics in the 6:1::Al:Si nitride films were essentially similar to those made on the pure nitride films, viz., currents followed an Ohmic behavior at low voltage then rose steeply as the voltage was increased; a further voltage increment induced a time dependent instability followed by breakdown or a major change in the I-V characteristic.

In the 1:1::Al:Si nitride films, however, a reproducible and highly stable I-V behavior was followed, Fig. 40. The slopes of the curves at the low and high voltage values represent Ohmic and trap-filled space-charge behavior, respectively. The voltage at which the transition between the main conduction mechanisms occurred, the traps-filled-limit, was low ($\sim$ 10 V) relative to the values for pure AlN films. In addition, the slope of this transition was less steep and suggests that fewer but probably more active traps take part in conduction. Although the I-V characteristics of the 1:1 mixed nitride films were stabilized by the mixing, dielectric measurements showed a range of dispersion with frequency. The dielectric properties of pure Si_3N_4 are unfortunately not well characterized at various frequencies. Several reports list

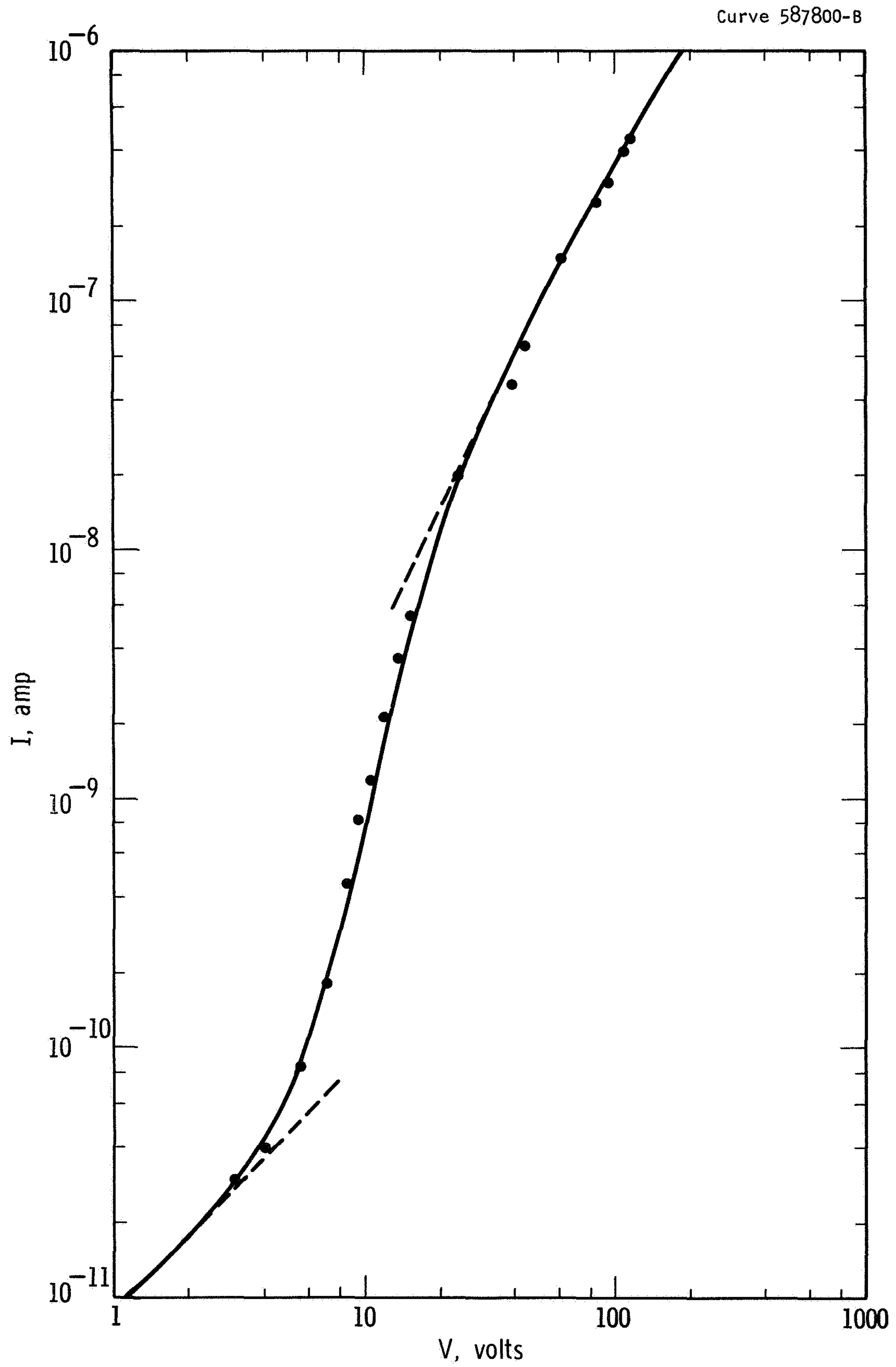

Fig. 40—I-V data for mixed $AlN-Si_3N_4$ film. Cathode Al:Si ratio is approximately 1:1

conflicting values of dielectric constant, e.g. 12.0 (Ref. 41) and 6.2-8.5 (Ref. 42) but this property seems to be strongly influenced by the density of the deposited layers and the given values seem only relative to this property. We suggest that both the conduction behavior and frequency dispersion of the dielectric properties are attributable to a modification of the numbers and levels of trapping, or impurity sites, relative to those operative in sputtered AlN films.

The 6:1::Al:Si nitride layers displayed no obvious dispersion with frequency showing, rather, dielectric properties similar to those of undiluted AlN.

3.4 Reactively Sputtered BN

A second nitride solid solution system (in the film form) now under investigation is AlN-BN, the interest in the latter component stemming from high temperature stability properties of the bulk compound (sublimation at 3000°C in pure form, Ref. 43). Prior to study of the mixed system, efforts were made to grow and characterize pure films of BN.

3.4.1 Preparation - The uhv, diode sputtering apparatus used for the preparation of AlN was modified only slightly. A cathode was fabricated by imbedding slices of bulk boron (99.9999) into a, "research grade", BN block. The combined surface area of the imbedded boron slices was approximately 5 cm^2. It was noted that with an applied voltage of -2800 Vdc, a current density of 4 ma/cm^2, a target-substrate spacing of 5 cm, and a substrate temperature of 1000°C, films could be formed at growth rates of 10 A/min.

3.4.2 Structures - Initial structure investigations via reflection electron diffraction showed a micro-crystalline pattern which could not immediately be indexed on the normal hexagonal bulk structures. Further deposits on Si, were examined by a transmission electron diffraction technique and the results are shown in Figs. 41 and 42. The variation in preparative temperature was introduced to note its influence on film structure and stoichiometry. As can be seen in the diffraction patterns, no differences due to temperature are evident. Using the diffraction spots (included with the diffraction rings for the unheated films and due to scattering from surrounding areas of the single crystal Si(100) substrate) for calibration, the transmission data can be indexed on a hexagonal cell with the following parameters.

$$a = 2.45 \quad , \quad c = 6.88 \text{ Å}$$

When compared to the bulk values (Ref. 44) for the hexagonal form, viz.,

$$a = 2.51 \quad , \quad c = 6.66 \text{ Å}$$

we note the difference to be of the order of 2-4%. The source of this deviation in the thin film lattice parameters is not known, but it appears possible that it may be associated with structural disorder, non-stoichiometry or the occlusion of trapped argon. A list of d-values and relative intensities are given for the bulk and thin film forms in Table VII.

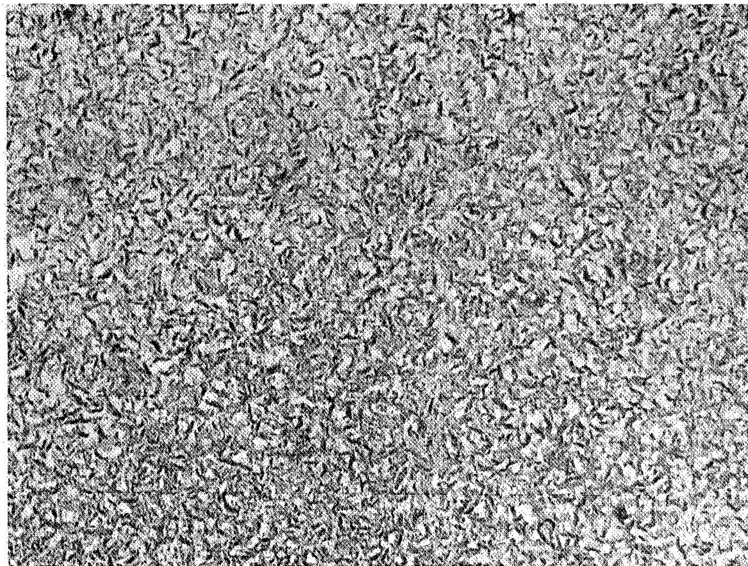

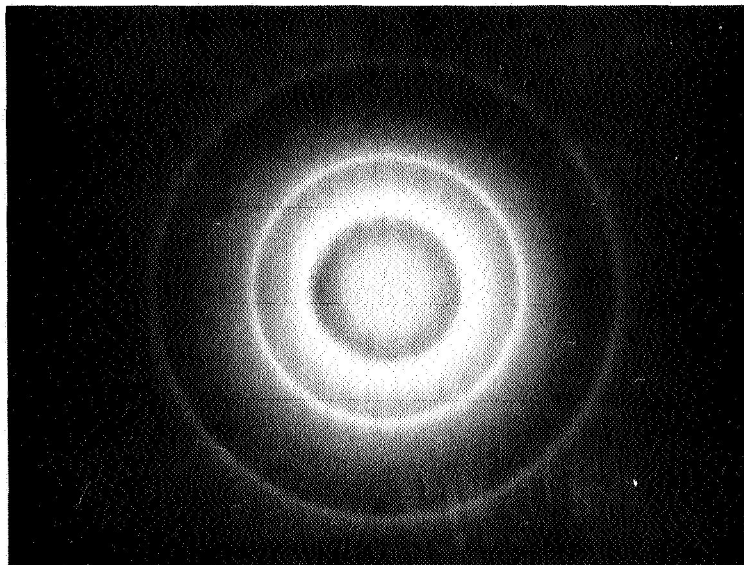

Fig. 41—Electron micrograph and selected area diffraction pattern from reactively sputtered BN film deposited on heated (800°C) Si substrate

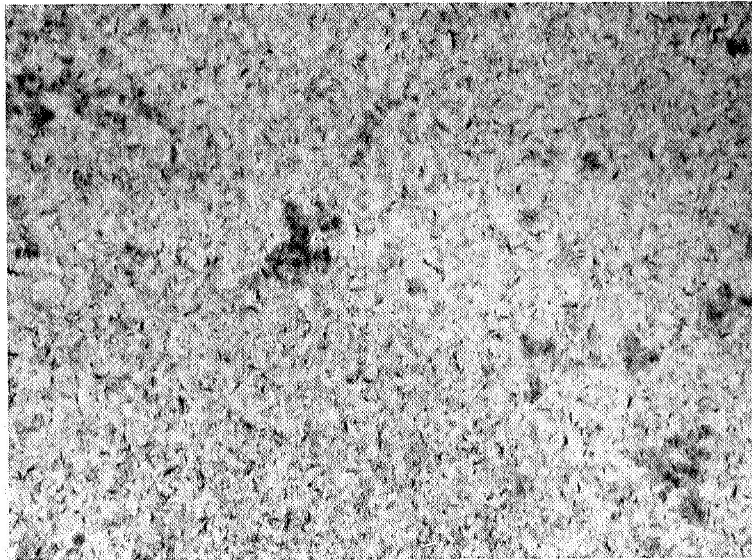

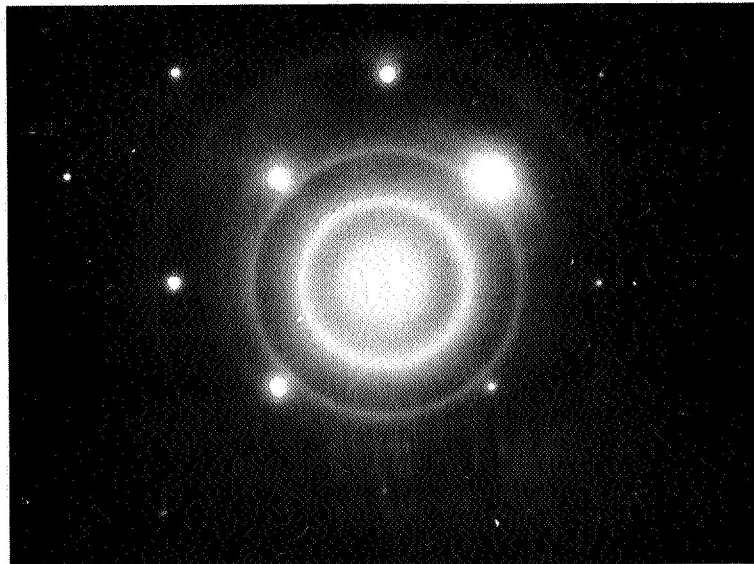

Fig. 42—Electron micrograph and selected area diffraction pattern from reactively sputtered BN film deposited on unheated Si substrate

Table VII   Diffraction Data for BN

BN (bulk)			BN (film)		
d(A)	I	(hk.1)	d(A)	I	(hk.1)
3.33	vs	00.2	3.48	vs	00.2
2.17	m	10.0	2.12	m	10.0
2.06	w	10.1			
1.82	m	10.2			
1.67	w	00.4	1.72	w	00.4
1.55	vw	10.3			
1.32	vw	10.4			
1.25	w	11.0	1.23	mw	11.0
1.17	w	11.2			
1.14	vvw	10.5			
1.11	vw	00.6	1.16		00.6
1.08	vw	20.0	1.06	vw	20.0
a = 2.51 c = 6.66			a = 2.45 c = 6.88		

3.4.3 Optical and Electrical Data - The optical absorption spectra for two BN films, deposited on vitreous silica substrates, under similar sputtering conditions is shown in Fig. 43. The apparent absorption edge for an unannealed film lies near 5.2 eV although an earlier film gave a value nearer to 4.8 eV. The film which was annealed at 800°C in N_2 shows a moderate shift of band edge toward higher energies, viz. 5.6 eV. The calculated direct band gap for the bulk hexagonal form is 7.53 eV (Ref. 45).

Measurement of dielectric constant and loss over a range of frequencies is given in Table VIII.

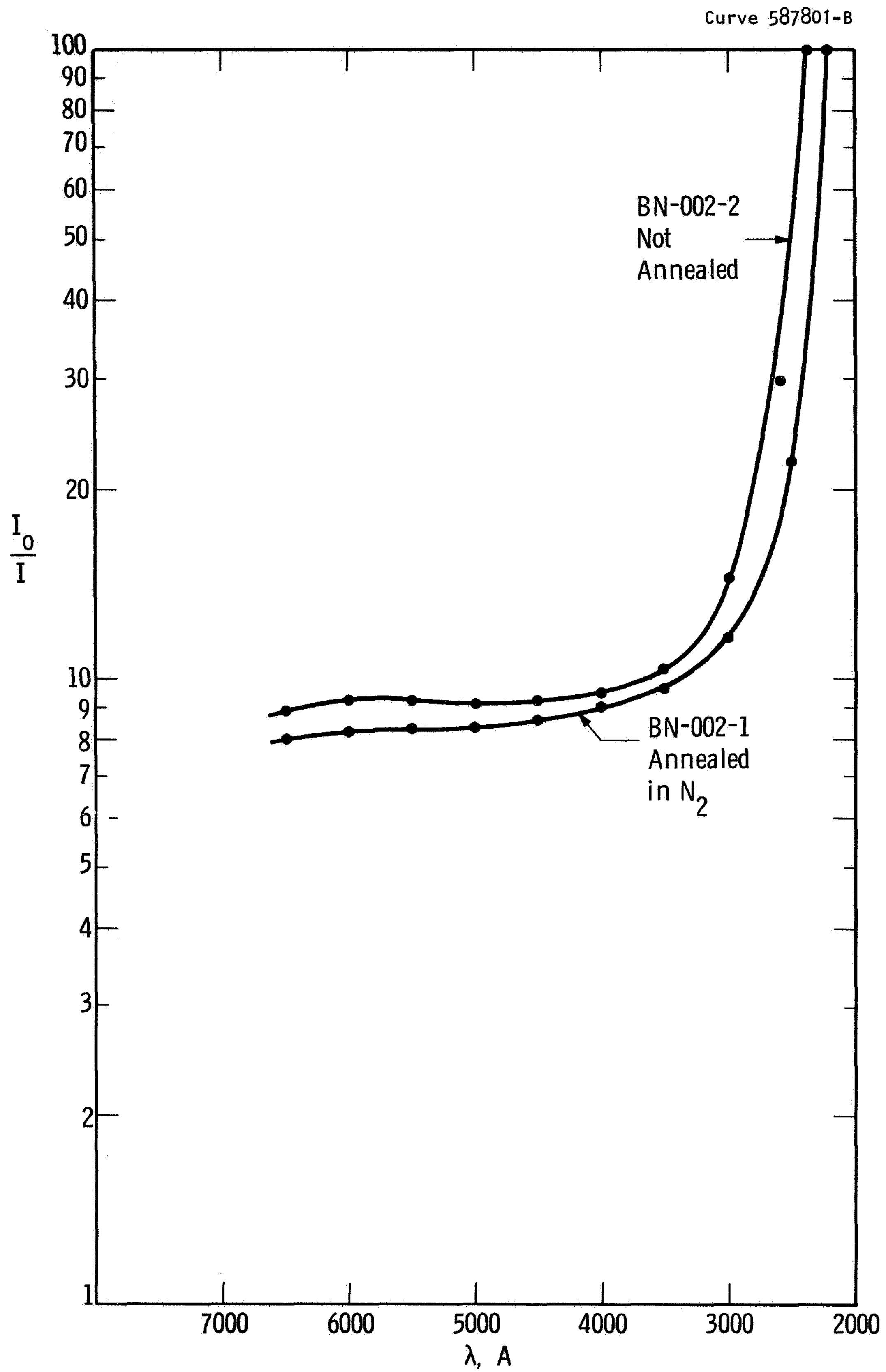

Fig. 43—Optical absorption data for two BN films deposited under similar sputtering conditions. BN-002-1 was annealed in pure N_2. Note the slight shift to shorter wavelength (higher energy)

Table VIII Dielectric Data for Reactively Sputtered BN Films

f(kHz)	0.5	1	2	5	10	20	50	100
K	3.9	3.9	3.8	3.8	3.8	3.8	3.75	3.5
D	.05	.02	.002	---	---	---	---	---

The reported value for the dielectric constant of bulk BN (hexagonal) is 5.12 (Ref. 46), a value for pyrolytic BN is 3.8 $\pm$ 0.2 (Ref. 48).

The wide range of absorption edge values and the altered dimensions of the basic hexagonal cell, when considered in relation to the previous results for AlN films, indicate that the sputtering ambient plays an important part in determining the properties of reactively sputtered BN films. Further studies before studying mixed Al-BN system will be devoted to (1) exploring more fully, the effects of annealing schedule and temperature and (2) preparing BN films by triode reactive sputtering.

3.5 Discussion

The excellent chemical stability of the reactively sputtered AlN films enabled a wide variety of measurements to be performed on these specimens. Included were X-ray and electron diffraction studies, optical absorption measurements, resistivity, capacitance and I-V measurements over a range of temperatures and the observation of MIS characteristics.

Since the films comprised oriented arrays of small crystals, it is perhaps not surprising that the observed properties bear some

resemblance to both bulk polycrystalline and single crystal characteristics. In general, the resemblance is strongest where compared to the latter. Structurally, films are found to adopt the hexagonal wurtzite structure of the bulk compound. However, an anomaly is noted in the optical absorption spectrum of films as deposited by diode reactive sputtering, viz., a shift of the absorption edge to lower energies. An analogous effect had been reported by Cox, et al. (Ref. 1) for argon-annealed bulk single crystals and explained as due to the formation or injection of nitrogen vacancies. By annealing in pure nitrogen, at temperatures near the temperature of deposition, the sputtered films can be made to dksplay bulk optical properties, thus appearing to corroborate the mechanism proposed by Cox, et al. That a surplus of argon should be occluded in the AlN film is not surprising since the argon to nitrogen ratio is of the order of 16:1. Films deposited by a triode reactive sputtering technique show no obvious shift of the absorption edge. The argon to nitrogen ratio in this instance is reduced to approximately 1:1.

Room temperature values of dielectric constant observed for the films correspond to those for pressed, sintered, bulk, polycrystalline forms (data for single crystals were unavailable). The dielectric constant, however, shows far smaller variation with temperature (up to 350°C) than is reported for bulk AlN. The dielectric loss characteristics followed a similar trend and both results seem indicative of a material less subject to the presence of conducting impurities. Although the films displayed excellent dielectric properties, it was possible to induce

significant conduction in them by the application of a high electric field (> 10^6 V/cm). The conduction behavior resembles that observed in single crystals (Ref. 33), viz., a space-charge limited current which is influenced by the presence of traps in the insulator. The correspondence, however, is not exact, and instabilities arise when high voltages are applied. Either breakdown or the adoption of a new "reversible" I-V characteristic usually is observed. The former could be attributed to leakage and eventual breakdown along grain boundaries. The latter property is unaccounted for but, in effect, represents the permanent filling of all traps.

Introduction, by co-sputtering, of Si_3N_4 into the AlN films appears to impart an amorphous character to them. However, the electron diffraction evidence, although inconclusive, suggests that the mixed films may have adopted a two-phase structure, comprising a microcrystalline AlN-type component and an amorphous Si_3N_4-type component.

Our preliminary evaluation of pure AlN and a dilute mixture of AlN-Si_3N_4 (cathode Al:Si ratio 6:1) as the insulating layer in MIS structures, indicates that these layers behave essentially in a similar fashion and show the presence of a considerable polarization effect, the degree and direction of which are determined by the applied bias voltage. Reported piezoelectric properties (Ref. 47) suggest that polarization is stress induced in the AlN. However, both the piezoelectric behavior of oriented AlN films and the MIS behavior of mixed films of varying proportions require further investigation in order to clarify the MIS results.

The I-V behavior of films still richer in Si_3N_4 (Al:Si::1:1) differs from that of the pure AlN material in several respects. Thus, a reversible characteristic fully consistent with space-charge limited conduction in an insulator with traps is obtained and the dielectric constant and dissipation factor show a greatly enhanced frequency dispersion. The former effect, is characterized by a low voltage ($\sim$ 10 V) traps-filled limit and a more gradual transition between the high and low voltage conduction mechanisms than was noted for the pure AlN films. Such behavior suggests the operation of fewer but more active traps. The interpretation of the dielectric constant values (Ref. 41, 42), presumably due to density differences induced by deposition parameters, have been observed but no reference to a systematic study over a range of frequencies has been found. It seems possible that both the modified conduction behavior and frequency dispersion of dielectric properties are attributable to a change in number and level of traps or impurity sites in the film structure. The nature of these sites remains speculative, however, but may include voids or isolated islands of Al, Si, AlN or Si_3N_4 in an overall matrix. The experience with triode sputtering in the reduction of argon inclusions in pure AlN suggests that this method might advantageously be used in the preparation of mixed films of more uniform composition.

The results obtained in our preliminary study of sputtered BN films are encouraging in that the film products possess excellent dielectric properties comparable with, or superior to, those found for AlN films. As with the AlN films, it appears that the optical properties may be sensitive to argon occlusion. However, in view of the few

results yet available, it would be premature to discuss this effect, or the anomalous distortion of the hexagonal film structure (cf. bulk parameters - Sec. 3.4.2) at this stage.

4. CONCLUSIONS AND FUTURE PLANS

4.1 Conclusions

4.1.1 - Evaporated films of AlAs and AlP have been prepared for the first time and the conditions of deposition leading to stoichiometric compositions have been defined. These conditions differ from those used for other III-V compound films due to the high decomposition temperatures of the Al-compounds.

4.1.2 - The structural and optical properties of the vacuum deposited AlSb, AlAs and AlP films agree with corresponding bulk properties. These properties degrade rapidly, however, when the films are exposed to air and water vapor environments.

4.1.3 - Resistivities measured in the antimonide, arsenide and phosphide, before film deterioration were comparable to bulk values. Mobilities, however, were very low and were attributed to the many grain boundaries inherent in films made up of small crystallites. This fact, as well as the difficulty experienced in producing epitaxial structures, render films grown by vacuum deposition unsuitable for the manufacture of junctions.

4.1.4 - Films of AlN have been sputtered for the first time in residual ultra-high vacuum conditions. Highly oriented deposits were prepared on amorphous substrates and partially epitaxial deposits on single crystal substrates.

4.1.5 - The structural, electrical, and dielectric properties of AlN films compared favorably to those of bulk polycrystalline and single-crystal material. The dielectric properties, in fact, seemed to surpass

those of sintered, polycrystalline AlN, in regard to dielectric loss and behavior at high temperature.

4.1.6 - An anomalous shift to lower energies in the position of the optical absorption edge for as-deposited films could be removed by annealing in N_2. As-deposited films were believed to contain occluded argon which gave rise to the shift. A similar effect had been reported for argon annealed bulk single crystals.

4.1.7 - Films of a mixed AlN-Si_3N_4 composition were deposited by the diode reactive sputtering of an Al-Si cathode of variable composition. Dilute mixtures retained properties similar to those observed for pure AlN. Deposits in which the Al-Si ratio was almost unity were partly amorphous (probably two-phase) and displayed a space-charge limited I-V characteristic. The dielectric properties of these films were frequency dependent, an undesireable characteristic. (Although these properties are representative of the films, they may also reflect some inherent features peculiar to the mode of deposition, e.g., argon occlusion. A more conclusive representation of film properties will require study of comparable film structures deposited by triode reactive sputtering.)

4.1.8 - Boron nitride (BN) films have been prepared by diode reactive sputtering and show some dielectric properties comparable to or superior to those of AlN. The thin film structure is not completely consistent with that of the bulk, adopting a hexagonal structure but with slightly modified lattice constants.

4.2 Future Plans

The forthcoming effort will be directed towards making a complete evaluation of the preparation and dielectric properties of AlN

films, and of other film compositions based on AlN, in relation to their application in solid state devices. Two primary device areas will be considered, i.e. MIS-type structures based on silicon, and transducer delay-line structures. A key objective of the study is the preparation of amorphous AlN-type film structures (e.g. in mixtures of the type AlN-Si_3N_4) for MIS application, and crystalline, highly-oriented films (e.g. pure AlN or AlN-BN mixtures) for transducer applications. The work we seek to accomplished is as follows:

4.2.1 - To deposit films of pure aluminum nitride AlN and of solid solutions of type type AlN-Si_3N_4 and AlN-BN on a variety of chemically inert substrates including silicon, vitreous silica, sapphire, and metal-film electroded substrates, at thicknesses in the range up to 4 microns. The techniques to be employed for film deposition will include both reactive and r-f. sputtering. Experimental conditions needed for optimum film growth rates and for epitaxial growth (in the case of AlN and the AlN-BN solid solutions) would be established.

4.2.2 - The crystallographic structure of the films will be evaluated by means of electron and X-ray diffraction and, in the case of films deposited on silicon, by transmission electron microscopy. The degree of crystallinity of the films will be established and their perfection of orientation graded in a semi-quantitative fashion using criteria such as widths of diffraction arcs. In the case of solid solutions, lattice parameter measurements are to be made and correlated with chemical analysis performed by electron microprobe or other appropriate techniques. Special attention will be paid to determining if solid-solution compositions form within the range in which an amorphous film structure is stabilized.

4.2.3 - Dielectric measurements will be performed on those films deposited on metallized substrates, in order to determine resistivity, capacitance, dissipation factor and the frequency dependence of these at frequencies up to 1 MHz. Breakdown strengths will be measured for all film compositions produced and the lowest film thickness at which the film is electrically stable under fields approaching the nominal breakdown strength would be established. Current-voltage characteristics will be measured in air and in vacuo to assess conductivity under high fields and to evaluate the role of electrode metals in possible barrier effects, and of ambient atmosphere in influencing film conductivity. These measurements will be made at different temperatures to test the validity of various possible conduction models. The temperature-dependence of permittivity, dissipation factor and resistivity will be measured in the range - 196 t0 500°C for each film composition studied.

4.2.4 - Films of pure AlN and of mixed nitrides (particularly those with amorphous structures) which have been deposited on silicon will be characterized electrically to evaluate their MIS behavior. Capacitance-voltage evaluation of metal-insulator silicon units will be made at 1 MHz to assess the charge behavior of mixed composition films of the type $AlN-Si_3N_4$. The films will be deposited on bare and oxide coated silicon substrates of appropriate resistivity. The surface state density will be evaluated for various film compositions, deposition temperatures and annealing schedules. Bias-temperature stress tests will be made over a temperature range of -196°C to 300°C. Results will be analyzed for

indications of ionic, injection-trapping or internal polarization effects. Correlations with conduction behavior will be made as applicable.

4.2.5 - A study will be made of the piezoelectric properties of AlN films with a view to their use as microwave acoustic transducers for bulk and surface wave delay lines. The electromechanical coupling coefficients of film-deposited on to Al_2O_3 and silicon single crystal delay lines will be measured and compared with those for ZnO, CdS and ZnS films using microwave pulse techniques. Measurements will be made to determine the piezoelectric constants needed for both compressional and shear wave generation. These studies will be performed on both fiber-textured and epitaxial films of pure AlN and on similar mixed with Si_3N_4 or BN. Measurements on epitaxial films will receive special emphasis since these would provide important information on shear mechanical energy conversion. Film thicknesses typically in the range 2000 A to 2 microns will be used, corresponding to a microwave frequency range from 1 to 10 GHz.

5. REFERENCES

1. Cox, G. A., Cummins, D. O., Kawabe, K. and Tredgold, R. H., J. Phys. Chem. Solids, 28, 1967, p. 543.

2. Grimmeiss, H. G., Kischio, W. and Rabenau, A., Phys. and Chem. of Solids, 16, 1960, p. 302-9.

3. Moss, T. S., Photoconduction in III-V Compounds. Semiconductors and Semimetals, Vol. 2 of Physics of III-V Compounds, Chap. 9, Sec. 11, Willardson, R. K. and Beer, A. C., ed., Academic Press (New York), 1966, p. 235.

4. Braunstein, R. and Kane, E. O., J. Phys. Chem. Solids, 23, 1962, p. 1423.

5. Reid, F. J., Miller, S. E., Goering, H. L., J. Electrochem. Soc., 113, 1966, p. 467.

6. Pastrnak, J. and Souckova, L., Phys. Stat. Solidi, 3, 1963, p. 71.

7. Chu, T. L., Ing. D. W. and Noreika, A. J., Solid-State Electron., 10, 1967, p. 1023-27.

8. Presnov, V. A. and Synorov, V. F., Zh.tekhn. fiz., 27, 1957, p. 123.

9. Sorokin, G. P., Izv. Vys. Uchebn. Zavedenii, Khim. tekhnol., 5, 1962, p. 407-12.

10. Johnson, J. E., J. Appl. Phys. 36, 1965, p. 3193.

11. David, J. P., Capella, L., Laude, L. and Martinuzzi, S., Rev. de Phys. Appl. 1, 1966, p. 172.

12. Gunther, K. G.: Compound Semiconductors. Willardson, R. K. and Goering, H. L., ed., Rheinhold (New York), 1962, p. 313.

13. Davey, J. E., J. Appl. Phys. 32, 1960, p. 877.

14. Molnar, B., Flood, J. J. and Francombe, M. H., J. Appl. Phys. 35, 1965, p. 3554.

15. Davey, J. E. and Pankey, T., J. Appl. Phys. 35, 1964, p. 2203.

16. Cardona, M.: Semiconductors and Semimetals, Vol. 3. Willardson, R. K. and Beer, A. C., ed., Academic Press (New York), 1967.

17. Abraham, A., Czech. J. Phys. 6, 1956, p. 624.

18. Mead, C. A. and Spitzer, W. G., Phys. Rev. Letters 11, 1963, p. 358.

19. Fomenko, V. S., Handbook of Thermionic Properties, Plenum Press (New York), 1966.

20. Kover, F., Solid State Phys. Electron. Telecommun. 2, 1960, p. 768.

21. Shaw, D. and McKell, H. D., Brit. J. Appl. Phys. 14, 1963, p. 295.

22. Minden, H. T., Sylvania Tech. 11, 1958, p. 13.

23. Gunther, K. G., The Use of Thin Films in Physical Investigations, Anderson, J. C., ed., Academic Press (London), 1966, p. 213.

24. Agrain, P. and Balkanski, M., Selected Constants Relative to Semiconductors, Pergamon Press, 1961.

25. Weisberg, L., Contract SD-182, AD-432-272, March 1964.

26. Wieder, H. H., Solid-State Electron. 9, 1966, p. 373.

27. Bube, R. H., Photoconductivity of Solids, John Wiley and Sons, 1960.

28. Madelung, O. (Meyerhofer, D., Trans.) Physics of III-V Compounds John Wiley and Sons, 1964.

29. Rhodin, T. N., Disc. Faraday Soc. 5, 1949, p. 215.

30. Jeffrey, G. A. and Parry, G. S., J. Chem. Phys. 23, 1955, p. 406.

31. Taylor, K. M. and Lenie, C., J. Electrochem. Soc., 107, 1960, p. 308.

32. von Hippel, A. R., Dielectrics and Waves, John Wiley and Sons (New York), 1954, p. 5.

33. Kawabe, K., Tredgold, R. H., and Inuishi, Y., Elec. Engr. in Japan, 87, 1967, p. 62.

34. Lampert, M. A., Phys. Rev., 103, 1956, p. 1648.

35. Grove, A. S., Deal, B. E., Snow, E. H., and Sah, C. T., Solid State Electron., 8, 1965, p. 145.

36. Krikorian, E. and Sneed, R. J., Technical Report AFAL-TR-67-139, August 1967, p. 112.

37. Murray, L. A. and Scott, J. H., Paper 152, Proc. Electrochem. Soc. (Philadelphia), October 1966.

38. Hu, S. M., Paper 156, Proc. Electrochem. Soc. (Philadelphia), October 1966.

39. Doo, V. Y., Nichols, D. R. and Silvey, G. A., J. Electrochem. Soc., 113, 1966, p. 1279.

40. Deal, B. E., Fleming, P. J. and Castro, P. L., J. Electrochem. Soc., 115, 1968, p. 300.

41. Barnes, C. R. and Geesner, C. R., J. Electrochem. Soc., 107, 1960, p. 98-100.

42. Gregor, L. V., Study of Silicon Nitride as A Dielectric Material for Microelectronic Applications, Tech. Rpt. AFAL-TR-67-248, September 1967.

43. Staff of Southern Reserve Inst.: The Thermal Properties of Twenty-Six Solid Materials to 5000°F or Their Destruction Temperature, ASD-TDR-62-765, Contract No. AF 33-616-7319, January 1963, ASTIA AD-298-061.

44. Pease, R. S., Acta Cryst. 5, 1952, p. 356-61.

45. Bassani, F. and Yoshimine, M., Phys. Rev. 130, 1963, p. 20-33.

46. Li, P. C., Chemically Vapor Deposited Boron Nitride, NASA, N65-11827, June 1964.

47. Winslow, D. K., Wauk, M. T., and Malbon, R. M., Microwave Device Techniques for Aerospace Surveillance, Stanford University, Tech. Rept. No. RADC-TR-67-401, August 1967.

48. Rand, M. J. and Roberts, J. F., J. Electrochem. Soc., 115, 423 (1968).

6. APPENDIX (NEW TECHNOLOGY)

Preparation of Stoichiometric Al-V Films by Three Temperature Evaporation

The following conditions were used to ensure the preparation of stoichiometric evaporated films of the compounds AlSb, AlAs and AlP. Al source temperatures should be in the range 1000-1200°C to provide incidence rates up to 600 A/min. The Group V element should be screened from the Al source to prevent formation of the compound at the surface of the melt. Adjustment of the source temperatures should be such that the Group V element flux is 1 to 1.5 times that for Al. Substrate temperatures must be greater than 700°C, high enough to prevent or reduce significantly the deposition of Al alone. The upper limit for the substrate temperature is set only by the decomposition temperature of the respective compound.

More detailed data are given for the individual compounds in Sec. 2.1.1 (AlSb), Sec. 2.3.1 (AlAs) and Sec. 2.4.1 (AlP).

Report Distribution List for Contract NAS 12-568

National Aeronautics & Space
Administration
Attn: US/Winnie M. Morgan
Sci. and Tech. Info. Division
Washington, D. C. 20546
2 copies

National Aeronautics & Space
Administration
Attn: REE/Mr. C. E. Pontious
Washington, D. C. 20546

National Aeronautics & Space
Administration
Attn: Office of Technology
Utilization
Washington, D. C. 20546

National Aeronautics & Space
Administration
Attn: Mr. S. Gaudiano, Code EE-2
Manned Spacecraft Center
Houston, Texas 77058

National Aeronautics & Space
Administration
Attn: Dr. Alvis M. Holladay, R-ASTR-R
Geo. C. Marshall Space Flight Center
Huntsville, Alabama 35812

National Aeronautics & Space
Administration
Attn: Mr. C. A. Hermach, Code SVM
Ames Research Center
Moffett Field, California 94035

National Aeronautics & Space
Administration
Attn: Mr. C. Husson, Mail Stop 470
Langley Research Center
Hampton, Virginia 23365

National Aeronautics & Space
Administration
Attn: Mr. R. Van Allen, Code 711
Goddard Space Flight Center
Greenbelt, Maryland 20771

Jet Propulsion Laboratory
Attn: Mr. R. Powell
Research Programs Office
4800 Oakgrove Drive
Pasadena, California 91103

Department of the Army

Commanding General
U.S. Army Electronics Command
Attn: AMSEL-KL-S, Dr. H. Jacobs
Fort Monmouth, New Jersey 07703

Commanding General
U.S. Army Electronics Command
Attn: AMSEL-KL-I, Mr. R. A. Gerhold
Fort Monmouth, New Jersey 07703

US Army Electronics Command
Attn: Mr. H. Mette
Code AMSEL-KL-ID
Fort Monmouth, New Jersey 07703

Army Research Office Durham
Attn: Dr. R. Mace
Director, Physics Division
Box CM
Duke Station, North Carolina 27706

Commanding Officer
Harry Diamond Laboratories
Attn: Mr. N. Doctor
Washington, D. C. 20438

Commanding Officer
USAMERDC
Attn: SMEFB-IR (Mr. K. Steinbach)
Fort Belvoir, Virginia 22060

Commanding Officer
Picatinny Arsenal
Attn: Mr. A. Hendrickson, SMUPA-T
Dover, New Jersey 07801

Department of the Navy

Naval Weapons Center
Attn: Dr. H. H. Weider, Code C 6134
Corona Laboratories
Corona, California 90720

Department of the Navy Cont.

Department of the Navy
Naval Electronic Systems Command
Attn: Mr. A. H. Young, ELEX-05143A
Washington, D. C. 20360

Director, Naval Research Laboratory
Attn: Mr. G. Abraham, Code 2027
Washington, D. C. 20390

Res. Coordinator Materials
Office of Naval Research
Attn: Mr. Ancel E. Cook, Code 403C
Department of the Navy
Washington, D. C. 20360

U.S. Naval Ordnance Laboratory
Attn: Mr. Albert D. Krall
White Oak
Silver Spring, Maryland 20910

Department of the Air Force

Air Force Avionics Laboratory
Attn: J. Blasingame
Chief, Electronic Res. Branch
Wright Patterson AFB, Ohio 45433

Air Force Avionics Laboratory (AVTA)
Attn: Mr. H. H. Steenbergen
Wright Patterson AFB, Ohio 45433

Air Force Office of Scientific Res.
Attn: Dr. T. Ratchford
Office of Aerospace Research
Washington, D. C. 20333

Commander, RADC
Attn: Mr. J. Brauer, EMERM
Griffiss Air Force Base
New York 13440

Air Force Materials Laboratory
Attn: Mr. L. F. Salzberg
Wright Patterson AFB, Ohio 45433

Other Government Agencies

Director, National Security Agency
Attn: Mr. Oliver H. Bartlett Jr., R-42
Fort George G. Meade,
Maryland 20755

Private Organizations

Dr. R. D. Baxter
Battelle Memorial Institute
505 King Avenue
Columbus, Ohio 43201

Dr. H. Manasevit
North American-Rockwell Corp.
Antonetics Division
Miraloma Avenue
Anaheim, California

Dr. G. S. Kamath
Xerox Corporation
Research Laboratory
Webster, New York

Dr. T. B. Light
IBM Corporation
Thomas Watson Research Center
Yorktown Heights, New York

Applies Physics Laboratory
The John Hopkins University
Attn: Dr. Charles Feldman
Silver Spring, Maryland 20910

Lincoln Laboratory, MIT
Attn: Mr. Donald J. Eckl
P.O. Box 73
Lexington, Massachusetts 02173

J. L. Moll
Stanford University
Stanford, California 94304

P. L. Hower
Research and Development Laboratory
Fairchild Semiconductor
Palo Alto, California

L. Cohen
General Telephone & Electronics
Laboratories, Incorporated
Bayside, New York

H. C. Casey
Bell Telephone Laboratories, Inc.
Murray Hill, New Jersey

Private Organizations Cont.

W. W. Hooper
Research and Development Laboratory
Fairchild Semiconductor
Palo Alto, California

A. M. Barnet
General Electric Company
Electronics Laboratory
Syracuse, New York

Dr. J. J. Tietjen
David Sarnoff Research Center
Princeton, New Jersey

G. E. Renner
General Electric Research and
Development Center
Schenectady, New York

H. Rupprecht
T. J. Watson Research Laboratory
IBM Corporation
Yorktown Heights, New York

W. G. Spitzer
Department of Materials Science
and Electrical Engineering
University of Southern California
Los Angeles, California

F. J. Reid
General Telephone & Electronics
Laboratories, Incorporated
Bayside, New York

C. M. Wolfe
Lincoln Laboratories
Mass. Institute of Technology
Lexington, Massachusetts 02173

J. Kinoshita
Central Research Laboratories
Varian Associates
Palo Alto, California

C. S. Kang
Hewlett-Packard Laboratories
Palo Alto, California

Private Organizations Cont.

M. Ilegems
Stanford Electronics Laboratory
Stanford University
Stanford, California 94304

R. Solomon
Fairchild Semiconductor Research &
Development Laboratory
Palo Alto, California

K. L. Ashley
Southern Methodist University
Dallas, Texas 75222

G. L. Pearson
Stanford Electronics Laboratory
Stanford University
Stanford, California 94304

M. T. Wauk
Microwave Laboratory
Stanford University
Stanford, California 94305

D. K. Winslow
Microwave Laboratory
Stanford University
Stanford, California 94305

J. DeKlerk
Westinghouse Research Center
Pittsburgh, Pa. 15235

R. E. Stapleton
Westinghouse Electric Corp.
Aerospace Elec. Div.
Lima, Ohio

R. A. Lindberg
NASA/Lewis Research Center
Space Power Systems Div.

S. E. Miller
Columbus Laboratories
Battelle Memorial Inst.
Columbus, Ohio

H. L. Goering
Columbus Laboratories
Battelle Memorial Inst.
Columbus, Ohio

S. M. Hu
IBM Components Div.
E. Fishkill Facility
Hopewell Junct., New York 12533

L. V. Gregor
IBM Components Div.
E. Fishkill Facility
Hopewell Junct., New York 12533

A. R. Janus
Research & Development Labs.
Sprague Elect. Co.
North Adams, Mass.

G. A. Shirn
Research & Development Labs.
Sprague Elect. Co.
North Adams, Mass.

L. A. Murray
Radio Corp. of America
Electronic Components & Devices
Somerville, New Jersey

J. H. Scott
Radio Corp. of America
Electronic Components & Devices
Somerville, New Jersey

J. R. Rairden
General Electric Corp.
Research and Development Center
Schenctady, New York

M. J. Rand
Bell Telephone Labs, Inc.
Allentown, Pa.

J. F. Roberts
Bell Telephone Labs, Inc.
Allentown, Pa.

D. Richman
RCA Laboratories
Princeton, New Jersey

Contracting Center Distribution List

NASA Electronics Research Center
575 Technology Square
Cambridge, Massachusetts 02139

AT/Technical Information Branch
(20 + 1 reproducible) copies
Technical Monitor - 5 copies
T/Technology Utilization
M/Patent Counsel